Abstract

FisB Mediated Membrane Fission during Sporulation in *Bacillus Subtilis*

Martha Braun

2021

Membrane fusion and fission are important to all forms of life as they are required for processes such as cellular division, intracellular trafficking, and synaptic vesicle recycling. While membrane fission is extensively studied in eukaryotes, little is known about bacterial membrane fission even though it is required for every cell cycle. Membrane fission also occurs during sporulation. When nutrients are scarce, certain bacteria (e.g. *Bacillus subtilis*) are able to sporulate, thereby creating resistant endospores that can withstand harsh environmental conditions, such as radiation and drought, for hundreds of years.

The first step of sporulation is asymmetric cell division which generates a larger mother cell and a smaller forespore. The mother cell then engulfs the forespore in a process similar to phagocytosis. When engulfment is complete, the leading membrane edge forms a small pore or membrane neck. Membrane fission of this neck connecting the engulfment membrane to the rest of the mother cell membrane, releases the forespore into the mother cell's cytoplasm. Our lab and collaborators had previously identified that fission protein B (FisB) is required for this membrane fission step. The mother cell nurtures the forespore and once it is mature, lysis of the mother cell releases the spore into the environment.

FisB is expressed shortly after asymmetric division and the only dedicated membrane fission machinery described for bacteria so far. It forms small, mobile clusters during engulfment and a large immobile cluster at the engulfment pole where membrane fission occurs. FisB is predicted to have a small N-terminal cytoplasmic domain, one

transmembrane domain, and a larger extracellular domain (FisB(ECD)) which binds the phospholipid cardiolipin (CL). CL is a negatively charged lipid with spontaneous, negative curvature and is implicated in membrane fusion and fission reactions. However, the physiological significance of these findings was not clear.

Overall, the aims of my thesis were to determine (1) how FisB localizes to the fission site and (2) the mechanism by which it mediates fission.

First, we tested if FisB is recruited to the fission site by interaction with another protein, a specific lipid domain, or by membrane curvature. We were unable to identify a protein that interacts with FisB and found that FisB localization and membrane fission do not depend on membrane microdomains of CL or phosphatidylethanolamine (PE), another lipid that previously had been implicated in membrane fission and fusion. Additionally, our results suggest that FisB does not sense or induce membrane curvature, thus localization to the highly curved membrane fission site must rely on a separate mechanism. However, by using mutagenesis, we found that FisB self-oligomerization and binding to acidic lipids is required for targeting of FisB to the fission site.

Next, we characterized interactions of FisB(ECD) with artificial membranes and found that FisB(ECD) forms an extended stable network on GUV membranes which is so stable that it persists even when the lipids are subsequently removed with detergent. Moreover, we found that FisB(ECD) bridges membranes of small liposomes and GUVs.

Finally, we noticed a strong correlation between forespore inflation during sporulation and membrane fission. We found that forespores of cells that have undergone fission are inflated, while spores of pre-fission cells are not, even if engulfment appears complete. DNA translocation from the mother cell into the forespore by the protein SpoIIIE leads to forespore inflation and requires membrane flow from the peripheral mother cell membrane through the membrane neck into the engulfment membrane. We hypothesize that by forming a stable network in the membrane neck when engulfment is complete,

FisB opposes lipid flow, leading to increased stress in the neck and ultimately membrane fission. Future work will test this hypothesis rigorously.

Altogether, our results suggest that FisB localizes to the fission site by relying largely on FisB-FisB and FisB-lipid interactions. Since the larger portion of FisB faces into the extracellular space, the membrane geometry at the end of engulfment allows for FisB molecules to interact in *trans*. Therefore, we propose that a FisB cluster gets trapped in the membrane neck by interacting with other FisB molecules and/or the membrane in *trans* across the neck. Thus, FisB exploits the high curvature geometry of the membrane fission site without relying on an intrinsic membrane curvature sensing mechanism. Our results also suggest that membrane fission and forespore inflation are linked. We suggest that FisB accumulation in the membrane neck resists membrane flow leading to friction between the FisB network and the membrane which when high enough can lead to membrane fission.

FisB Mediated Membrane Fission during Sporulation in *Bacillus Subtilis*

A Dissertation

Presented to the Faculty of the Graduate School

Of

Yale University

In Candidacy for the Degree of

Doctor of Philosophy

By
Martha Braun

Dissertation Director
Erdem Karatekin

June 2021

Acknowledgements

First, I would like to thank my advisor, Dr. Erdem Karatekin for all his help and guidance throughout my time in the lab. I felt fully supported to pursue any direction of research. His enthusiasm, continuous positivity, and creative ideas helped me to become the scientist I am today.

Next, I would like to thank Dr. Ane Landajuela. Without her, the project would not have advanced as much as it did. Her assistance with designing experiments and discussions about analyzing results were exceptionally helpful.

My sincere thanks also go to all my committee members, Dr. Christine Jacobs-Wager, Dr. Julien Berro, and Dr. Hesper Rego for many helpful suggestions over the past years.

I am grateful to all members of the laboratory, past and present, for creating a supportive environment, stimulating discussions, and camaraderie.

I would also like to thank all our collaborators who helped immensely to advance the project with insightful discussions and by providing us with bacterial strains. Specifically, I would like to thank the laboratories of David Rudner, Thierry Doan, and Christopher Rodrigues. Furthermore, I would like to thank the laboratory of Karin Reinisch, especially Florian Horenkamp, who assisted with obtaining structural information for our protein FisB.

I big thank you also goes to the Bacillus Genetic Stock Center, for providing us with bacterial strains but also for their help and advice concerning molecular cloning.

I am grateful to all my friends. Boardgame nights, potlucks, hiking, and camping adventures all kept me sane during this stressful time.

I am also grateful to my parents for their love and support throughout my whole life. They have helped me find my passions and made sure I had the ability to pursue them.

I would also like to express my gratitude to my parents-in-law Debra and Steve Debs. Thank you for letting Garrett and me stay at your place, for endless days and nights of playing settlers and for all the ice cream.

I would like to thank my best friend and husband Garrett Debs who always believed in me, even when I did not. You were incredibly supportive, and I am not sure if I could have made it this far without your help.

Finally, I am grateful to my cats, Oscar and Mr. Kitty, for keeping both of us sane while being quarantined.

Table of Contents

Abstract i

Acknowledgements vi

Table of Figures xiii

Frequently used abbreviations xv

1 Introduction 1

1.1 Eukaryotic membrane fission mechanisms 2

1.2 Bacterial membrane fission 7

1.2.1 Membrane fission during vegetative growth 7

1.2.2 Sporulation and membrane fission 7

1.3 Determinants of subcellular protein localization 11

1.3.1 Membrane curvature 11

1.3.2 Functional membrane microdomains (FMM) 12

1.3.3 Lipid domains 12

1.3.4 Nucleoid occlusion 13

1.3.5 Proton motive force (PMF) 13

1.4 Role of lipids in membrane fission 15

1.5 FisB mediates membrane fission at the end of engulfment during sporulation 18

2 FisB localization and membrane fission during sporulation in *Bacillus subtilis* 22

2.1 Localization of FisB to the membrane fission site requires FisB self-oligomerization and lipid binding 23

2.1.1 FisB is a single-pass transmembrane protein with a large extracellular domain 24

2.1.2 Membrane fission always occurs in the presence of a cluster of FisB molecules 28

2.1.3 Localization of FisB is not coupled to cell wall remodeling, the protonmotive force, or the membrane potential 32

2.1.4 FisB localization and membrane fission are independent of cardiolipin, phosphatidylethanolamine and flotillins 38

2.1.5 FisB binds to acidic lipids 44

2.1.6 $FisB^{173-220}$ binds acidic lipids 48

2.1.7 The extracellular domain of *C. islandicus* FisB binds to acidic lipids 49

2.1.8 Purified FisB(ECD) forms soluble oligomers 52

2.1.9 $FisB^{G175A,I176S,I195T,I196S}$ ($FisB^{GIII}$) is selectively impaired in self-oligomerization 55

2.1.10 $FisB^{K168D,K170E}$ ($FisB^{KK}$) is selectively impaired in binding acidic lipids 59

2.1.11 FisB-lipid interactions and homo-oligomerization are important for targeting FisB to the fission site 63

2.2 Interactions of FisB with giant unilamellar vesicles, forespore inflation, and a possible mechanism of membrane fission 67

2.2.1 Soluble FisB(ECD) binds to and aggregates negatively charged artificial membranes 68

2.2.2 FisB(ECD) forms a stable, extended network on GUV membranes 72

2.2.3 FisB does not permeabilize membranes 78

2.2.4 At very high concentrations FisB(ECD) deforms and disrupts membranes 81
2.2.5 FisB does not sense or induce membrane curvature 84
2.2.6 Interaction of FisB(ECD) mutants with artificial membranes 92
2.2.7 Correlation between forespore size and membrane fission 102
2.2.8 A possible mechanism for FisB mediated membrane fission 104
2.3 Discussion 106
2.4 Outlook 116
3 Materials and Methods 121
3.1 Materials 121
3.2 Methods 121
3.2.1 Generation of *B. subtilis* Strains 121
3.2.2 Overnight cultures of *B. subtilis* 122
3.2.3 Sporulation by resuspension (synchronous sporulation) 123
3.2.4 Substituted Cysteine Accessibility Method (SCAM) 123
3.2.5 Western Blot 124
3.2.6 Inhibition of cell wall synthesis and analyses of FisB motions 125
3.2.7 Dissipation of membrane potential 126
3.2.8 Thin Layer Chromatography (TLC) 126
3.2.9 Determination of sporulation efficiency (Heat Kill assay) 127
3.2.10 Determination of membrane fission efficiency 127
3.2.11 Widefield live-cell fluorescence microscopy of *B. subtilis* 128

3.2.12 Expression and purification of recombinant FisB(ECD) 128
3.2.13 Liposome preparation.....129
3.2.14 Liposome-protein co-floatation 130
3.2.15 Determination of binding constants.....130
3.2.16 Analytical size-exclusion chromatography (SEC) and negative-stain electron microscopy (EM).....131
3.2.17 Image analysis 131
3.2.18 Giant Unilamellar Vesicles (GUVs).....132
3.2.19 Permeabilization of giant unilamellar vesicles.....133
3.2.20 Permeabilization of large unilamellar vesicles (LUVs).....133
3.2.21 Fluorescence recovery after photobleaching (FRAP) 134
3.2.22 Determination of mean GUV intensity.....134
3.2.23 Transfection of HEK293 cells 134
3.2.24 Determination of spore surface area.....135
3.2.25 *Bacillus subtilis* giant protoplasts.....135
3.2.26 Micropipette aspiration 135
4 Leukocyte Cytoskeleton Polarization Is Initiated by Plasma Membrane Curvature from Cell Attachment.....144
4.1 Introduction.....144
4.2 Increasing membrane curvature drives SRGAP2 and PI4P polarization 146
4.3 Discussion 149
4.4 Material and Methods 150

4.4.1 Neutrophil Preparation and Transfection 150

4.4.2 Micropipette Aspiration Assay 150

Appendix: *In vitro* reconstitution of FisB into GUVs.....152

References.....158

Table of Figures

Figure 1. Membrane fission mechanisms. 5

Figure 2. Sporulation in *Bacillus subtilis*.....10

Figure 3. Cardiolipin localization during sporulation in *B. subtilis.* 17

Figure 4. FisB is required for membrane fission at the end of engulfment during sporulation.....19

Figure 5. Domain structure and topology of FisB. 26

Figure 6. Membrane fission always occurs in the presence of a cluster of FisB molecules. 30

Figure 7. Motion of FisB clusters is not coupled to cell wall synthesis, or pH and voltage gradients across the cell membrane. 36

Figure 8. Membrane fission is insensitive to membrane lipid composition. 42

Figure 9. FisB(ECD) binds acidic lipids via electrostatic interactions. 46

Figure 10. The most hydrophobic region of FisB(ECD) binds to liposomes containing acidic lipids. 50

Figure 11. His6-FisB(ECD) forms soluble aggregates *in vitro.* 54

Figure 12. FisB mutants selectively impaired in oligomerization and membrane binding. 57

Figure 13. Identification of FisB lipid binding mutants. 61

Figure 14. FisB clustering and binding to acidic lipids are both required for ISEP formation and membrane fission. 65

Figure 15. Interactions of FisB(ECD) with GUV membranes.....70

Figure 16. FisB(ECD) forms a stable, extended network on GUV membranes. 74

Figure 17. FisB(ECD) forms a stable network on GUV membranes.....77

Figure 18. FisB does not permeabilize membranes at 1 μM. 80

Figure 19. At high coverage, FisB(ECD) causes membrane invaginations and collapse. 83
Figure 20. Curvature-sensing versus curvature-inducing. 85
Figure 21. FisB does not sense or induce membrane curvature. 90
Figure 22. Interaction of FisB(ECD) WT and mutants with GUV membranes. 95
Figure 23. FisB(ECD) WT and mutants aggregate membranes of GUVs and SUVs. 99
Figure 24. At 1 μM FisB(ECD) mutants also form a stable network on GUV membranes. 101
Figure 25. Determination of forespore surface area. 103
Figure 26. Possible mechanism for FisB mediated membrane fission. 105
Figure 27. Comparison of FisB with eukaryotic fission proteins. 115
Figure 28. Method for generating giant *B. subtilis* protoplasts. 119
Figure 29. Curvature dependent localization of FBAR-GFP and GFP-P4M. 148
Figure 30. Reconstitution of FisB into GUVs. 155
Figure 31. Fluorescence intensity profiles along GUV contours. 157

Frequently used abbreviations

AH	Amphipathic helix
AMS	4-acetamido-4′-maleimidylstilbene-2,2′-disulfonic acid
CCCP	Carbonyl cyanide m-chlorophenyl hydrazone
CCTOP	Constrained Consensus TOPology
CF	Carboxyfluorescein
CI	Confidence interval
CL	Cardiolipin
CME	Clathrin-mediated endocytosis
DMC	Dim mobile clusters
ECD	Extracellular domain
ESCRT	Endosomal sorting complex required for transport
FMM	Functional membrane microdomains
FRAP	Fluorescence recovery after photobleaching
FS	Forespore
GFP	Green fluorescent protein
GUV	Giant unilamellar vesicle
ID	Index of dispersion
ISEP	Intense spot at the engulfment pole
LUV	Large unilamellar vesicle
MC	Mother cell
MIP	Maximum intensity projection
MPB	3-(N-maleimidylpropionyl) biocytin
MSD	Mean square displacement

NAO	Nonyl acridine orange
PA	Phosphatidic acid
PC	Phosphatidylcholine
PE	Phosphatidylethanolamine
PG	Phosphatidylglycerol
PI(4,5)P2	Phosphatidylinositol-4,5-bisphosphate
PM	Plasma membrane
SCAM	Substituted Cysteine Accessibility Method
SDC	Spinning disk
SEC	Size exclusion chromatography
SUV	Small unilamellar vesicles
TIRFM	Total internal reflection microscopy
TMA-DPH	N,N,N-trimethyl-4-(6-phenyl-1,3,5-hexatrien-1-yl)-benzamine
TMD	Transmembrane domain
WT	Wild type
YFP	Yellow fluorescent protein

1 Introduction

Membrane fusion and fission are essential to all forms of life and can be viewed as opposite processes (Figure 1A). During membrane fusion two initially separate membranes merge into one continuous bilayer, while during membrane fission an initially continuous membrane divides into two separate lipid bilayers. Membrane fission is required for complex processes such as endocytosis, membrane trafficking, enveloped virus budding, phagocytosis, cell division, and sporulation [1-3]. While several membrane fission mechanisms have been described in eukaryotes at molecular detail [4-8], our knowledge of membrane fission in bacteria is more limited. During my thesis, using a combination of biochemical, biophysical, and live-cell imaging approaches, I studied mechanisms by which the only known dedicated bacterial membrane fission protein, FisB, localizes to the membrane fission site and catalyzes membrane fission during sporulation. Our results suggest novel mechanisms of sub-cellular localization and membrane fission. They also allow us, for the first time, to compare eukaryotic and bacterial membrane fission machineries.

Membrane fusion and fission share many similarities as both require local membrane deformations and transient disruptions. While both processes require the formation of a membrane neck, the key difference between these processes is that while during membrane fusion this neck expands, during membrane fission this neck must be constricted (Figure 1A). For membrane fission to occur the neck needs to be constricted to less than 3 nm [9]. At this distance, two forces dominate: a repulsive hydration force which arises from water molecules bound to the polar lipid head groups and an attractive hydrophobic force between the hydrophobic interior acyl chains of the membranes [10]. Therefore, for fission to occur, this repulsive hydration force must be overcome and molecular contact between the membranes must be created. Additionally, the energy

barrier for fission is determined by the mechanical properties of the membranes (e.g. membrane tension or membrane bending modulus) as well as the overall geometry of the system. Usually, specialized proteins localize to the fission site to generate the work required to merge membranes [11-15].

Numerous mechanisms by which membrane fission can be achieved have been discovered (Figure 1B) and it is still an active research field. While it was originally believed that membrane fission reactions require a cellular energy source (active membrane fission), pathways that do not require an energy source (passive membrane fission) have more recently been described [1].

1.1 Eukaryotic membrane fission mechanisms

In eukaryotes, many active membrane fission reactions are mediated by dynamin and the endosomal sorting complex required for transport III (ESCRT-III) [4, 5]. Dynamin is a GTPase involved in endocytosis and mitochondrial genesis. During clathrin-mediated endocytosis (CME), dynamin is recruited to the membrane neck connecting the clathrin-coated pit (CCP) to the plasma membrane by endophilin and amphiphysin to cooperatively mediate membrane fission [16]. Endophilin and amphiphysin are N-Bar domain-containing proteins. BAR domains (Bin, amphiphysin and Rvs) are banana-shaped dimeric protein domains, which can bind membranes with their curved surfaces and thereby either induce or stabilize curved membranes. Endophilin and amphiphysin are recruited to the membrane neck due to their preference for the curvature of the membrane neck. Here, they induce higher curvature and promote dynamin recruitment [17].

To catalyze membrane fission, dynamin oligomerizes into a helical scaffold around the outside of a membrane neck. GTP hydrolysis leads to changes in dynamin's helical conformation which is believed to promote membrane fission (Figure 1B, panel D) [18]. Additionally, binding to the negatively charged phospholipid L-α-phosphatidylinositol-4,5-

bisphosphate (PI(4,5)P2) was shown to be critical for dynamin mediated membrane fission [19, 20].

While proteins of the ESCRT-III membrane fission machinery also bind negatively charged lipids, they oligomerize on the inside of membrane necks in form of inward growing spirals (Figure 1B, panel E). However, final membrane fission requires the activity of the AAA-ATPase Vps4 [21].

In contrast, passive membrane fission processes do not need energy in the form of ATP or GTP. These processes may rely on insertion of amphipathic helices (AH) [6], formation of lipid domains and line tension [22] or protein crowding [7].

Insertion of a high number of amphipathic helices (Figure 1B, panel A) has been shown to induce membrane bending and was shown to promote a shift from tubulating membranes to vesiculation [23]. Small GTPases, Atg proteins, proteins containing ENTH/ANTH domains, or proteins with a BAR-domain have all been shown to be involved in AH induced fission reactions [6]. For membrane fission to occur, these AH-containing proteins frequently work together with another protein (e.g. a lipid-modifying enzyme such as phospholipase A2 [24]) or lipid (e.g. phosphatidylinositol 4,5-bisphosphate (PI(4,5)P2) [23, 25], phosphatidic acid (PA) [26, 27], or cardiolipin (CL) [28, 29]).

Another way to achieve passive membrane fission is through energy minimization at a phase boundary. Depending on their lipid composition and the proteins present, biological membranes show phase separation resulting in phases that differ in their physical properties such as thickness or stiffness. The boundaries of those phases are energetically unfavorable, resulting into line tension [22]. One way to decrease the excess free energy associated with these phase boundaries is to shorten the length of the interface [30, 31]. For a planar membrane this could be achieved by formation of a membrane bud where the connecting neck containing the phase boundary would be

narrower than the domain. In this case a high enough line tension can lead to severing of the membrane neck [32].

More recently protein crowding has been suggested as a new way to achieve membrane fission (Figure 1B, panel C) [7]. In this case, collisions between proteins bound to one side of the membrane generate lateral pressure which can lead to membrane budding and fission. The efficiency of membrane fission does not depend on how proteins are anchored to the membrane. Replacement of amphipathic helices with synthetic membrane-binding motifs did not affect membrane fission. Instead, protein coverage and hydrodynamic radius determine fission efficiency.

Finally, membrane fission can be achieved by friction generated through a BAR protein scaffold in combination with molecular motors (Figure 1B, panel G) [8]. In this case, BAR proteins form a scaffold on a membrane tube via interaction with lipid headgroups. This scaffold creates a resistance for lipid flow. If the lipid tube is rapidly extended by a molecular motor, tension builds up in the lipid membrane and if large enough can lead to scission of the tube.

While much progress has been made in understanding the molecular mechanisms underlying the fission mechanisms described above as well as in identifying new fission mechanisms, it seems likely that even more fission mechanism will be discovered in the future. This leads to the question: Why would cells need so many ways to mediate membrane fission? It is likely that different fission machineries work together to effectively regulate the fission reaction and make it more efficient. However, future work is necessary to understand how interconnected these fission machineries are and their role in controlling various fission reactions within a cell.

Figure 1. Membrane fission mechanisms. ***(A)*** Membrane fission and fusion as opposite processes. ***(B)*** Membrane fission mechanisms, borrowed from [1]. Comparison of passive (no cellular energy source required, left) and active (hydrolysis of GTP or ATP required, right) mechanisms. Passive membrane fission can be achieved by insertion of amphipathic helices, generation of line tension by lipid domains or protein crowding. Active membrane fission can be achieved by the GTPase dynamin which assembles a helical scaffold on the outside of a membrane neck or the ESCRT-III complex. The latter requires activity of the ATPase Vps4 to constrict a membrane neck from the inside. Additionally, actin polymerization or CtBP/BARS complexes are believed to modify the lipid composition or membrane organization which in turn can generate membrane domains and line tension. High enough line tension can finally sever a membrane neck.

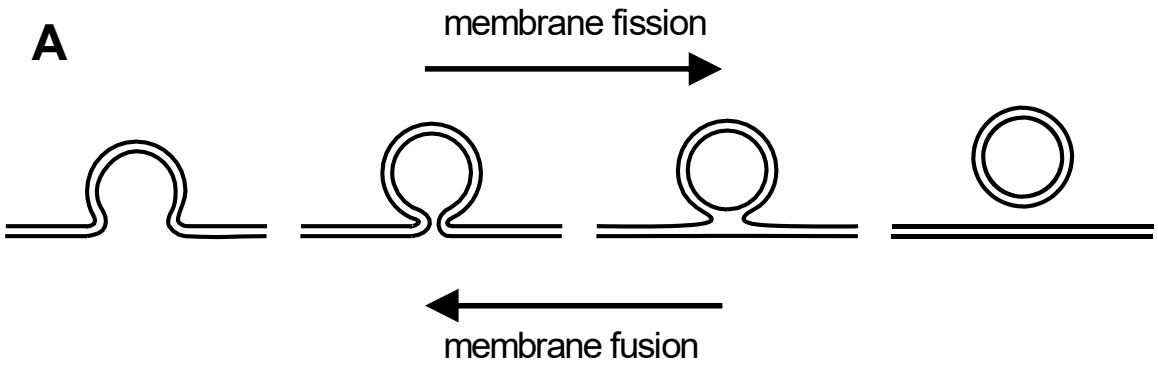

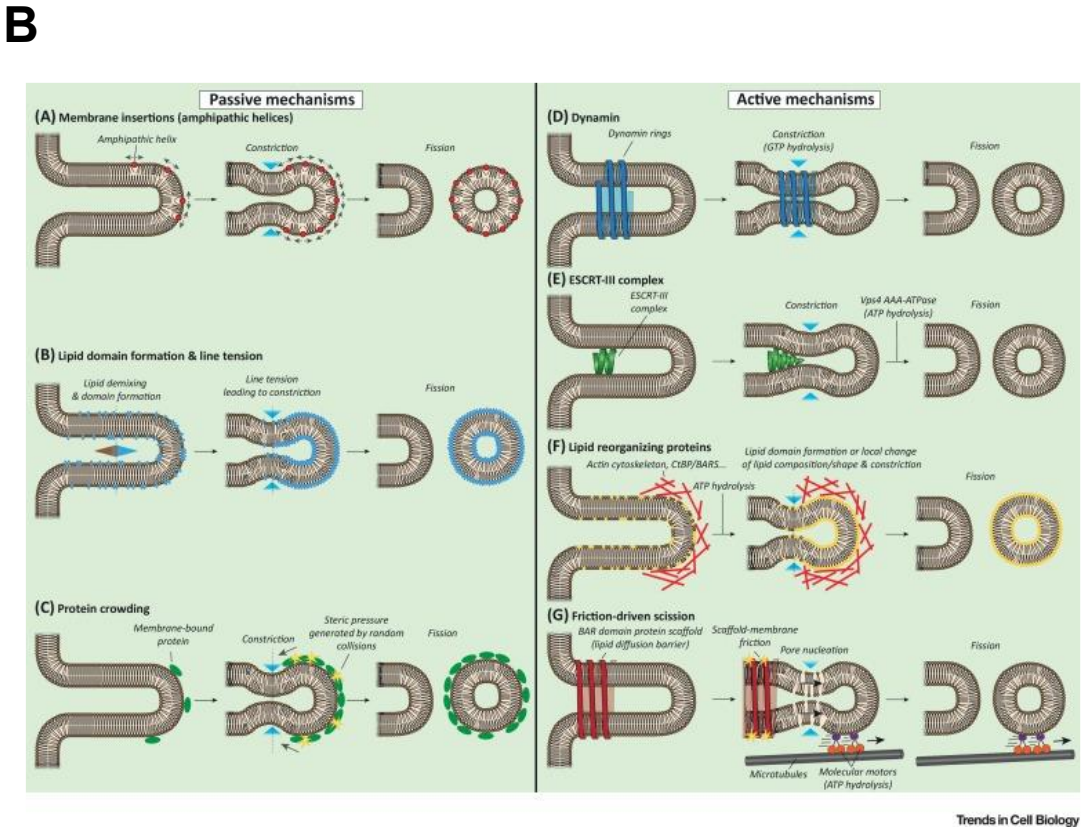

Figure 1. Membrane fission mechanisms.

1.2 Bacterial membrane fission

While eukaryotic membrane fission reactions have been studied extensively, much less is known about bacterial membrane fission even though they rely on membrane fission for every cell cycle and during sporulation.

1.2.1 Membrane fission during vegetative growth

Binary fission during vegetative growth usually starts with the assembly of a Z-ring in the middle of the cell [33]. This Z-ring is mainly composed of the tubulin-like GTPase FtsZ which forms dynamic filaments together with the actin-like protein FtsA (FtsAZ). The Z-ring recruits other proteins required for septum formation and ultimately cell division. Among those are peptidoglycan synthases. Recent studies suggest that treadmilling of FtsZ regulates the synthesis of new peptidoglycan at the division site which is believed to be the main driver for membrane constriction during cytokinesis [34].

What drives membrane fission at the end of constriction is not known. In archaea, a distant ESCRT-III homologue mediates membrane fission during cell division [35, 36]. However, bacteria do not have an ESCRT homologue. While bacterial dynamin homologs have been described [37], they are not involved in fission during regular division [37] or sporulation (Figure 4A) [38]. While binary fission is required during vegetative growth, membrane fission is also critical for membrane fission at the end of engulfment in sporulating bacteria (see below).

1.2.2 Sporulation and membrane fission

Under conditions of environmental stress, certain bacteria (e.g. *Bacillus subtilis*) are able to produce endospores which are highly resistant to physical and chemical assaults and help the bacterium to survive these adverse conditions. This developmental program

is controlled by four sporulation specific sigma factors, which are proteins that are required to initiate transcription in bacteria. During sporulation σ^F, σ^E, σ^G and σ^K are activated at different stages to regulate specific gene expression [39].

Sporulation starts with an asymmetric cell division, resulting in a larger mother cell (MC) and a smaller forespore (FS) (Figure 2). This process requires the sporulation-specific increased expression of FtsAZ and SpoIIE which colocalizes with the polar Z-rings [40]. While the exact molecular mechanisms underlying this process are still unknown, asymmetric division requires a largely overlapping set of proteins as for binary cell division during vegetative growth.

After asymmetric division, the mother cell engulfs the forespore in a process similar to phagocytosis. When engulfment is complete the leading edge of the mother cell membrane forms a tube or neck that connects the engulfment membrane to the rest of the mother cell membrane (Figure 2 i). Upon membrane fission, the forespore is released into the cytoplasm of the mother cell and now surrounded by two membranes (Figure 2 ii).

During the early stages of sporulation, the chromosome is fully replicated. One chromosome remains in the mother cell and the other one will be transported into the forespore. During asymmetric division, ~1/3 of the forespores chromosome gets trapped in the newly created asymmetric division site. The remainder of the chromosome is translocated into the forespore throughout engulfment by the DNA pump SpoIIIE [41]. Pumping of the DNA as well as membrane synthesis were shown to increase fore spore size [42].

Following engulfment, the mother cell nurtures the forespore and provides it with a protective coat. When the spore is mature, the mother cell lyses and the spore is released into the environment. Once environmental conditions improve and are favorable for vegetative growth again, the spore will germinate and can restart the vegetative life cycle [39].

Thus, membrane fission occurs twice during sporulation: first for the asymmetric division, and then at the end of engulfment. Molecules required for the first membrane fission event are largely the same proteins needed for symmetric division during vegetative growth [40]. By contrast, the mother cell protein FisB is required for the second membrane fission event which releases the forespore into the cytoplasm of the mother cell [38]. Currently, how FisB localizes to the fission site and the mechanism by which fission is mediated is unknown.

Previous research by the Pogliano laboratory suggested that in addition to translocating the chromosome into the forespore, SpoIIIE is also necessary for this membrane fission reaction [43, 44]. They found that a SpoIIIE-GFP fusion protein localizes to the engulfment pole around the time of membrane fission and that cells lacking SpoIIIE are deficient in membrane fission. However, our lab and collaborators previously found that cells lacking SpoIIIE show engulfment defects prior to membrane fission, suggesting that SpoIIIE might not be directly involved in membrane fission [38]. In contrast, in cells lacking FisB, engulfment is not impaired and only the final fission step is impaired [38] (see chapter 1.5).

The two major goals of this thesis were to determine 1) the mechanisms underlying how FisB localizes to the membrane fission site and 2) how FisB mediates membrane fission. In the remaining sections below, I briefly review what is known about sub-cellular protein localization in bacteria, lipids previously implicated in membrane fission reactions, and properties of FisB that were known at the beginning of my thesis.

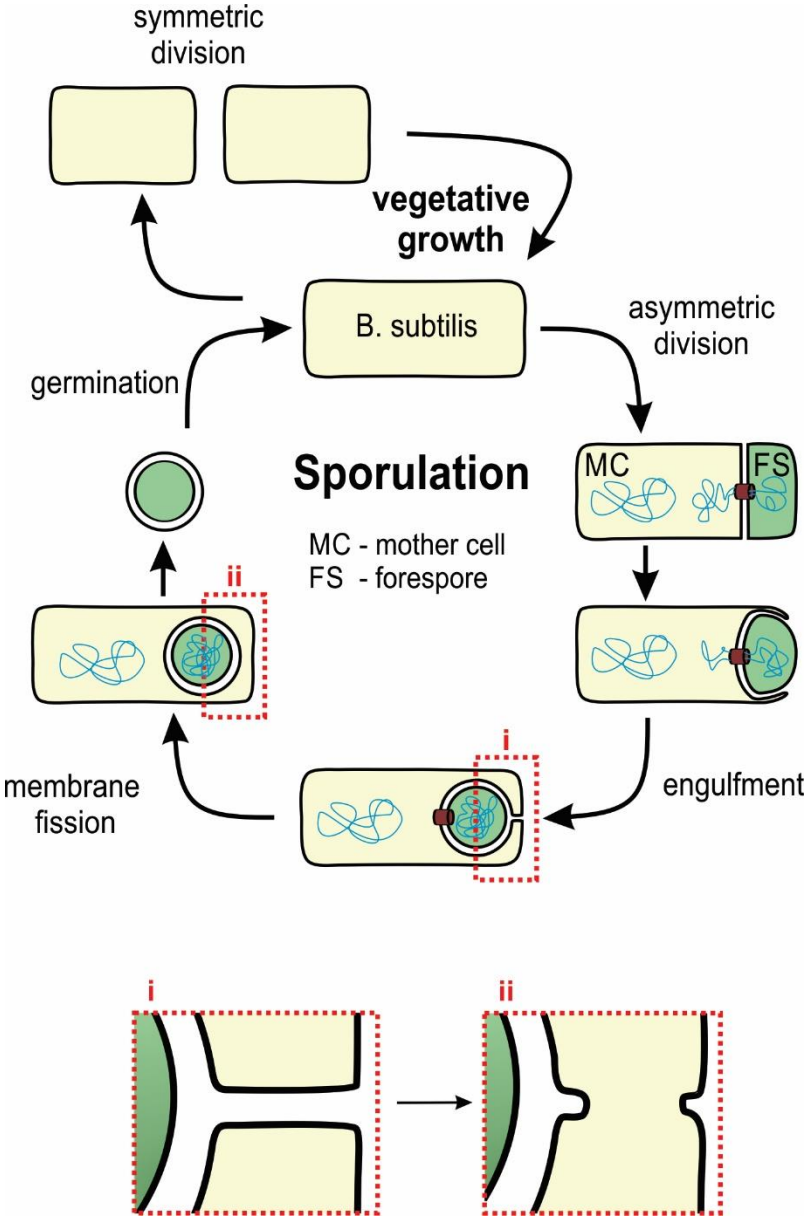

Figure 2. Sporulation in *Bacillus subtilis*. When nutrients are scarce, *B. subtilis* divides asymmetrically into a mother cell (MC) and a forespore (FS). The MC then engulfs the FS in a process similar to phagocytosis. During engulfment, the protein SpoIIIE translocates the forespore chromosome into the forespore. When engulfment is complete, membrane fission (highlighted in panels i and ii) releases the forespore into the cytoplasm of the MC where it is now surrounded by two membranes. The MC nurtures the FC and provides it with a protective coat. When the spore is mature, the mother cell lyses and releases the spore into the environment. Once environmental conditions improve, the spore can germinate and is able to enter the vegetative growth cycle.

1.3 Determinants of subcellular protein localization

For complex cellular processes such as endocytosis in eukaryotic cells or sporulation in bacteria to occur, many proteins need to localize to specific subcellular locations. In bacteria, several mechanisms have been described for subcellular localization of proteins and lipids. These include membrane curvature, functional membrane microdomains, lipid domains, nucleoid occlusion, and the proton motive force. They are briefly reviewed below.

1.3.1 Membrane curvature

In bacteria as well as eukaryotic cells, many proteins localize to a specific subcellular location due to their intrinsic preference for positive or negative membrane curvature. As described above, BAR-domain containing proteins recognize the high positive membrane curvature of the membrane neck during endocytosis. In rod-shaped bacteria such as *E. coli* or *B. subtilis*, many proteins are recruited to the cell poles due to their intrinsic preference for negative membrane curvature. However, on the scale of a single nanometer-sized protein (or lipid) within a micrometer-sized cell, the cell membrane at the pole is essentially flat. Therefore, formation of larger oligomeric structures is necessary in order to efficiently sense the membrane curvature at the poles in bacterial cells.

In *B. subtilis,* the DivIVA protein was described to localize to regions of high negative curvature such as the septum in dividing cells as well as the cell poles [45, 46]. While membrane binding of DivIVA requires its N-terminal amphipathic helix, the whole protein is required for DivIVA oligomerization [47] and therefore proper targeting to the cell pole or division site [48].

During sporulation, the Stage V sporulation protein M (SpoVM) localizes to the engulfing membrane of the mother cell due to its preference for positively curved

membranes. However, in contrast to DivIVA, it is believed that SpoVM's amphipathic helix directly senses membrane curvature by detecting packing differences of acyl chains [49].

1.3.2 Functional membrane microdomains (FMM)

Bacteria organize their membranes into functional membrane microdomains (FMM) which serve as a platform to coordinate many signal transduction cascades and protein oligomerization [50]. These FMMs can be considered loose analogs of eukaryotic lipid rafts and can also be purified from bacterial cells as the detergent insoluble membrane fraction [51]. FMMs are enriched in special lipids, however the exact lipid composition of these FMM's varies among species. In *B. subtilis* these FMMs are enriched in polyisoprenoid lipids and contain the flotillin-like proteins, FloT and FloA, which form mobile foci in the plasma membrane [52, 53]. In *B. subtilis* cells lacking FloT, sporulation is impaired, however which step of sporulation is affected is currently unknown [54].

1.3.3 Lipid domains

Proteins can also localize to specific subcellular locations by binding specific phospholipids that are enriched in these regions. The phospholipid cardiolipin (CL) has been shown to serve as a landmark for recruiting proteins in eukaryotes and prokaryotes [55, 56]. CL is comprised of two phosphatidic acid groups that are connected by a glycerol backbone resulting in a lipid with four acyl chains (Figure 3A). CL is a cone-shaped lipid, which is thought to favor non-bilayer structures. It forms microdomains that localize to regions of negative membrane curvature, for example the poles of rod-shaped bacteria [57, 58]. Wingreen and colleagues proposed that CL can form finite-sized microdomains large enough (100-1000 lipids) to sense the membrane curvature at the cell poles as a

consequence of short-range CL-CL attraction combined with long range elastic repulsion [59].

In bacteria, CL was shown to act as a landmark for the polar recruitment of the proline transporter ProP, or the mechanosensitive channel MscS in *E. coli* [60, 61].

In eukaryotes, CL is involved in stabilizing and activating many mitochondrial enzymes, especially those involved in oxidative phosphorylation [62, 63]. Additionally, CL is also involved in mitochondrial protein import/export, maintaining cristae morphology, and apoptosis [56]. Interestingly, CL has also been shown to be important for mitochondrial fusion and fission (see chapter 1.4).

1.3.4 Nucleoid occlusion

In addition to membrane curvature or binding to a lipid, another way for proteins to localize to the bacterial cell pole is via nucleoid occlusion [64]. The cell poles of bacteria are usually free from chromosomal DNA. DNA can be considered a quite bulky polymer and formation of larger oligomeric complexes would be more energetically favorable in regions devoid of DNA [65]. This has been described for the self-assembling *C. crescentus* protein PopZ, which forms an *in vivo* matrix in regions devoid of DNA such as the poles of *C. crescentus* or *E. coli* or in non-polar DNA-free regions of filamentous C*. crescentus* or *E. coli* with segregated nucleoids [66, 67]. Since FisB is a membrane protein, it is unlikely that this mechanism would play a role in FisB's localization.

1.3.5 Proton motive force (PMF)

It is well established that eukaryotes and prokaryotes require a proton motive force (PMF) across the membrane generated by the respiratory chain for ATP production by F_1F_o-ATPases [68]. However, more recently it was shown that the PMF can directly influence

the localization of proteins involved in cell division such as MinD, FtsA, and the bacterial cytoskeletal protein MreB [69]. For MinD, the authors also showed that its C-terminal amphipathic helix is sensitive to changes in the membrane potential component of the PMF.

1.4 Role of lipids in membrane fission

As mentioned above CL is a dimeric phospholipid with four acyl chains which prefers to localize to regions of negative membrane curvature. The cross-sectional area and volume of its head group is small relative to the acyl chains thereby conferring CL a predominantly inverted cone shape. As a result, CL can display a remarkable range of lipid phases favoring inverted, non-lamellar hexagonal phases [70]. In eukaryotes, CL is involved in mitochondrial fission and fusion. Fusion of the inner mitochondrial membranes requires the GTPase Opa1. CL binds to Opa1 and stimulates Opa1 dimerization as well as GTPase activity which is required for the fusion reaction [71]. During mitochondrial fission, the dynamin related protein 1 (Drp1) stably binds CL. This interaction enhances oligomerization and GTP hydrolysis [72, 73]. Moreover, it was proposed that the helical assembly of Drp1 induces localized lamellar to non-lamellar phase transition in CL-containing membranes and thereby priming it for membrane fission [72].

In addition to CL, phosphatidylethanolamine is another cone-shaped lipid that was shown to be involved in membrane budding, fusion and fission [74-76]. However, PE was also shown to work as a chaperone for membrane proteins [77].

While the role of cone-shaped lipids in membrane fission is well studied in artificial systems and eukaryotic cells, their role in bacterial membrane fission is less clear. In bacteria, CL and PE form microdomains at similar subcellular locations [54]. In *E. coli*, PE is important for cell division, as a strain lacking PE grows into filamentous cells and is defective in cell division [78]. However, *B. subtilis* cells lacking PE have no phenotype [79] and CL seems to be dispensable for binary fission during vegetative growth in *E. coli* [80] and *B. subtilis* [58]. Still, it is believed that due to their propensity for non-bilayer structures, PE and CL might locally alter membrane properties and thereby facilitating cellular processes such as cell division, creation of adhesion sites between the outer and the inner

membranes in gram-negative bacteria and integration and stabilization of membrane proteins [81]. Additionally, CL seems to play an important role during sporulation in *B. subtilis* as its levels rise from 1 % to 5 % during spore-formation [82]. CL is enriched in the engulfing membranes as well as the spore membrane (Figure 3B). Spores usually contain 25-50 mole % CL [82, 83]. When all three known genes for CL synthases (ywnE, ywiE, and ywjE) are disrupted, no CL is detected in membranes of cells during vegetative growth. Interestingly, CL levels rise to detectable levels in this strain during sporulation, suggesting a yet undiscovered sporulation specific pathway to produce CL further implying an important role for CL in spore-formation [58, 82]. However, if CL plays a role in membrane fission at the end of engulfment during sporulation is not known. Interestingly Doan et al. [38] found that FisB specifically interacts with CL and hypothesized that this interaction might be important for FisB localization to the fission site as well as membrane fission. This let us to investigate the role of CL in FisB localization and membrane fission (section 2.1.4 below).

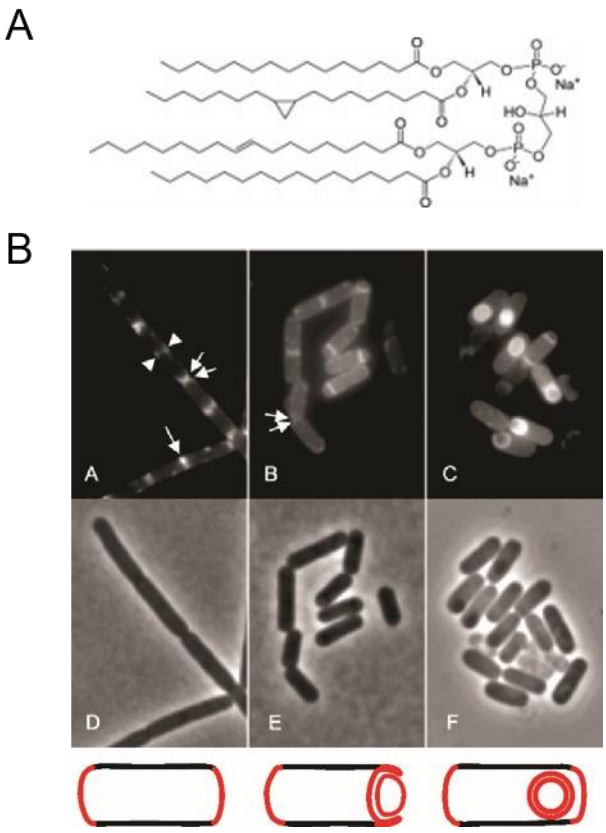

Figure 3. Cardiolipin localization during sporulation in *B. subtilis.* *(A)* Structure of *E. coli* CL (Avanti Polar Lipids). ***(B)*** Localization of CL during sporulation, adapted from [58]. *B. subtilis* 168 were stained with 100 nM nonyl acridine orange (NAO) to visualize CL during exponential growth (A,D), and 2h (B,E) and 4h (C,F) into sporulation. CL is enriched in the division septa, the engulfing membranes as well as the forespore membrane as indicated with schematics.

1.5 FisB mediates membrane fission at the end of engulfment during sporulation

The mother cell protein FisB was identified to be required for membrane fission at the end of engulfment [38]. Expression of FisB starts shortly after asymmetric division upon activation of the sporulation specific transcription faction σ^E. FisB is predicted to have a short N-terminal domain located in the cytoplasm, one transmembrane domain (TMD) and a larger extracellular C-terminus (FisB(ECD)) (Figure 5B). In FisB knock-out cells, engulfment is indistinguishable from wild type (WT) cells, but the final membrane fission step is impaired (Figure 4B) [38]. During engulfment, FisB expressed under its native promoter and fused to a fluorescent protein (such as GFP or YFP) forms small mobile clusters in the engulfment membrane as well as the peripheral mother cell membrane (Figure 4D-F). After around 3h after inducing sporulation, most cells display a large immobile focus at the engulfment pole where fission occurs.

Figure 4. FisB is required for membrane fission at the end of engulfment during sporulation. Adapted from [38]. ***(A)*** Percentage of cells that have undergone membrane fission 3h into sporulation for wild-type (wt) cells, cells lacking the bacterial dynamin homolog DynA, wild-type cells that were treated with 5 mM fosfomycin 1.5h after sporulation was induced and cells lacking FisB. ***(B)*** Time course of membrane fission for wt cells and cells lacking FisB. ***(C)*** Determination of membrane fission. Prior to membrane fission, the lipophilic dye FM4-64 labels the peripheral mother cell membrane, the engulfing membrane as well as the forespore membrane. FM4-64 is unable to cross the membrane. Therefore, after membrane fission, the dye cannot label the forespore membrane. The presence of a forespore inside the mother cell is assessed by a fluorescent forespore reporter (P_{spoIIQ}-*cfp*). ***(D)*** Localization of GFP-FisB at native expression levels at 3h into sporulation. Membranes were stained with TMA-DPH. Examples of sporulating cells with a discrete GFP-FisB focus at the fission site are highlighted with yellow arrowheads. ***(E)*** Images from a time lapse movie showing dynamic GFP-FisB foci at 2.5h into sporulation. Images were acquired every 2 min. The bottom image shows the average image of the entire time lapse movie and yellow arrowheads indicate immobile GFP-FisB clusters at the fission site. ***(F)*** Localization of YFP-FisB expressed at approximately 8-fold lower expression compared to native expression levels. Images show YFP-FisB localization 2h and 3h into sporulation. Small YFP-FisB clusters mainly localize to engulfing membrane at 2h into sporulation and are indicated with white arrowheads. 3h into sporulation most cells display a discrete YFP-FisB focus at the cell pole (yellow arrowheads). A schematic representation of FisB localization is shown below the images. Bar, 1 µm.

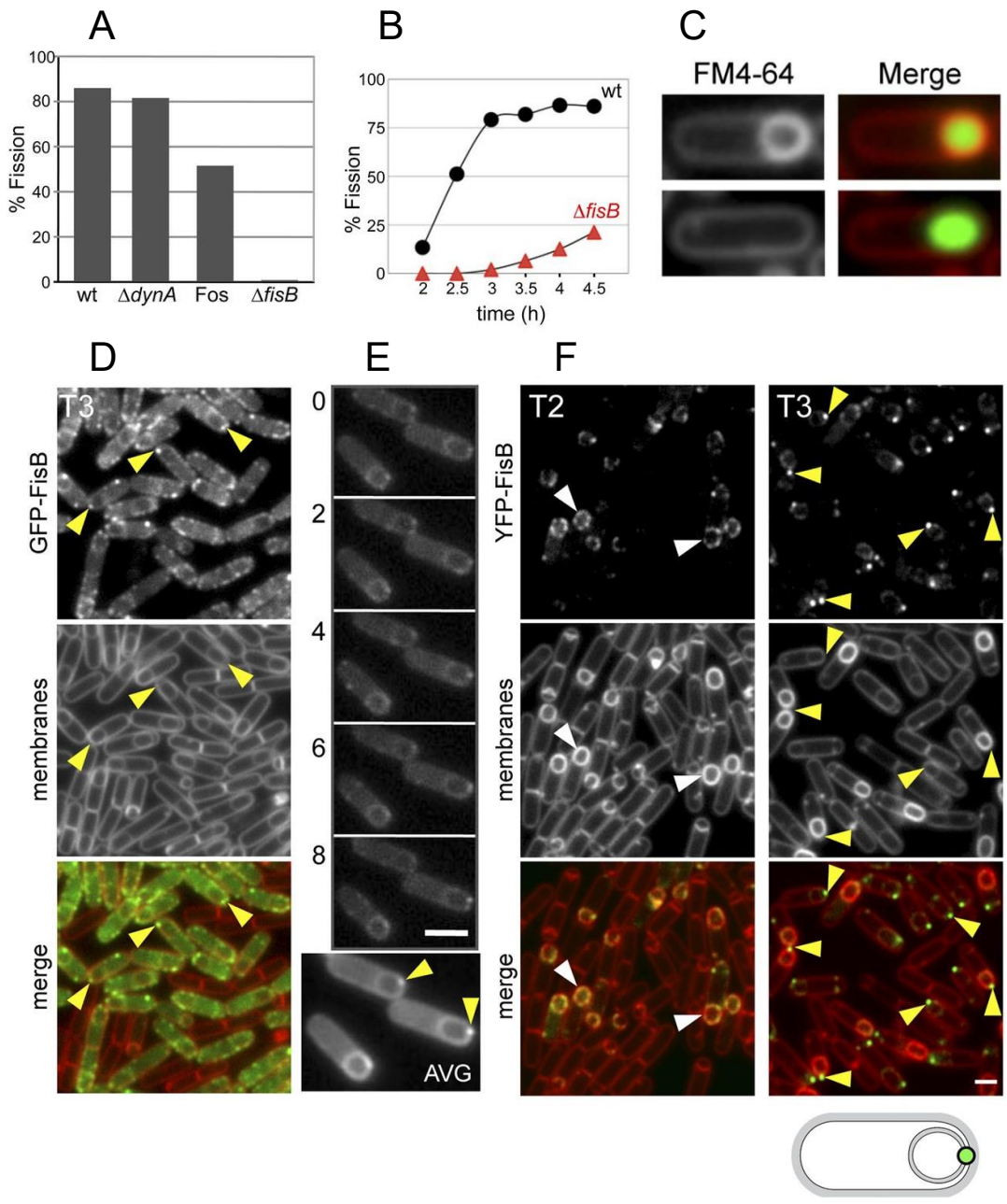

Figure 4. FisB is required for membrane fission at the end of engulfment during sporulation.

Our laboratory and collaborators had previously reported that FisB(ECD) specifically interacts with the CL [38]. As mentioned above, CL has been shown to act as a landmark for recruiting proteins to specific subcellular regions and has a well-established role in mitochondrial fission and fusion (see section 1.4) . Therefore it was hypothesized that FisB - CL interactions might be important for localization of FisB to the fission site and membrane fission [38].

Throughout my thesis, I will describe our work to determine how FisB localizes to the fission site and how it mediates membrane fission.

In section 2.1, I will mainly describe our findings concerning the mechanism by which FisB is recruited to the fission site. We investigated if CL or PE microdomains, flotillin-dependent functional membrane microdomains, cell wall synthesis machinery, and proton or voltage gradients across the membrane influence FisB dynamics and membrane fission.

In section 2.2, I will first describe the interactions of FisB(ECD) with artificial model membranes *in vitro* and how I investigated if FisB has an intrinsic preference for curved membranes. Then I will describe how forespore size and membrane fission are linked and finally present a model of how FisB might mediate membrane fission.

2 FisB localization and membrane fission during sporulation in *Bacillus subtilis*

2.1 Localization of FisB to the membrane fission site requires FisB self-oligomerization and lipid binding

2.1.1 FisB is a single-pass transmembrane protein with a large extracellular domain

All spore-forming bacteria possess a FisB homolog, however no experimental structural information about FisB is available. I therefore first established the topology of FisB within the membrane. Pfam [84] identifies a consensus region (residues 130-223) defining the FisB protein family (Figure 5B). Most topology prediction tools predict that FisB has a small cytoplasmic N-terminal domain, one predicted transmembrane domain (TMD) and a larger extracellular domain (FisB(ECD)) (Figure 5A and B). However, the topology prediction tool Prodiv predicts a second TMD spanning amino acids 130 -150 (Figure 5A,C and D). If this were indeed the case, the C-terminus of FisB would now face the cytosol rather than the extracellular space. Additionally, Memset also predicts a single TMD, but with the N-terminus facing the extracellular space, while the C-terminus would be located in the cytoplasm (Figure 5A).

Since the interpretation of all our results relies on the topology of FisB, I established FisB's topology experimentally using the substituted cysteine accessibility method (SCAM) [85]. To this end, I tested accessibility of cysteine residues introduced at various positions to a membrane impermeable, biotinylated, sulfhydryl-reactive reagent, 3-(*N*-maleimidylpropionyl) biocytin (MPB) [86] (wild-type FisB lacks cysteines) (Figure 5D-F).

I generated three Myc-tagged FisB mono-cysteine variants (Myc-tagged FisB G6C, FisB L137C and FisB A245C) and tested separately whether these cysteines were intra- or extracellular. First, I determined the sporulation efficiency of these mutants using a heat kill assay to verify that the mutants are still functional. In this assay sporulation is induced by nutrient exhaustion in DSM medium [87] and the sporulation efficiency is determined after 24 – 30 h as the number of heat-resistant (80°C for 20 min) colony forming units

(CFUs) compared to wild-type heat-resistant CFUs (see section 3.2.9 in Material and Methods for details). The mutants showed a slight reduction in sporulation efficiency (Figure 5E). However, this reduction was small enough for us to assume that FisB's topology was not affected.

To test if each of the cysteines is accessible to MPB, I first lysed protoplasts of sporulating cells, solubilized membranes with detergent and subsequently pulled down FisB using a polyclonal Anti-Myc tag antibody. Biotinylation was detected by Western Blot using an HRP-conjugated-avidin antibody. Only residues 6 and 245 were accessible (Figure 5F, right panel) suggesting residue 137 may be restricted by secondary/tertiary structures and/or the membrane. In intact protoplasts only residue 245 was labeled by MPB, indicating the C-terminus faces the extracellular space (Figure 5F, middle panel). In contrast, only residue 6 was biotinylated when extracellular cysteines were blocked by 4-acetamido-4′-maleimidylstilbene-2,2′-disulfonic acid (AMS) prior to cell lysis and incubation with MPB. That is, residue 6 faces into the cytoplasm (Figure 5F, right panel). To confirm the presence of FisB, I stripped every Western Blot and probed it with anti-FisB antibody (Figure 5F, bottom row). Altogether, these results confirm a topology in which the larger C-terminus of FisB is extracellular, the N-terminus faces the cytoplasm, and residue 137 is inaccessible to biotinylation, possibly residing inside a globular domain, shielded at the oligomerization interface, or by the membrane.

We were unable to determine the structure of FisB. However, a computational model of FisB covering residues 44 to 225 (most of the extracellular domain) is available [88] and is shown in Figure 5G. The model predicts that FisB(ECD) has a curved structure which is about 8 nm long and the inner and outer radii of curvatures are ~3 nm and ~5 nm. Overall, our results confirm the prediction that FisB has a short cytoplasmic N-terminal domain, a single TMD and a larger, extracellular domain with a curved, banana-like shape.

Figure 5. Domain structure and topology of FisB.*(A)* FisB topology prediction from 10 different algorithms, and the consensus prediction by Constrained Consensus Topology Prediction Server (CCTOP, [89]). ***(B)*** Predicted domain structure of FisB. ***(C)*** Kyte-Doolittle hydropathicity profile of the FisB sequence, with a potential second TMD indicated. ***(D)*** Possible topologies of FisB. Left: a single TMD with a cytoplasmic N-terminus and extracellular C-terminus. Right: With two TMDs, both the N- and the C-termini face into the cytoplasm. Cysteine residues introduced for SCAM analysis at positions 6 or 245 are indicated. ***(E)*** Sporulation efficiencies of Myc-tagged mono-cysteine FisB variants determined by heat kill. ***(F)*** Accessibility of the cysteines at positions 6, 137, and 245 to a biotinylated, sulfhydryl-reactive compound, 3-(N-maleimidoypropionlyl) biocytin (MPB). Myc-tagged monocysteine FisB variants were produced in ΔfisB cells and reacted with MPB before or after blocking extracellular cysteines with 4-acetamido-4'-maleimidylstilbene-2,2'-disulfonic acid (AMS). FisB was pulled down using an anti-myc antibody and biotinylation was probed by western blot using an HRP-conjugated avidin antibody. Lysed cells were probed to ensure accessibility of MPB to the cysteine labels. ***(G)*** Predicted model of FisB(44-225) comprising most of the extracytoplasmic domain (ECD) of FisB [88].

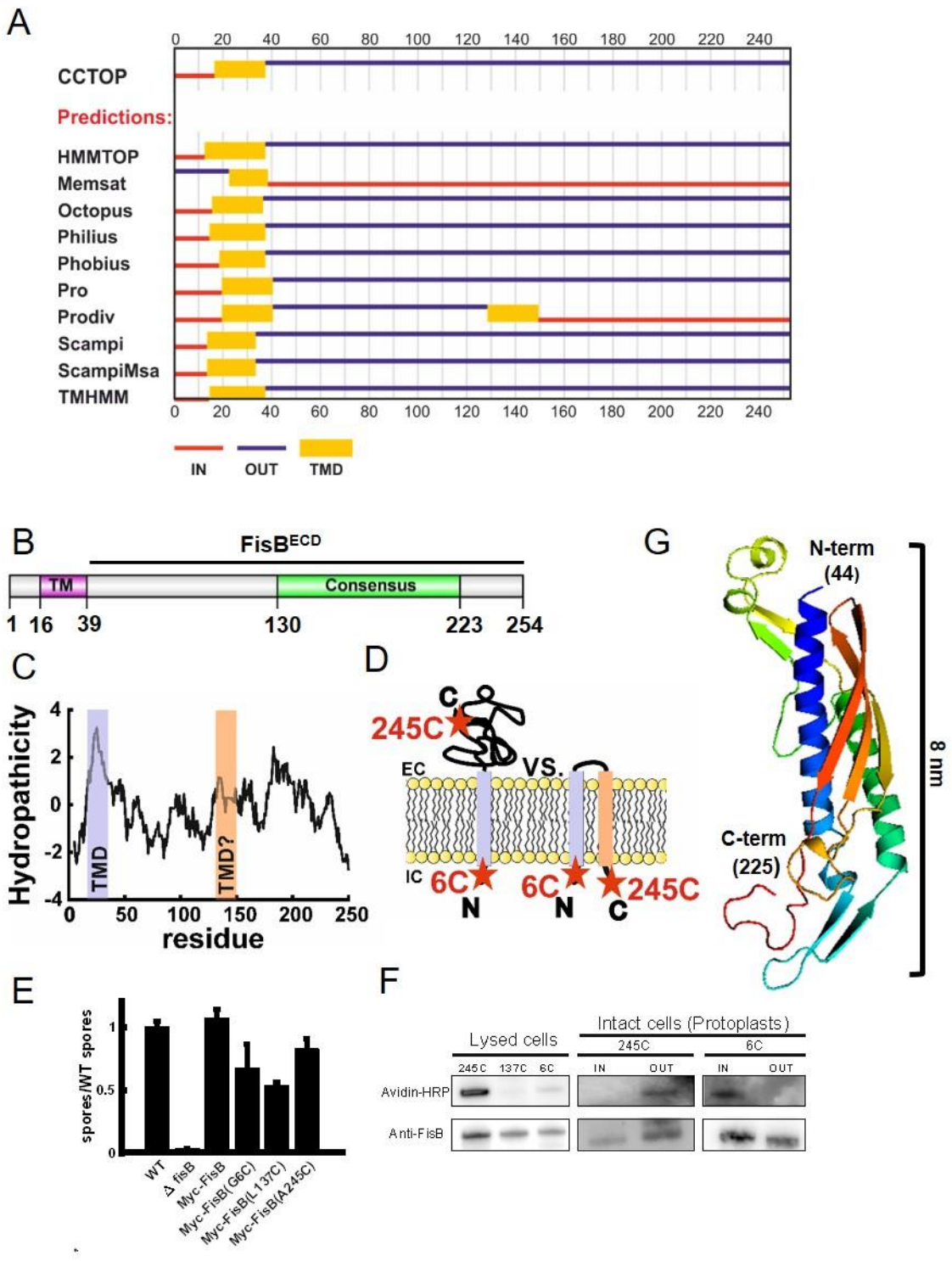

Figure 5. Domain structure and topology of FisB.

2.1.2 Membrane fission always occurs in the presence of a cluster of FisB molecules

Contribution statement: All experiments and analysis reported in this section were carried out by Ane Landajuela and are puplished [90].

After confirming the topology of FisB, we wondered if a certain number of FisB molecules need to be recruited to the fission site for membrane fission to occur.

During engulfment, FisB expressed under its native promoter and fused to a fluorescent protein (such as GFP or YFP) forms dim mobile clusters (DMC) in the engulfment membrane as well as the peripheral mother cell membrane (Figure 6B) [90]. After around 3h after inducing sporulation, most cells display an intense spot at the engulfment pole (ISEP) where fission occurs (Figure 6B). Using quantitative analysis, Ane Landajuela from our lab showed that the DMCs contain ~12 FisB molecules while at the time of fission about ~ 40 molecules have accumulated at the fission site [90]. She also monitored mGFP-FisB dynamics and membrane fission using TMA-DPH simultaneously (Figure 6B). TMA-DPH is a lipophilic dye that does not fluoresce in aqueous solution and only inefficiently crosses membranes. Prior to membrane fission, the dye has access to the engulfment, forespore and mother cell membranes, thus shows intense labeling where these membranes are adjacent to one another (Figure 6A top). After membrane fission, the dye has only direct access to the mother cell membrane and therefore labels internal membranes weakly (Figure 6A bottom). 3h after sporulation was induced, around 70% of cells have undergone fission (Figure 6D), which is similar to the percentage of cells that show an ISEP (Figure 6E). Lastly, Ane expressed FisB at about ~8 fold lower expression (Figure 6C) [38] which led to an initial delay in membrane fission and ISEP formation (Figure 6D and E). Importantly, we found a strong correlation between cells that have

undergone fission and the fraction of cells with an ISEP (Figure 6F) and conclude that membrane fission always occurs in the presence of a large immobile cluster at the fission site.

Figure 6. Membrane fission always occurs in the presence of a cluster of FisB molecules.*(A)* Detection of membrane fission. The lipophilic dye TMA-DPH does not fluoresce in the aqueous solution and crosses membranes inefficiently. Prior to membrane fission, the dye has access to the engulfment, FS and MC membranes, thus shows intense labeling where these membranes are adjacent to one another (top). After membrane fission, the dye labels internal membranes weakly (bottom). ***(B)*** Images show mGFP-FisB (strain BAM003, native expression level) at indicated times during sporulation. Membranes were visualized with TMA-DPH. Examples of sporulating cells with mGFP-FisB enriched at the septum (1.5 h), forming dim mobile cluster (DMC; 2 h) and with a discrete mGFP-FisB focus at the cell pole (intense spot at engulfment pole, ISEP, 3 h) are highlighted with white arrowheads and magnified in the insets. ***(C)*** Similar to D, but using a strain (BAL003) that expresses mGFP-FisB at ~ 8-fold lower levels in a ΔfisB background. ***(D)*** Time course of membrane fission for wild-type cells, ΔfisB cells, or ΔfisB cells complemented with mGFP-FisB expressed at native (BAM003) or low levels (BAL003). Lower expression of mGFP-FisB leads to a delay in membrane fission kinetics. ***(E)*** The percentage of cells with an intense spot at the engulfment pole (ISEP) for low and native level expression of mGFP-FisB as a function of time into sporulation. ***(F)*** Correlation between percentage of cells that have undergone fission and percentage of cells having an ISEP for all time points shown in (D) and (E). Scale bars represent 1 μm.

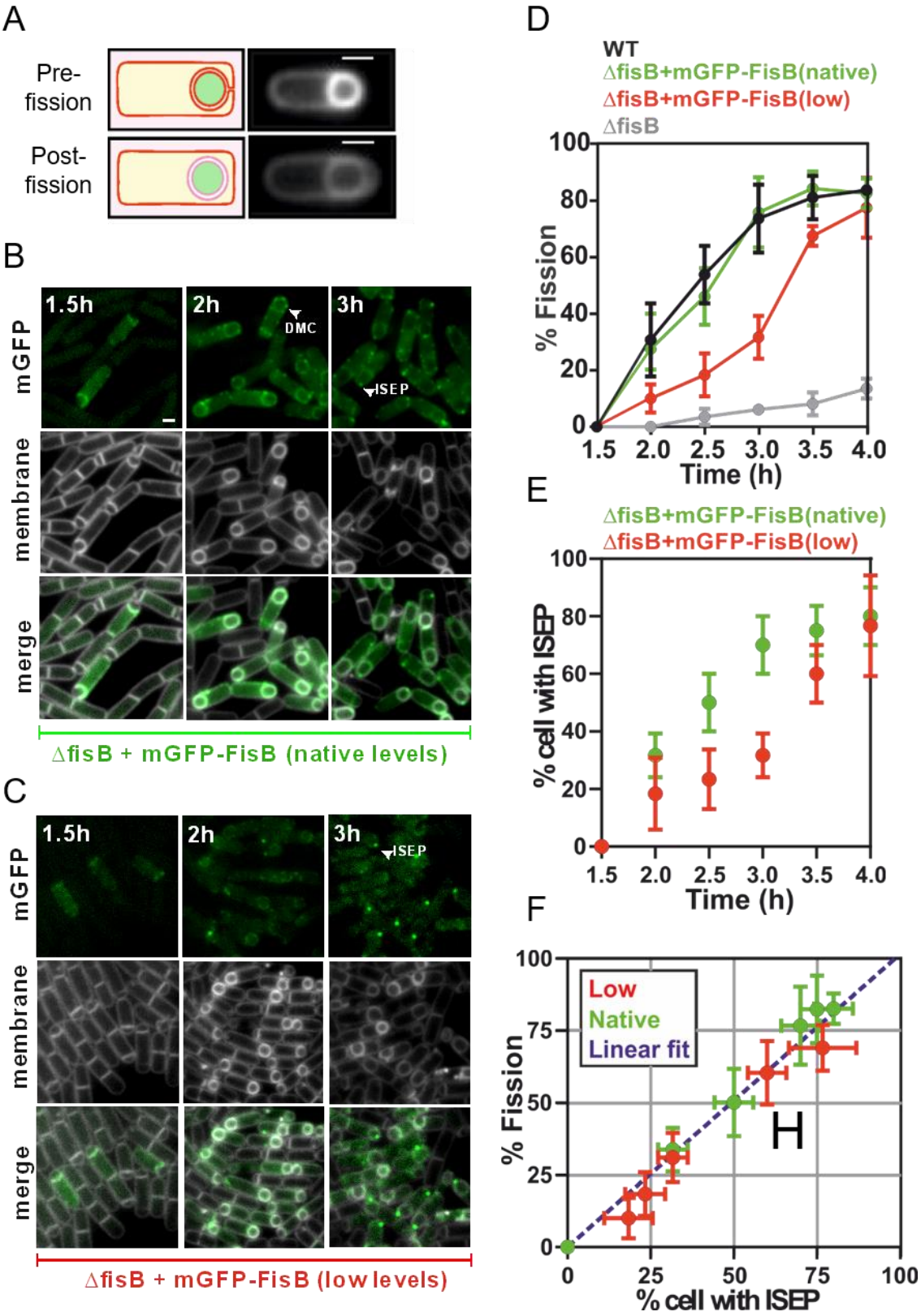

Figure 6. Membrane fission always occurs in the presence of a cluster of FisB molecules.

2.1.3 Localization of FisB is not coupled to cell wall remodeling, the protonmotive force, or the membrane potential

After determining the number of FisB molecules present in the small clusters during engulfment and in the large cluster at the time of membrane fission, we investigated how FisB is recruited to the fission site.

The sub-cellular localization and motion of many cellular components depend on the cell-wall remodeling machinery [91-93], the protonmotive force and the membrane potential [69]. *B. subtilis* is surrounded by a peptidoglycan cell wall which must be remodeled for binary fission to occur [94]. Treadmilling of FtsZ and FtsA filaments is required for this process as these filaments control the recruitment and activity of peptidoglycan synthesizing enzymes to the division site [33]. Interestingly, cell wall synthesis and degradation also drive engulfment during sporulation [95, 96]. It was suggested that cell wall remodeling might also drive membrane fission at the end of engulfment [96].

Doan et al. showed that membrane fission was reduced from 81% to 51% when cell wall synthesis was inhibited 1.5 h after induction of sporulation suggesting that cell wall remodeling alone cannot be a major driver for membrane fission [38]. However, we still wondered whether FisB dynamics could be coupled to cell wall remodeling. Since inhibition of cell wall synthesis leads to engulfment defects, we expressed mGFP-FisB from an inducible promoter during vegetative growth and investigated effects of inhibition of cell wall synthesis by the antibiotic fosfomycin on the motion of FisB clusters [97]. As a control, we chose to image GFP-Mbl in parallel experiments. Mbl is an actin homologue that controls cell wall synthesis and cell shape. Mbl forms filaments that are associated with the cell membrane and rotate around the cell circumference together with enzymes

required for cell wall synthesis [98]. Fosfomycin blocks the formation of N-acetylmuramic acid, a building block of the bacterial cell wall [99]. Upon depletion of these cell wall precursors, Mbl filaments stop moving and eventually disassemble [100].

I imaged cells expressing either mGFP-FisB or GFP-Mbl using total internal reflection fluorescence microscopy (TIRFM) (Figure 7A,C). In TIRFM, only fluorophores within ~100 nm of the glass-aqueous buffer interface are detected [101]. That is, only the spots near the substrate-proximal side a cell would be visible. Small mGFP-FisB spots, similar to the ones present during early stages of engulfment, moved around in the cell membrane seemingly randomly. By contrast, GFP-Mbl spots moved along the short axis of the cell, as previously reported [102]. To quantify these motions, we used four different approaches. First, we computed kymographs of mGFP-FisB or GFP-Mbl along the short and long axes of a cell, as indicated with blue and red lines in Figure 7A and C. Before treatment, GFP-Mbl moved around the cell circumference, reflected by stripes across the cell in the maximum intensity projections (MIP) and spots that appear and disappear in the kymographs along the long axis (marked with a red frame). Spots also appear and disappear along the short axis as GFP-Mbl spots move in and out of the evanescent field as they move along the cell circumference (kymographs marked by blue frames). Addition of fosfomycin stopped the motion of GFP-Mbl, resulting in small spots in the MIP and continuous lines in the kymographs. By contrast, mGFP-FisB MIPs and kymographs were not appreciably modified upon fosfomycin treatment. Second, we tracked individual GFP-Mbl and mGFP-FisB spots and calculated the mean-squared displacement (MSD) (Figure 7B,D). Addition of fosfomycin reduced the motility of GFP-Mbl filaments whereas the motion of mGFP-FisB was unaffected. Third, the average total distance that GFP-Mbl filaments traveled within 3 s was reduced in the presence of fosfomycin, whereas no such effect was found for the distance traveled by mGFP-FisB spots (Figure 7E). Finally, we

computed the asymmetry (see section 3.2.6 in Material and Methods for details) [103] of the individual GFP-Mbl and mGFP-FisB trajectories, and computed averages (Figure 7F). Asymmetry is a measure of the tendency for a persistently preferred direction of motion: asymmetry is zero for a perfectly symmetric trajectory, whereas it diverges for a straight-line trajectory. For simulated 2-dimensional Brownian trajectories, the asymmetry rapidly converges to ~ 0.26 for a large number of steps and/or particles [90]. Because GFP-Mbl moves on nearly linear tracks, the asymmetry of GFP-Mbl trajectories before fosfomycin treatment is high, equal to 0.58 ± 0.06 (mean ± SEM). Upon treatment, GFP-Mbl spots stop moving, and the asymmetry is reduced to 0.30 ± 0.07. By contrast, the asymmetry of mGFP-FisB trajectories before (0.22 ± 0.03) and after treatment (0.23 ± 0.06) were similar (Figure 7F). Thus, the motion of FisB clusters is independent of cell-wall synthesis.

The PMF is important for the localization of proteins that are involved in maintaining cell shape, such as MreB and Mbl, or cell division (e. g. FtsZ/FtsA) [69]. We tested if the localization of FisB depends on the PMF by imaging mGFP-FisB in the absence and presence of carbonyl cyanide m-chlorophenyl hydrazone (CCCP), a proton-ionophore that dissipates the membrane PMF. We found that the localization of GFP-FisB at T3 of sporulation is not affected by the PMF unlike the localization of Mbl (Figure 7G).

All proteins, whose localization depends on the PMF, also require an intact membrane potential. To see if the membrane potential affected FisB dynamics, we imaged mGFP-FisB in the presence and absence of valinomycin, an antibiotic that functions as a potassium carrier that depletes the transmembrane electric potential component of the PMF. We found that GFP-Mbl mislocalizes in the presence of valinomycin (Figure 7G), whereas the localization of FisB is not affected (Figure 7G).

Together, these results show that the localization of FisB is independent of cell wall remodeling, the PMF, and the membrane potential. Therefore, we continued to investigate

if the presence of lipid microdomains are important for localization of FisB and membrane fission.

Figure 7. Motion of FisB clusters is not coupled to cell wall synthesis, or pH and voltage gradients across the cell membrane.*(A)* Representative TIRFM images of cells expressing GFP-Mbl (BDR2061) before and after treatment with fosfomycin. Red and light blue lines indicate the directions along the long and short axes of the cell used to compute the kymographs on the right. Before treatment, GFP-Mbl moved around the cell circumference, reflected by stripes across the cell in the maximum intensity projections (MIP) and spots that appear and disappear in the kymographs along the long axis (marked with a red frame). Spots also appear and disappear along the short axis as GFP-Mbl spots move in and out of the evanescent field as they move along the cell circumference. Addition of fosfomycin stopped the motion of GFP-Mbl, reflected in small spots in the MIP and continuous lines in the kymographs. ***(B)*** Mean-squared displacement (MSD) as a function of lag time for GFP-Mbl before (24 tracks) and after (20 tracks) fosfomycin treatment. Colored lines connect averaged points, whereas gray areas represent standard deviation and error bars represent the standard error of the mean (SEM). Movies were acquired at 1 frame/s. The short-time diffusion coefficient, estimated from a parabolic fit to the MSD, was $D_{Mbl} = 505\, nm^2/s$ (95% confidence interval CI=439-571 nm^2/s) and $D_{Mbl}^{fos} = 112\, nm^2/s$ (CI=79-146 nm^2/s) before and after fosfomycin treatment, respectively. ***(C)*** Similar to (A) but cells express mGFP-FisB (BMB014). Motion of GFP-FisB was not affected by addition of fosfomycin. ***(D)*** MSD as a function of lag time for GFP-FisB before (18 tracks) and after (12 tracks) fosfomycin treatment. Acquisition rate was 1 frame/s. The short-time diffusion coefficient was $D_{FisB} = 6270\, nm^2/s$ (95% confidence interval CI=5810-6740 nm^2/s) and $D_{FisB}^{fos} = 6370\, nm^2/s$ (CI=5580-7160 nm^2/s) before and after fosfomycin treatment, respectively. ***(E)*** Average total distance traveled by GFP-Mbl and mGFP-FisB spots over 3 s in the presence and absence of fosfomycin. GFP-Mbl (20 tracks), GFP-Mbl + fosfomycin (24 tracks), mGFP-FisB(18 tracks) and mGFP-FisB + fosfomycin (12 tracks). Fosfomycin decreased the total distance traveled by Mbl filaments ($p = 0.024$, Student's t-test), whereas FisB was not affected ($p = 0.433$). ***(F)*** Average asymmetry of the GFP-Mbl and mGFP-FisB trajectories. Upon treatment with fosfomycin, GFP-Mbl filaments stop moving, which is reflected as a decrease in asymmetry ($p = 0.0044$), whereas mGFP-FisB's motion is unaffected ($p = 0.8655$). ***(G)*** Localization of GFP-Mbl (BDR2061) during vegetative growth and mGFP-FisB (BAM003) at 3h into sporulation in the presence or absence of 100 μM CCCP or 30 μM valinomycin. GFP-Mbl mislocalizes in the presence of either drug, whereas the localization of mGFP-FisB is unaffected. Scale bar is 3 μm.

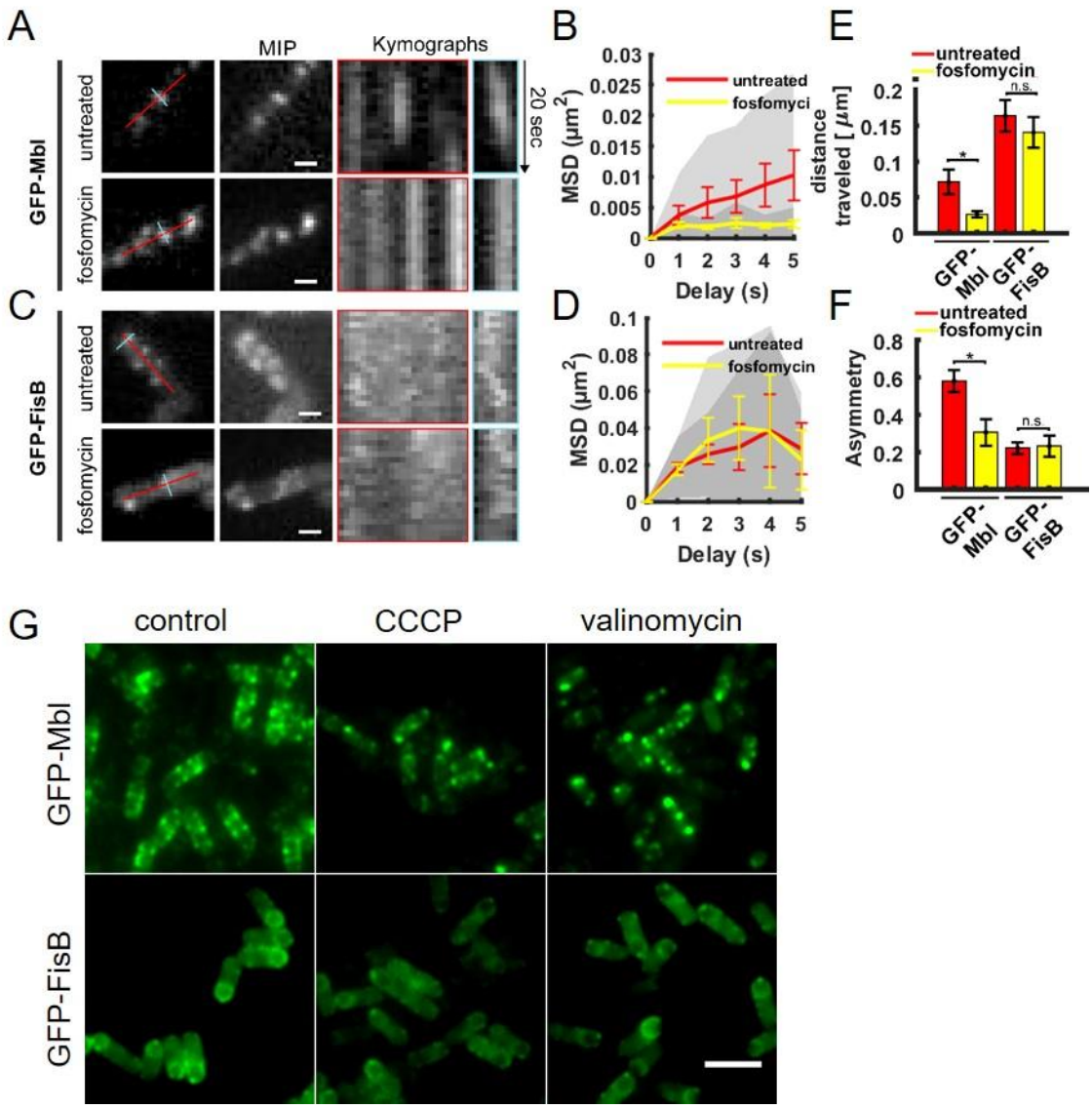

Figure 7. Motion of FisB clusters is not coupled to cell wall synthesis, or pH and voltage gradients across the cell membrane.

2.1.4 FisB localization and membrane fission are independent of cardiolipin, phosphatidylethanolamine and flotillins

Contribution statement: All experiments and analysis reported in this section, except the one involving zaragozic acid, were carried out by Ane Landajuela.

It was previously reported that FisB(ECD) specifically interacts with lipid bilayers containing the phospholipid cardiolipin (CL) [38]. CL has been implicated in membrane fusion and fission reactions [7], its levels rise during sporulation and it is enriched in the forespore membrane as well as the engulfing membrane [58, 82, 104]. Additionally, CL has been shown to serve as a landmark for recruiting proteins [65] and is involved in membrane fission and fusion of mitochondria [72]. Therefore, we tested the possibility that FisB - CL interactions could be important for localization of FisB to the fission site as well as membrane fission.

To test this hypothesis, we used strain BAM234 in which all known genes for CL synthases (Figure 8A) (*ywnE (clsA)*, *ywjE (clsB)* and *ywiE (clsC))* were deleted [105]. First, we verified the absence of CL in this strain. Wild type (PY79) and *ΔclsABC* cells were induced to sporulate by resuspension. Briefly, an overnight culture was diluted in fresh medium and grown until it reached mid-log phase. The culture was then harvested by centrifugation and resuspended in nutrient poor resuspension medium. This is the beginning of sporulation (see section 3.2.3 in Material and Methods). 3h after sporulation was induced (T3 of sporulation) lipids were extracted and analyzed by thin layer chromatography (TLC). While CL is readily detectable in wild type cells, no CL was observed in the CL synthase deficient (*ΔclsABC)* strain (Figure 8B). During vegetative growth, wild type and CL deficient cells show the same double time, but cells lacking CL are strongly reduced in their ability to produce heat-resistant spores (Figure 8C) which is

consistent with previous reports [82].

A reduction of sporulation efficiency determined using the heat kill assay could be due to a defect at one or several steps during spore formation or germination. We continued to determine if membrane fission is impaired in the absence of detectable CL using the TMA-DPH assay (Figure 8D). TMA-DPH is a lipophilic dye that does not fluoresce in aqueous solution and only inefficiently crosses membranes. Prior to membrane fission, the dye has access to the engulfment, FS and MC membranes, thus shows intense labeling where these membranes are adjacent to one another (Figure 8D, top). After membrane fission, the dye labels internal membranes weakly (Figure 8D, bottom).

We found that the membrane fission time course of *ΔclsABC* is indistinguishable from wild type cells (Figure 8E). This result suggests that the reduction in sporulation efficiency is a result of a defect downstream of membrane fission. This is in line with previous research suggesting that CL plays a role in spore germination [82].

Moreover, the dynamics and localization of mYFP-FisB at T3 of sporulation is similar in a wild type (BAL002) or *ΔclsABC* background (BAL006) (Figure 8H). The fraction of cells that had an intense spot at the engulfment pole (ISEP), and the intensity of the ISEP, which reflects the number of FisB molecules recruited to the membrane fission site, were indistinguishable for wild-type and *ΔclsABC* cells (Figure 8I and J). Therefore, we conclude that CL is not required for the subcellular localization of FisB or membrane fission.

Another lipid implicated in membrane fission or fusion is phosphatidylethanolamine (PE) [106, 107]. Like CL, PE is a cone-shaped phospholipid with the tendency to form non-bilayer structures [106, 107]. Furthermore, it has been shown to accumulate in the membranes of the asymmetric division septum during sporulation and in the engulfing membranes as well as the spore membrane [108].

We generated cells lacking PE (strain BAL007) by deleting the gene pssA which encodes a phosphatidylserine (PS) synthase. The PS synthase mediates the first step in synthesizing PE (Figure 8A). We again used TLC to confirm the absence of PE (Figure 8B). Sporulation efficiency as well as the time course of membrane fission in cells lacking PE was indistinguishable from wild type cells (Figure 8C and E), suggesting that PE does not play a significant role in membrane fission.

PE and CL microdomains localize to the same subcellular regions and are both implicated in membrane fusion and fission. To exclude the possibility that CL and PE might be able to compensate for each other we created a quadruple mutant that lacks all CL synthase genes as well as pssA (BAL005). The membranes of BAL005 consist mostly of phosphatidylglycerol (PG) (Figure 8B). Interestingly, the quadruple mutant also underwent fission with indistinguishable kinetics compared to wild type (Figure 8E). Thus, two lipids with negative spontaneous curvature and implicated in membrane fusion and fission reactions, have no significant role in FisB mediated membrane fission during sporulation.

Besides CL and PE microdomains, bacteria organize many signal transduction cascades and protein-protein interactions into functional membrane domains (FMMs) similar to lipid rafts in eukaryotic cells [50]. In *B. subtilis* these FMMs are enriched in polyisoprenoid lipids as well as two different flotillin-like proteins, FloT and FlotA. These proteins form mobile foci in the membrane and recruit other FMM-associated proteins to facilitate their interaction and oligomerization [52, 53]. We observed that *ΔfloA* (BAL035), but not *ΔfloT* (BAL036), cells are impaired in sporulation as assayed by heat-resistant colony forming units (Figure 8C). However, when we monitored engulfment and membrane fission during sporulation, we found engulfment proceeded normally (Figure 8E and F) and that *ΔfloA* cells underwent fission at the same rate as wild type cells (Figure

8E). Thus, the sporulation defect in *ΔfloA* cells lies downstream of engulfment and membrane fission. This was confirmed by blocking formation of FMMs through inhibition of the squalene synthase during sporulation by addition of 50 μM zaragozic acid [51] to the sporulation medium. No effect on the localization of mGPF-FisB at T3 of sporulation was observed (Figure 8G).

Altogether, our results suggest that FisB-mediated membrane fission at the end of engulfment during sporulation does not depend on the negative-curvature lipids CL, PE, or FloA/T-dependent lipid domains.

While the presence of CL did not affect FisB localization and membrane fission, binding of FisB to a negatively charged lipid other than CL might still be important for FisB mediated membrane fission. Therefore, we further investigated the interaction of FisB(ECD) with negatively charged phospholipid *in vitro.*

Figure 8. Membrane fission is insensitive to membrane lipid composition. (*A)* Pathways for membrane lipid synthesis in *B. subtilis*. Lipid synthetases responsible for each step are highlighted in blue. **(*B)*** Thin-layer chromatography (TLC) of the total lipid extracts of wild-type and indicated lipid synthesis-deficient cells. Phospholipid spots (PLs) were visualized by staining with Molybdenum Blue spray reagent. Purified CL, PG, and PE were used as standards to identify the PLs of *B. subtilis*. Arrows indicate locations to which individual standards migrate. **(*C)*** Sporulation efficiency (% of WT) for each indicated strain. Means ± SD for four replicates per condition. **(*D)*** Detection of membrane fission. The lipophilic dye TMA-DPH does not fluoresce in the aqueous solution and crosses membranes slowly. Prior to membrane fission, the dye has access to the engulfment, FS and MC membranes, thus shows intense labeling where these membranes are adjacent to one another (top row). After membrane fission, the dye has only direct access to the mother cell membrane and therefore labels internal membranes poorly (bottom row). **(*E)*** Percentage of cells from indicated strains that have undergone membrane fission as a function of time after initiation of sporulation. **(*F)*** Membranes from cells of the indicated genetic backgrounds were visualized with TMA-DPH at t=3h. Cells were mounted on agarose pads containing sporulation medium. Bar,1 μm. **(*G)*** Images of mGFP-FisB (strain BAM003) at T3 after treatment with the squalene-synthase inhibitor zaragozic acid. **(*H)*** Images show cells expressing mYFP-FisB (low expression levels) in either a wild type (BAL002) or in a CL deficient background strain (BAL006) at T3. Membranes were visualized with the fluorescent dye TMA-DPH. Examples of sporulating cells with a discrete mYFP-FisB focus at the cell pole are highlighted (white arrows). Foci were semi-automatically selected with SpeckletrackerJ *[109]*. ***(I)*** the percentage of cells with an ISEP for wild-type (BAL002) or cardiolipin-deficient (BAL006) mYFP-FisB expressing cells at T3 (low expression). **(*J)*** Distributions of total fluorescence intensities (sum of pixel values) at ISEP for wild-type (BAL002) or cardiolipin-deficient (BAL006) mYFP-FisB cells at 3h into sporulation.

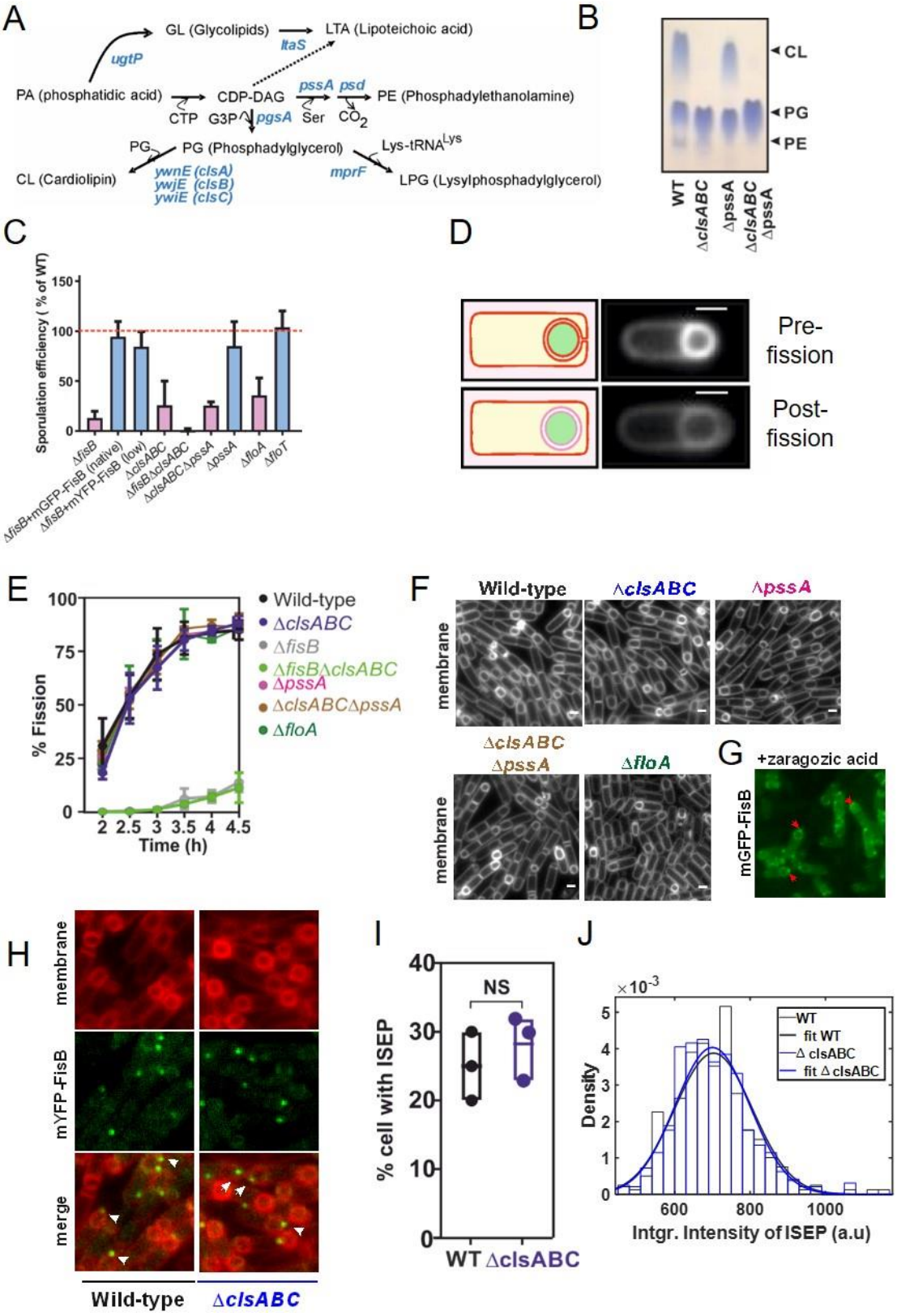

Figure 8. Membrane fission is insensitive to membrane lipid composition.

2.1.5 FisB binds to acidic lipids

While our results suggest that FisB-mediated membrane fission does not depend on the negative-curvature lipids CL, PE, or FloA/T-dependent lipid domains, lipid binding itself might still be important. For many CL binding proteins, it has been described that PG, the substrate for cardiolipin synthases (Figure 8A), may substitute as a binding partner in the absence of CL [110, 111]. Since the absence of CL did not affect localization of FisB or membrane fission, we wondered if PG could substitute for CL's function in its absence. Because removing PG from *B. subtilis* membranes, by knocking out the gene for PG synthesis (pgsA), is lethal [112], we characterized binding of FisB(ECD) to negatively charged lipids *in vitro.* To this end, I probed the interaction of FisB(ECD) with liposomes containing various acidic lipids using the co-flotation assay shown in Figure 9B.

Purified recombinant FisB(ECD) (200 pmol) was incubated with liposomes (40 nmol) in a total volume of 100 µl for 1 hour at room temperature and subsequently layered at the bottom of an iodixanol discontinuous density gradient. Upon equilibrium ultracentrifugation, the lighter liposomes float up to the interface between the two lowest density layers together with bound protein, while unbound protein remains at the bottom. I collected fractions as indicated in Figure 9B and determined the percentage of protein co-floated with liposomes using SDS-PAGE and densitometry, as shown in Figure 9C. We first determined that binding of FisB(ECD) to liposomes containing 45% CL was not dependent on pH or Ca^{2+} (Figure 9D and E). By contrast, the fraction of liposome-bound protein decreased rapidly as the ionic strength increased (Figure 9F). These results indicate that binding of FisB(ECD) to acidic lipids is mainly mediated by electrostatic interactions.

CL carries two negative charges, whereas PG and phosphatidylserine (PS), a lipid not normally found in *B. subtilis* [113], carry only a single negative charge. If binding is

mediated mainly by electrostatic interactions and no specific affinity for one lipid species or another is present, we reasoned that liposomes carrying PG or PS at two times the mole fraction of CL should bind the same amount of FisB(ECD), since the surface charge density would be the same. Indeed, similar amounts of FisB(ECD) were bound to liposomes carrying 30% CL, 60% PG, or 60% PS (Figure 9G). FisB(ECD) did not bind neutral phosphatidylcholine PC liposomes [38].

To quantify the affinity of FisB(ECD) for CL and PG, I titrated liposomes containing either 45 mole % CL or PG and measured binding of 100 nM FisB(ECD) (Figure 9H). In these experiments, I used iFluor555 labeled FisB(ECD) (iFluor555-FisB(ECD)) and detected liposome-bound protein using fluorescence rather than densitometry of SYPRO-stained gels, which extended sensitivity to much lower protein concentrations. The resulting titration curves were fit to $f_b = K[L]/(1 + K[L])$, where f_b is the bound fraction of protein, $[L]$ is the total lipid concentration (assumed to be $\gg$ [protein bound]), and $K = 1/K_d$ the apparent association constant while K_d is the apparent dissociation constant [114]. Best fit values for K_d were 1.0 μM for CL (95% confidence interval CI=0.7-2.1 μM) and 3.6 μM for PG, respectively (CI=2.8-5.0, Figure 9I). Together, these results suggest that while FisB(ECD) has higher affinity for CL than for PG, the higher affinity likely results from the higher charge carried by CL. FisB does not bind CL with any specificity; at the same surface charge density, FisB(ECD) binds PG, or even PS which is not present *B. subtilis* membranes, with similar affinity. Thus, *in vivo* FisB is likely to bind CL as well as PG which constitutes up to 50% of the bacterial membrane [115]. We investigated if this interaction is important for localization of FisB to the fission site by creating lipid binding mutants (see section 2.1.10).

Figure 9. FisB(ECD) binds acidic lipids via electrostatic interactions. (*A)* Domain structure of FisB and its His_6-tagged extracytoplasmic domain (ECD) used in floatation experiments. ***(B)*** Schematic of the floatation assay. Liposomes (40 nmol total lipid) and FisB ECD (200 pmol) were incubated for 1 hour at room temperature and layered at the bottom of an iodixanol density gradient. Upon ultracentrifugation, liposomes float to the top interface, whereas unbound protein remains at the bottom. Four fractions were collected as indicated and analyzed by SDS-PAGE. ***(C)*** SYPRO orange stained gel of FisB(ECD) incubated with liposomes containing 45 mole % CL. The percentage of recovered protein is determined by comparing the intensity of the band in fraction B to the input band intensity. ***(D-F)*** FisB(ECD) binding to liposomes is independent of calcium or pH, but decreases rapidly with increasing ionic strength. ***(G)*** Indistinguishable amounts of FisB(ECD) are recovered when FisB(ECD) is incubated with liposomes containing different acidic lipid species if the charge density is similar. CL30, PG60, PS60 indicate liposomes containing 30 mole % CL, 60 mole % PG and 60 mole % PS, respectively. CL carries 2 negative charges, whereas PG and PS carry one each. The rest of the liposome composition is eggPC. ***(H)*** Fraction of liposome-bound iFluor555-labeled FisB(ECD) (iFluor555-FisB(ECD)) recovered after floatation as a function of lipid concentration. Titration curves were fit to $\boldsymbol{f_b = K[L]/(1 + K[L])}$, where $\boldsymbol{f_b}$ is the bound fraction of protein, $[\boldsymbol{L}]$ is the total lipid concentration (assumed to be $\gg$ [protein bound]), and $\boldsymbol{K = 1/K_d}$ the apparent association constant, and $\boldsymbol{K_d}$ is the apparent dissociation constant. ***(I)*** Best fit values for $\boldsymbol{K_d}$ were 1.0 μM for CL (95% confidence interval, CI=0.7-2.1 μM) and 3.6 μM for PG (CI=2.8-5.0 μM), respectively. 100 nM iFluor555-FisB(ECD) was incubated with10^{-8} to 10^{-4} M lipids for 1 h at room temperature before floatation. Liposomes contained 45 mole % of CL or PG and 55% PC.

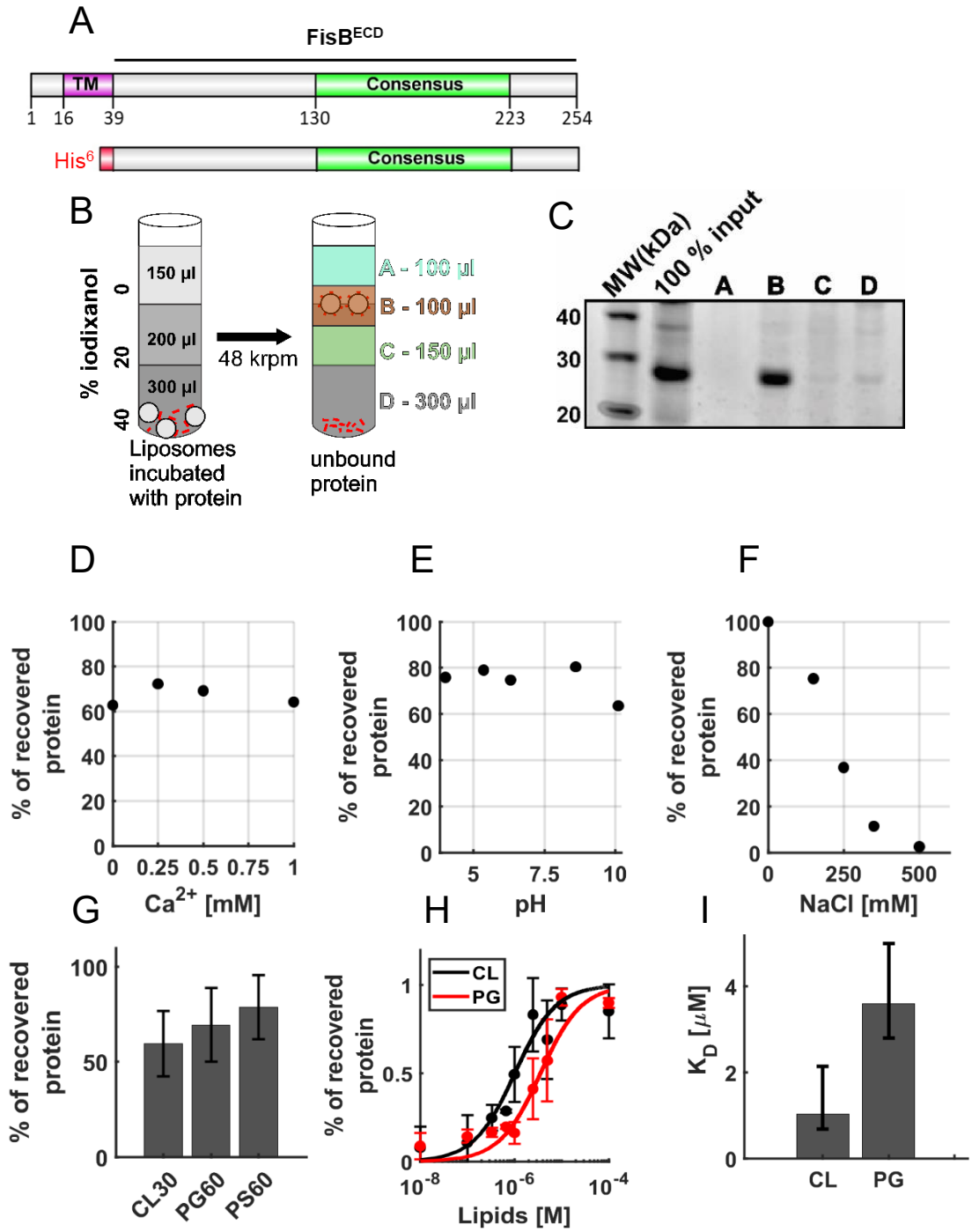

Figure 9. FisB(ECD) binds acidic lipids via electrostatic interactions.

2.1.6 FisB$^{173-220}$ binds acidic lipids

We aimed to determine the region of FisB that is responsible for binding to negatively charged lipids. To this end, I expressed and purified peptides (as indicated as P1 – P4 in Figure 10A) corresponding to different regions of FisB(ECD) and tested for binding to CL – containing liposomes in the co-floatation assay.

I first purified P1 (16 kDa) and P2 (9.5 kDa) from *E. coli* using a hexa-histidine tag. The purification of P2 showed a ladder pattern (Figure 10D, 100% input lane). We assume these correspond to different oligomeric states of P2 due to its high hydrophobicity. While I did not observe any binding to liposomes containing 45% CL for P1 (no band visible in fraction B in (Figure 10C), I saw some binding for P2 (Figure 10D). Interestingly binding occurs mainly as a dimer. We continued by testing 2 more peptides (P3 and P4). Only the more hydrophobic P3 bound to the liposomes (Figure 10B,E) and again showed bands corresponding to different oligomeric states. While P3 corresponding to FisB(173-220) spans the most hydrophobic region of the protein besides the transmembrane domain, binding to liposomes was still mediated by electrostatic interactions, as P3 did not bind to neutral liposomes containing 100% eggPC (Figure 10F).

Altogether, these results indicate that lipid binding is mediated by positively charged residues within or close to the most hydrophobic part of the protein which also corresponds to the most conserved region (consensus region) suggesting that lipid binding might be important for FisB's function and conserved among different FisB homologs.

2.1.7 The extracellular domain of *C. islandicus* FisB binds to acidic lipids

To test if binding to negatively charged lipids is a conserved property, I expressed the ECD of the FisB homolog of *C. islandicus* in *E. coli* ($FisB^{Cisl}$(ECD)), purified the protein using a hexa-histidine tag and tested for binding to negatively charged lipids in the co-floatation assay (Figure 10G). Similar to $FisB^{Bsubti}$(ECD), $FisB^{Cisl}$(ECD) also efficiently bound liposomes containing 45% CL supporting the idea, that lipid binding is important for FisB's function.

In addition to lipid binding, another property of FisB seems to be self-oligomerization, as FisB forms clusters of various sizes throughout sporulation. We investigated the physiological role of FisB self-oligomerization in the following sections.

Figure 10. The most hydrophobic region of FisB(ECD) binds to liposomes containing acidic lipids. ***(A)*** Domain structure of FisB with indicated peptides (P1 to P4) tested for binding to CL containing SUVs in the flotation assay. ***(B)*** Kyte-Doolittle hydropathicity plot. Blue shade indicates the transmembrane domain (TMD) and green shade indicates Peptide 3 (P3), corresponding to the most hydrophobic region within FisB(ECD). ***(C-E)*** Flotation results of P1-P4. Fractions were collected as indicated in Figure 9B. Only P2 and P3 show a band in fraction B, indicating that the peptide binds to liposomes containing acidic lipids. ***(F)*** P3 only binds to liposomes containing 45% CL and not to neutral liposomes consisting of 100% eggPC. ***(G)*** Binding to acidic lipids is conserved among FisB homologs. The ECD of *C. islandicus* FisB also binds to liposomes containing acidic lipids.

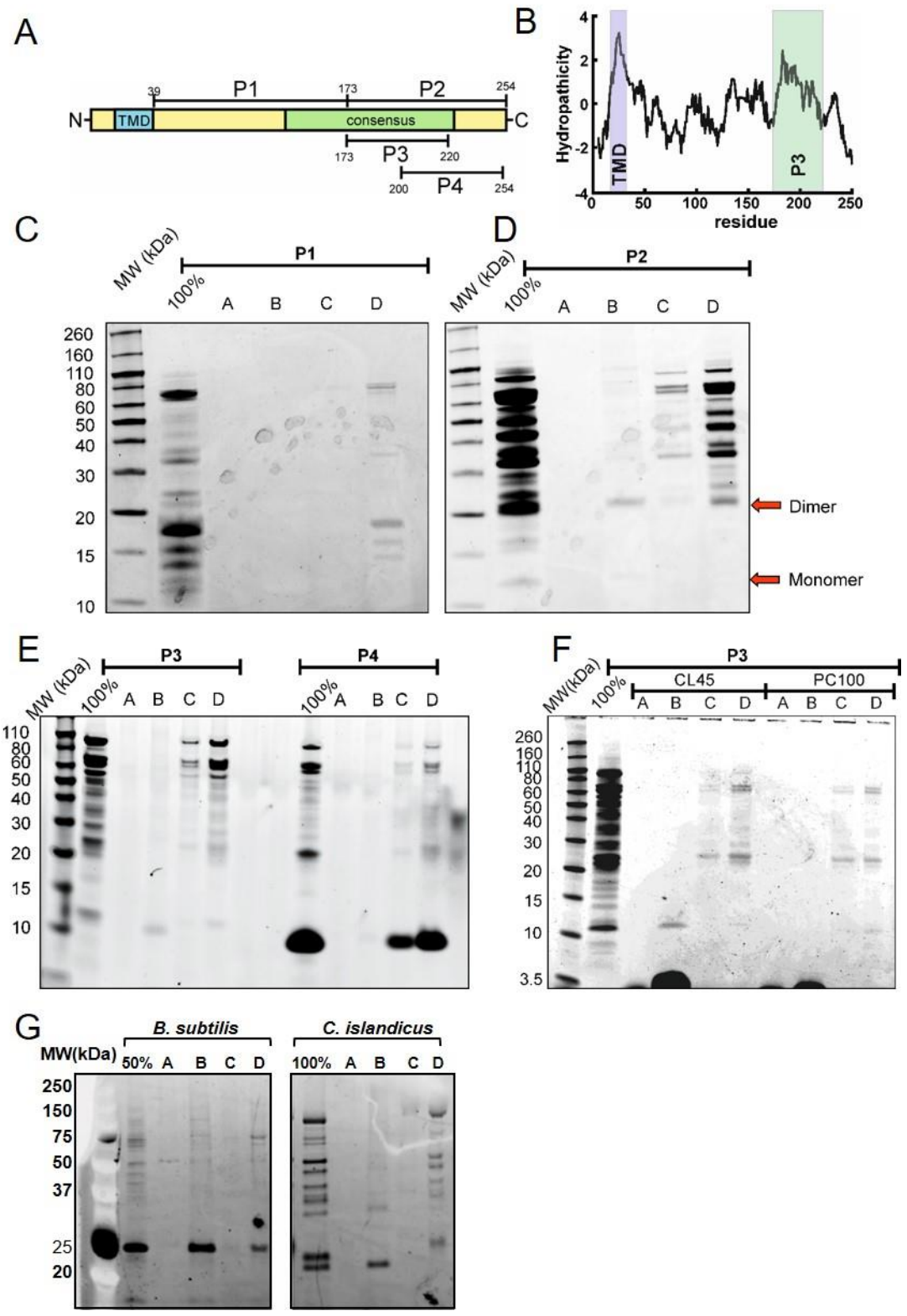

Figure 10. The most hydrophobic region of FisB(ECD) binds to liposomes containing acidic lipids.

2.1.8 Purified FisB(ECD) forms soluble oligomers

Contribution statement: The protein purification shown in Figure 11A was carried out by me. Size exclusion chromatography, the corresponding SDS Page gel and electron microscopy were carried out by Ane Landajuela in collaboration with Florian Horenkamp (laboratory of Karin Reinisch).

Pull-down of GFP-FisB from sporulating cells using an anti-GFP antibody and mass spectroscopy failed to identify proteins interacting with FisB other than itself [38]. However, during sporulation, FisB fused to a fluorescent protein forms clusters of various size (see section 2.1.2). Therefore, we reasoned that FisB self-oligomerization might be important for FisB's function and characterized FisB's tendency to oligomerize *in vitro.* We purified FisB(ECD) from *E. coli* using a hexa-histidine tag to homogeneity by affinity chromatography. Samples analyzed by SDS-PAGE show multiple bands corresponding to different oligomeric states (Figure 11A, blue bracket).

Size-exclusion chromatography (SEC) of the purified protein showed mainly high molecular weight complexes, that eluted over a wide range of sizes (Figure 11B,C). Lower molecular weight peaks were only minor components with the peak at ~ 18 ml (24kDa) corresponding to monomeric FisB(ECD). Additionally, the peak at ~15 ml (~400kDa) could potentially be FisB co-eluting with the chaperone GroEL, a common contaminant in recombinant proteins purified from *E. coli* (Figure 11B,C) [116]. The high molecular weight peaks collected from the initial chromatogram did not show a redistribution when re-analyzed (Figure 11B, bottom), suggesting that once formed, the oligomeric structures are stable for an hour or longer.

Using negative stain electron microscopy, we found that the high molecular-weight SEC fractions (peaks 1 and 2) form fairly homogenous rod-like structures approximately

50 nm long and ~10 nm wide. However, these structures showed conformational flexibility, precluding structural analysis using cryoEM (and likely hampered our attempts to crystallize FisB(ECD)). We estimate every rod-like oligomer can accommodate ~40 copies of the predicted structure of $FisB^{44-225}$ shown in Figure 5G, similar to the number of FisB molecules recruited to the membrane fission site in cells [90].

Next, we investigated if FisB self-oligomerization is important for FisB localization and membrane fission by analyzing a mutant impaired in oligomerization *in vitro* and *in vivo* (sections 2.1.9 and 2.1.11).

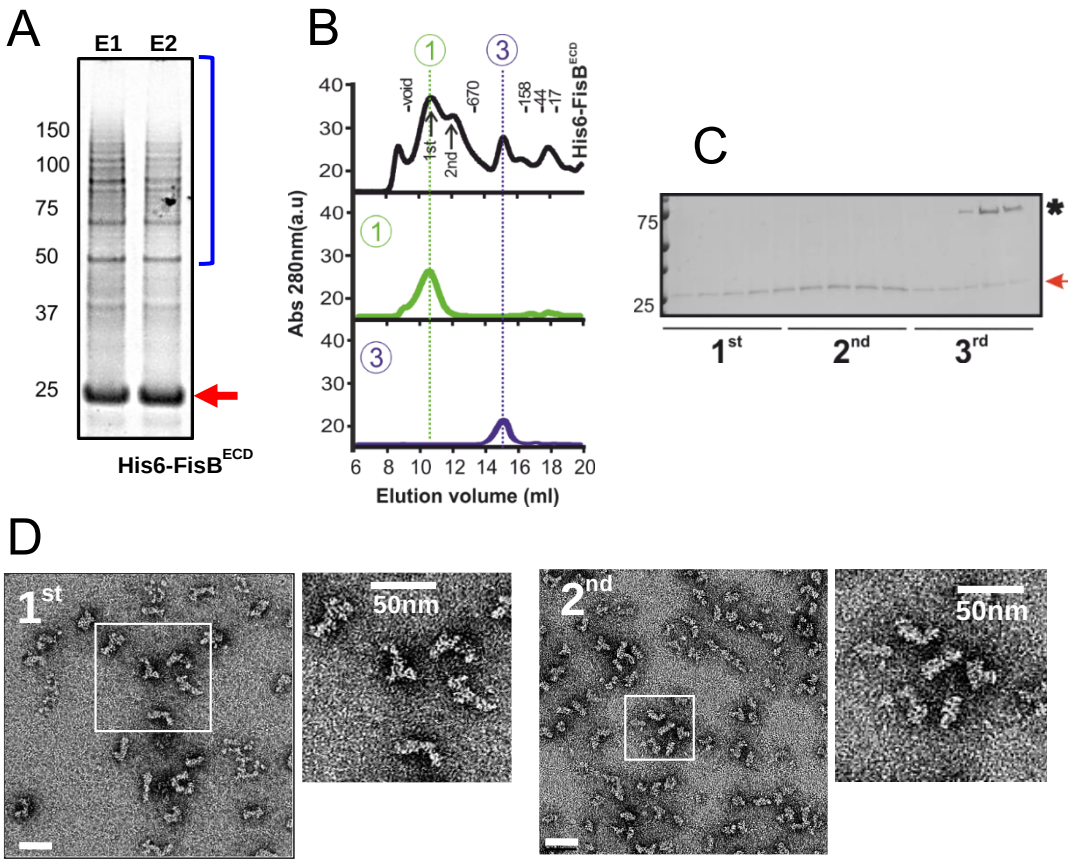

Figure 11. His6-FisB(ECD) forms soluble aggregates *in vitro*. *(A)* Second and third elution fractions from the affinity column were analyzed by SDS-PAGE and stained with SYPRO™ Orange. The red arrow indicates the monomeric form of His6-FisB (23 kDa) and the blue bracket highlights SDS-resistant His_6-FisB multimers. ***(B)*** Gel filtration elution profile of His6-$FisB^{ECD}$ in Superose 6 Increase 10/300 GL column (top). Two fractions comprising the indicated peaks were re-injected in the same column under the same conditions and eluted at the same volume as in the original sample. Elution volumes of molecular weight markers are indicated. ***(C)*** Peaks labeled 1-3 in (C) were analyzed by Coomassie Blue-stained SDS-PAGE. Molecular weight markers are indicated on the left (in kDa). The band that corresponds to His_6-$FisB^{ECD}$ is indicated with a red arrow. The black asterisk indicates a chaperone that co-elutes with monomeric His_6-FisB(ECD). ***(D)*** Representative electron micrographs of fractions comprising the 1st and 2nd peaks from C. Scale bar is 50 nm.

2.1.9 FisB^{G175A,I176S,I195T,I196S} (FisB^{GIII}) is selectively impaired in self-oligomerization

Contribution statement: In this section, protein purification for Western Blot analysis, size exclusion chromatography and electron microscopy were carried out by Ane Landajuela in collaboration with Florian Horenkamp (laboratory of Karin Reinisch). Determination of binding constants by floatation was carried out by me.

FisB forms dim, mobile clusters (DMC) during engulfment [90]. When engulfment is complete, an intense, immobile mGFP-FisB spot at the engulfment pole (ISEP) is formed. Additionally, recombinant FisB(ECD) forms soluble aggregates that bind negatively charged lipids yet changing the lipid composition of the membrane did not influence FisB targeting or membrane fission (see section 2.1.4). Therefore, we wondered whether self-oligomerization and lipid-binding are important for FisB's function and generated mutants that are selectively deficient in one or the other, characterized aggregation and lipid-binding of purified mutant proteins, and tested the phenotypes of these mutations in *vivo* (section 2.1.11).

We speculated that self-oligomerization of FisB may be at least partially mediated by hydrophobic interactions. Our collaborator Thierry Doan created a mutant, FisB(G175A,I176S,I195T,I196S) (referred to FisB^{GIII} from here on) in which conserved residues in a highly hydrophobic patch were mutated (Figure 12A,B and C). Since these residues can be found on the surface of the predicted structure (Figure 5G), they are not expected to interfere with protein folding.

Western Blot analysis of *E. coli* expressing His_6-FisB^{GIII} (ECD) revealed a reduction of high oligomeric weight complexes (Figure 12D). Additionally, when purified recombinant FisB^{GIII}(ECD) is analyzed by SEC, we found that the mutant also displayed less high

molecular weight complexes (Figure 12E). Though much reduced in amplitude, a broad, high molecular weight peak was still present in size exclusion chromatograms. Negative-stain EM analysis of this fraction revealed oligomerization with less defined size and structure compared to wild type FisB(ECD) (Figure 12G).

We used the co-floatation assay shown in Figure 12H to determine whether these mutations affected lipid binding and determined the apparent dissociation coefficients as described above (section 2.1.5). Despite being impaired in self-oligomerization, FisB^{GIII}(ECD) has lipid binding properties similar to wild-type with a dissociation constant $K_d^{GIII} = 1.6$ μM (95% confidence interval CI=0.9-5.1 μM), which is indistinguishable from that of wild type FisB(ECD) ($K_d^{wt} = 1.0\ \mu\mathrm{M}, \mathrm{CI} = 0.7 - 2.1\ \mu\mathrm{M}$, Figure 12I and J).

Next, we identified a mutant that is impaired in lipid binding, but not impaired in self-oligomerization and finally investigated the effect of these mutants on FisB localization and membrane fission.

Figure 12. FisB mutants selectively impaired in oligomerization and membrane binding. ***(A)*** Mutated residues indicated on the FisB domain structure. ***(B)*** Kyte-Doolittle hydrophobicity profile of the FisB sequence for wild-type (WT), FisB(K168D,K170E) ($FisB^{KK}$), and FisB(G175A,I176S, I195T, I196S) ($FisB^{GIII}$) mutants. ***(C)*** Mutations shown on the predicted model of FisB(44-225) [88]. Residue conservation (top) and electrostatic potential (bottom) are mapped onto the structure. ***(D)*** Western Blot of cell lysates from *E. coli* cells expressing FisB(ECD) WT, $FisB^{GIII}$(ECD), or $FisB^{KK}$(ECD), probed with an anti-histidine antibody. High molecular weight bands in the WT and KK lanes are largely absent in the GIII lane, indicating FisBGIII is less prone to forming oligomers. ***(E)*** Size-exclusion chromatography of FisB(ECD) WT and the $FisB^{GIII}$(ECD). The GIII mutant profile shows a lot less high molecular weight complexes compared to WT. ***(F)*** A fraction corresponding to the high-molecular peak in *(E)* (indicated by *) for FisB(ECD) WT was collected and imaged using negative-stain electron microscopy (EM), which revealed flexible, elongated structures of ~50 nm × 10 nm. ***(G)***. A similar analysis for $FisB^{GIII}$(ECD) revealed more heterogeneous and less stable structures. Scale bars in F, G are 50 nm. ***(H)*** Schematic of the flotation experiments to determine the apparent affinity of FisB(ECD) mutants for liposomes containing acidic lipids. iFluor555-FisB(ECD) (100 nM) was incubated with 10^{-8} to 10^{-4} M lipids for 1 h at room temperature before floatation. Liposomes contained 45 mole % of CL and 55% PC. ***(I)*** Fraction of protein bound to liposomes as a function of total lipid concentration. Data was fitted to a model as in Figure 9H. The data and fit for FisB(ECD) WT is copied from Figure 9H for comparison. ***(J)*** Best fit values for K_d were 1.0 μM for WT (95% confidence interval, CI=0.7-2.1 μM), 9.1 μM for KK (CI=6.5-15.3 μM), and 1.6 for GIII (CI=0.9-5.1 μM), respectively.

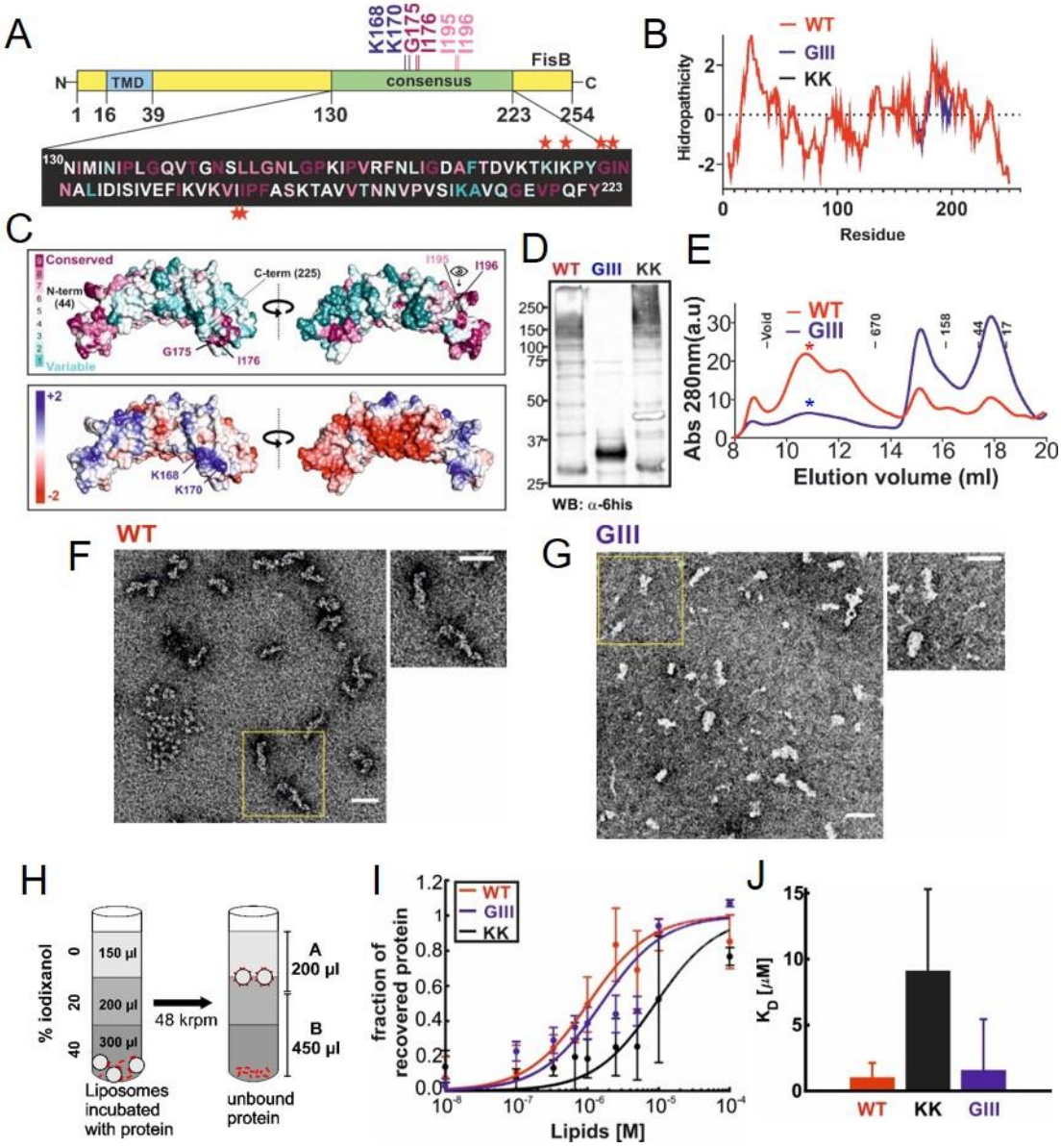

Figure 12. FisB mutants selectively impaired in oligomerization and membrane binding.

2.1.10 FisB^{K168D,K170E} (FisB^{KK}) is selectively impaired in binding acidic lipids

Contribution statement: Protein purification and floatation experiments were carried out by me. Determination of sporulation efficiencies and imaging was carried out by Ane Landajuela.

We found that lipid-binding is primarily mediated by electrostatic interactions (Figure 9F) within or close to the consensus domain. To identify lipid-binding mutants, we either neutralized or inverted up to four positively charged residues in FisB(ECD). I expressed the charge neutralization mutants in *E. coli*, purified the proteins using a hexa-histidine tag and tested for lipid binding in the co-floatation assay showed in Figure 9B. The largest reductions in lipid binding were observed when lysines in a region comprising residues 168-172 were neutralized (Figure 13A). This region corresponds to a highly positively charged pocket in the predicted model of FisB 44-225 (Figure 12C, bottom).

A partially overlapping set of FisB mutants were expressed as a fusion to monomeric YFP at low expression levels in a *ΔfisB* background and tested for sporulation efficiency using the heat kill assay (Figure 13B-E). Again, the strongest reductions in sporulation efficiency were found when lysines 168, 170 or 172 were mutated (Figure 13D). We decided to characterize the K168D, K170E mutation in more detail, as it produced the strongest reduction in sporulation efficiency.

We purified the ECD of FisB^{K168D,K170E} (FisB^{KK}) from *E. coli* and tested its binding to liposomes containing 45 mole % CL using the co-floatation assay (Figure 12H-J). The dissociation constant for FisB^{KK}-acidic lipid binding was $K_d^{KK} = 9.1$ μM (CI=6.5-15.3 μM), nearly 10-fold lower than that for wild-type FisB(ECD) ($K_d^{wt} = 1.0\ \mu\mathrm{M}, \mathrm{CI} = 0.7 - 2.1\ \mu\mathrm{M}$, Figure 9 H,J). Importantly, formation of oligomers was not affected (Figure 12D). Thus, FisB^{KK} is specifically impaired in binding to acidic lipids.

Additionally, we also designed mutations targeting hydrophobic residues (black) or inversions of negatively (red) charged residues, or deletions (Figure 13B) to identify potential other regions required for FisB localization and/or membrane fission. mYFP fusions of the mutated FisB were expressed at low levels in *ΔfisB* cells and tested for heat-resistant colony formation (Figure 13C,D) and imaged for localization (Figure 13E). However, most of these mutants were not correctly targeted to the membrane. (Figure 13E, red and cyan boxes) and therefore not informative.

Figure 13. Identification of FisB lipid binding mutants. ***(A)*** Mutations neutralizing up to four positively charged residues in the consensus region were introduced into FisB(ECD), purified from *E. coli* and tested for binding to negatively charged liposomes using the flotation assay depicted in Figure 9B. Neutralization of lysines around K170 produced the strongest reduction in binding. Liposomes were composed of 45 mole % CL and 55 mole % PC**.** ***(B)*** Other designed mutations targeted hydrophobic residues (black), inversion of positively (blue) or negatively (red) charged residues, or deletions. mYFP fusions of the mutated FisB were expressed at low levels in *ΔfisB* cells and tested for heat-resistant colony formation (C,D) and imaged for localization (E). ***(C)*** Sporulation efficiency of cells expressing mYFP-FisB with deletion and hydrophobic residue mutations shown in (B). ***(D)*** Sporulation efficiency of cells expressing mYFP-FisB with charge inversion mutations shown in (B). ***(E)*** Images of sporulating cells (at T3) expressing mYFP-FisB bearing some of the mutations in C,D. In half the cases, the mYFP signal was cytosolic, suggesting the fusion protein was not inserted into the membrane and degraded (images boxed in red). In other cases, some mYFP signal was on the membrane and some was cytosolic (cyan-framed images). Cases in which mutants were located exclusively to the membrane were rare and included neutral mutations (images boxed in green) as well as $FisB^{KK}$ and $FisB^{GIII}$.

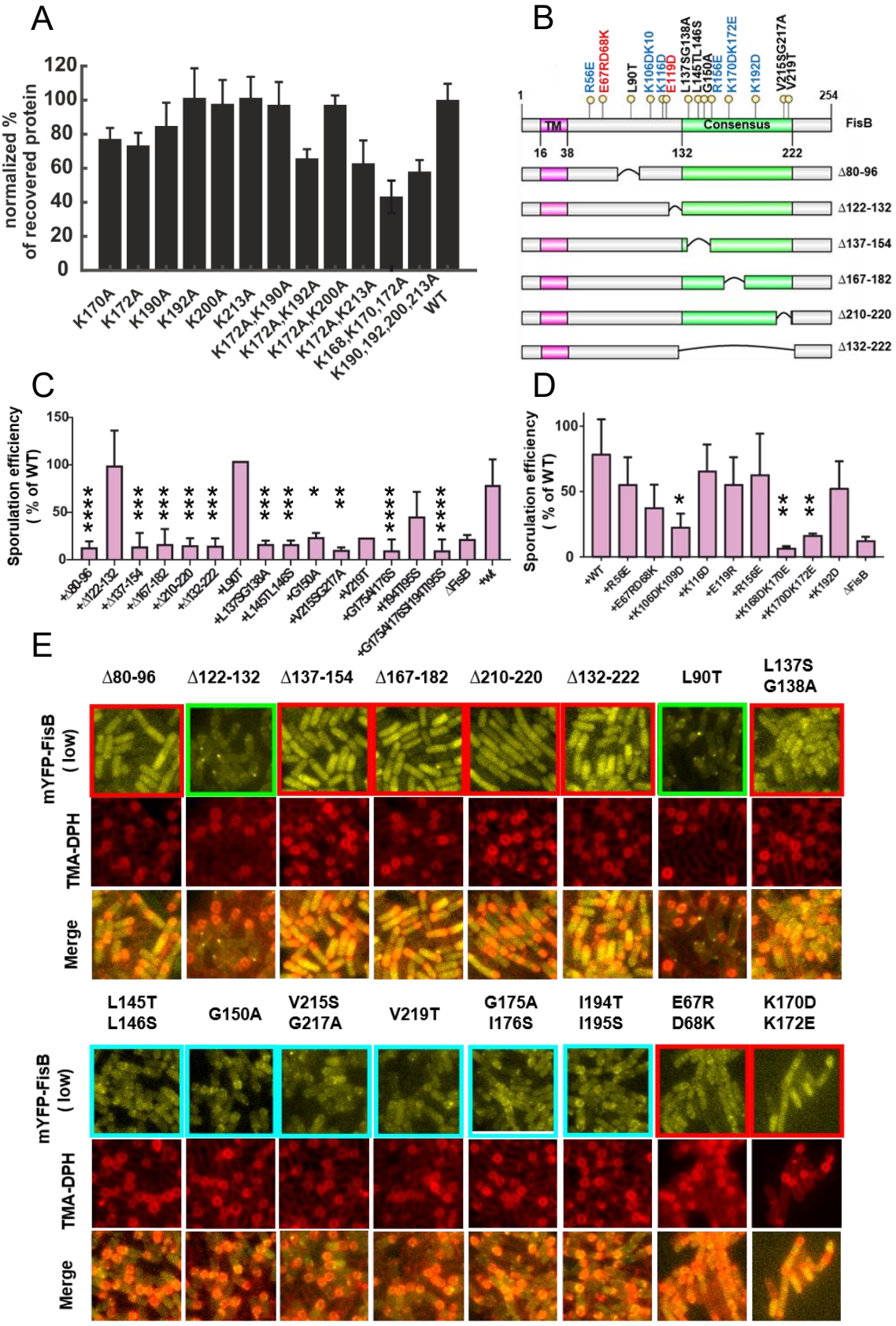

Figure 13. Identification of FisB lipid binding mutants.

2.1.11 FisB-lipid interactions and homo-oligomerization are important for targeting FisB to the fission site

Contribution statement: All experiments and analysis described in this sub-section were carried out by Ane Landajuela except the Western Blot shown in Figure 14G, which was done by Thierry Doan (Aix-Marseille Université – CNRS). These results are included here because they are relevant for our overall understanding of how FisB localizes to the membrane fission site and mediates fission.

We imaged the mYFP tagged FisB mutants selectively impaired in binding to lipids ($FisB^{KK}$) or self-oligomerization ($FisB^{GIII}$) to investigate whether these properties were important for FisB's function *in vivo* (Figure 14). We induced these strains to sporulate and monitored FisB dynamics and membrane fission using the lipophilic dye TMA-DPH. Both the lipid-binding ($FisB^{KK}$) and the oligomerization mutant ($FisB^{GIII}$) were targeted to the cell membrane. This was not the case for most of the other mutants we tested (Figure 13E, red and cyan boxes). 1.5 h after sporulation was induced (T1.5), mYFP-FisB signal was visible in all strains without any distinguishing features. While at T2.5 of sporulation, some cells expressing FisB wild type started to display an ISEP and these cells also had undergone membrane fission, no membrane fission or ISEPs were observed in either of the mutants.

By 3 h into sporulation, 25% of WT FisB cells had undergone fission, always with an accompanying ISEP. In the lipid binding $FisB^{KK}$ mutant, only 8% of the sporulating cells had accomplished membrane fission, but those that did had an ISEP (Figure 14A,B). Membrane fission events and the accompanying bright mYFP-FisB spots were very rare (0.6%) in the oligomerization-deficient $FisB^{GIII}$ mutant.

The distribution of fluorescence intensities of the foci from low-expression WT and KK

cells were indistinguishable (Figure 14C). Using quantitative imaging, we determined that about 6±2 copies of low-expression FisB WT or the KK mutant to have accumulated at the fission site (Figure 14F) [90]. For the GIII mutant, there were not enough cells with an intense spot to perform a similar analysis.

From TMA-DPH labeling, we determined the fraction of cells that successfully completed fission as a function of time (Figure 14D). Oligomerization-deficient $FisB^{GIII}$ was not able to induce fission, whereas the lipid-binding mutant $FisB^{KK}$ had a partial, but severe defect (~50% reduction compared to wild-type). Importantly, both mutants were expressed at levels similar to the wild type. We determined the total fluorescence per cell as indicated in Figure 14E and found no difference between WT and mutants (Figure 14F). Additionally, western blot analysis showed no difference in expression levels for WT and GIII mutant at T3 of sporulation (Figure 14G). Therefore, the defects to form an ISEP and undergo membrane fission are not due to lower expression levels.

Together, these results suggest FisB-lipid and FisB-FisB interactions are both important for targeting FisB to the fission site.

Altogether, our results in section 2.1 show that FisB is a single pass membrane protein with a small N-terminal domain facing into the cytoplasm and a larger C-terminal domain located in the extracellular space. FisB(ECD) binds negatively charged lipids non-specifically through electrostatic interactions and forms oligomers of various sizes *in vitro* and *in vivo*. Using mutagenesis, we identified FisB mutants that are deficient in either lipid-binding or oligomerization and found that FisB oligomerization as well as binding to acidic lipids are required for targeting FisB to the fission site. To gain insight into the mechanism by which FisB mediates membrane fission, we decided to study the interaction of FisB(ECD) with model membranes of GUVs and SUVs in the next section (2.2.1).

Figure 14. FisB clustering and binding to acidic lipids are both required for ISEP formation and membrane fission. ***(A)*** Snapshots of sporulating ΔfisB cells expressing mYPF-FisB WT (BAL002), mYPF-FisB^{KK} (BAL006), or mYPF-FisB^{GIII} (BAL007), at low levels. For each time point during sporulation cell membranes were labeled with TMA-DPH and images were taken for the membrane (left) and the YFP (right) channels. By T2.5, some foci at the engulfment pole (ISEP) are visible for WT cells that have undergone membrane fission (red boxes), but not for the KK or GIII mutants (white boxes). A small fraction of KK mutants accumulated FisB at the engulfment pole and underwent membrane fission at T3. Scale, 1 μm. ***(B)*** Percentage of cells with an intense spot at the engulfment membrane (ISEP) at T3 of sporulation, for WT FisB, FisB^{KK}, or FisB^{GIII}. ***(C)*** Distribution of background-corrected integrated intensities (sum of pixel values) of ISEP fluorescence for ΔfisB cells expressing mYFP-FisB WT or mYPF-FisB^{KK}. The distributions are indistinguishable. Since low-expression cells accumulate, on average, 6±2 FisB WT molecules at the ISEP [90], so do FisB^{KK} cells. ***(D)*** Percentage of cells that have undergone membrane fission at the indicated time points. ***(E-G)*** **FisB mutants selectively deficient in membrane binding or oligomerization are expressed at similar levels as wild-type FisB.** ***(E)*** Examples of cell contours detected using MicrobeJ. ***(F)***. Distributions of background-corrected total fluorescence intensity per cell for *ΔfisB* cells expressing mYFP-FisB^{WT} (BAL002), mYFP-FisB^{KK} (BAL006), or mYFP-FisB^{GIII} (BAL007) at low levels. The pixel values within the contours detected by MicrobeJ as in *(E)* were summed to define the total intensity per cell. This value was corrected for autofluorescence and background by subtracting the average total intensity per cell in cells (PY79) that did not express any fluorescent protein. The three distributions were indistinguishable, indicating that the mutants were expresses at the same level as the wild-type protein. ***(G)*** Expression levels of mYFP-FisB^{GIII} (BAL007) was similar to those of FisB^{WT} (BAL002) using Western blotting, probed using an anti-FisB antibody. Time points into sporulation probed are indicated above the blot.

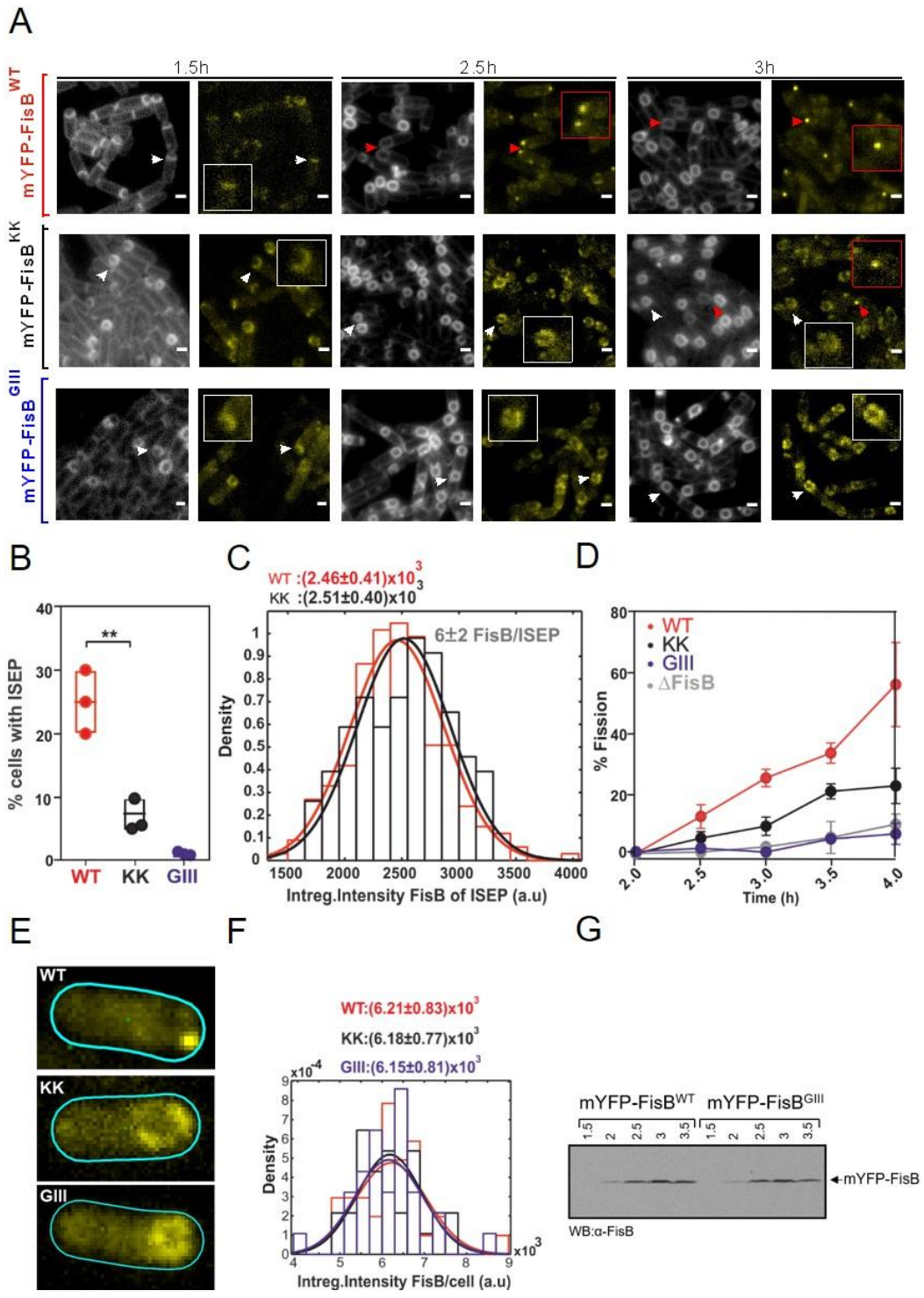

Figure 14. FisB clustering and binding to acidic lipids are both required for ISEP formation and membrane fission.

2.2 Interactions of FisB with giant unilamellar vesicles, forespore inflation, and a possible mechanism of membrane fission

2.2.1 Soluble FisB(ECD) binds to and aggregates negatively charged artificial membranes

To gain further insight into FisB-membrane interactions, self-oligomerization of FisB, and membrane remodeling, I studied interactions of FisB(ECD) with membranes of giant unilamellar vesicles (GUVs). To this end, I first incubated varying amounts of iFLuor555-FisB(ECD) with GUV membranes containing either 30 mole % CL, 69 mole % eggPC and 1 mole % NBD-PE or 99 mole % eggPC and 1 mole % NBD-PE in an Eppendorf tube for 1h. NBD-PE is a headgroup-labeled lipid which was included to visualize the GUV membrane. After incubation, GUVs incubated with protein were transferred into the imaging chamber shown in Figure 16C.

The reaction buffer used in all experiments was the same buffer used in the floatation experiments (25 mM HEPES at pH 7.4, 140 mM KCl, 1 mM EDTA, 0.2 mM tris(2-carboxyethyl) phosphine). Compared to the 250 mM sucrose solution inside the GUV, this buffer is slightly hypertonic by ~20 mOsm/l which deflates the GUVs. This results in lower membrane tension which would facilitate any membrane remodeling activity FisB(ECD) might have. After an incubation time of 1h, membranes and the labeled protein were visualized using spinning-disc confocal (SDC) microscopy, by alternating channels (Figure 15A). Starting at ~75 nM iFluor555-FisB(ECD), discrete fluorescent mobile spots in the iFluor555 channel became visible. At 200 nM, iFluor555-FisB(ECD) spots completely covered most GUVs. In regions of more intense iFluor555 labeling, often additional membrane signal was found. Even at 1 µM iFluor555-FisB(ECD) did not bind GUVs consisting of 99 mole % eggPC and 1 mole % NBD-PE (lacking any acidic lipids). As shown in Figure 15B, aggregates of GUVs can often be found in the presence of iFLuor555-FisB(ECD). Fluorescence profiles of the arcs indicated with blue, green, and red in Figure 15B are plotted in in Figure 15C and show that the protein signal is enhanced

at the adhesion patches and its rim. Interestingly, the iFluor555-FisB(ECD) intensity along a GUV contour is uniform in the adhesion patch, unlike in non-adhering regions. This result suggests that FisB(ECD) can bridge and aggregate membranes.

To further investigate the ability of FisB(ECD) to bridge membranes, I tested if FisB(ECD) can aggregate membranes of SUVs by measuring solution turbidity [117]. In this assay SUVs are incubated with protein and the apparent absorbance at 350 nm is measured. Aggregation of vesicles leads to an increase in particle size which is reflected in an increase of scattered light. An increase of scattered light leads to less transmitted light and therefore the absorbance increases. I prepared SUVs composed of 50 mole % *E. coli* PG, 25 mole % *E. coli* PE, 20 mole % eggPC, 5 mole % *E. coli* CL (BS mix) which roughly mimics the membrane composition of *B. subtilis*. I measured the apparent absorbance of 50 µM total lipid for 5 min, before addition of 1 µM FisB(ECD) (Figure 15D). Upon addition of FisB(ECD), the absorbance increased over time indicating FisB(ECD)-induced SUV aggregation. No increase in apparent absorbance was observed for vesicles or protein alone.

Altogether these results show that FisB(ECD) can bind to negatively charged membranes of GUVs *in vitro* and that it can bridge membranes of GUVs as well as SUVs.

Figure 15. Interactions of FisB(ECD) with GUV membranes. ***(A)*** Varying amounts of iFluor555-FisB(ECD) were incubated with either 30 mole % CL, 69 mole % eggPC and 1 mole % NBD-PE or 99 mole % eggPC and 1 mole % NBD-PE for 1h in an Eppendorf tube before imaging. At low concentration (75 nM) FisB(ECD) forms mobile clusters on the GUV. Labeling becomes more uniform as the concentration is increases to 1000 nM. No binding was observed in the absence of acidic lipids. ***(B)*** Aggregated GUVs can often be observed in the presence of 100 nM iFluor555-FisB(ECD) with the protein accumulating where the GUVs are attached. ***(C)*** Fluorescence intensity profiles along the attachment zones between GUVs shown in (B). FisB(ECD) accumulates uniformly within the adhesion zones and at the rim. ***(D)*** SUVs aggregate upon addition of FisB(ECD). Absorbance (350 nm) of SUVs is measured. After 5 min, 1 μM of FisB(ECD) is added resulting in an increase in absorbance, indicating that SUVs are aggregating.

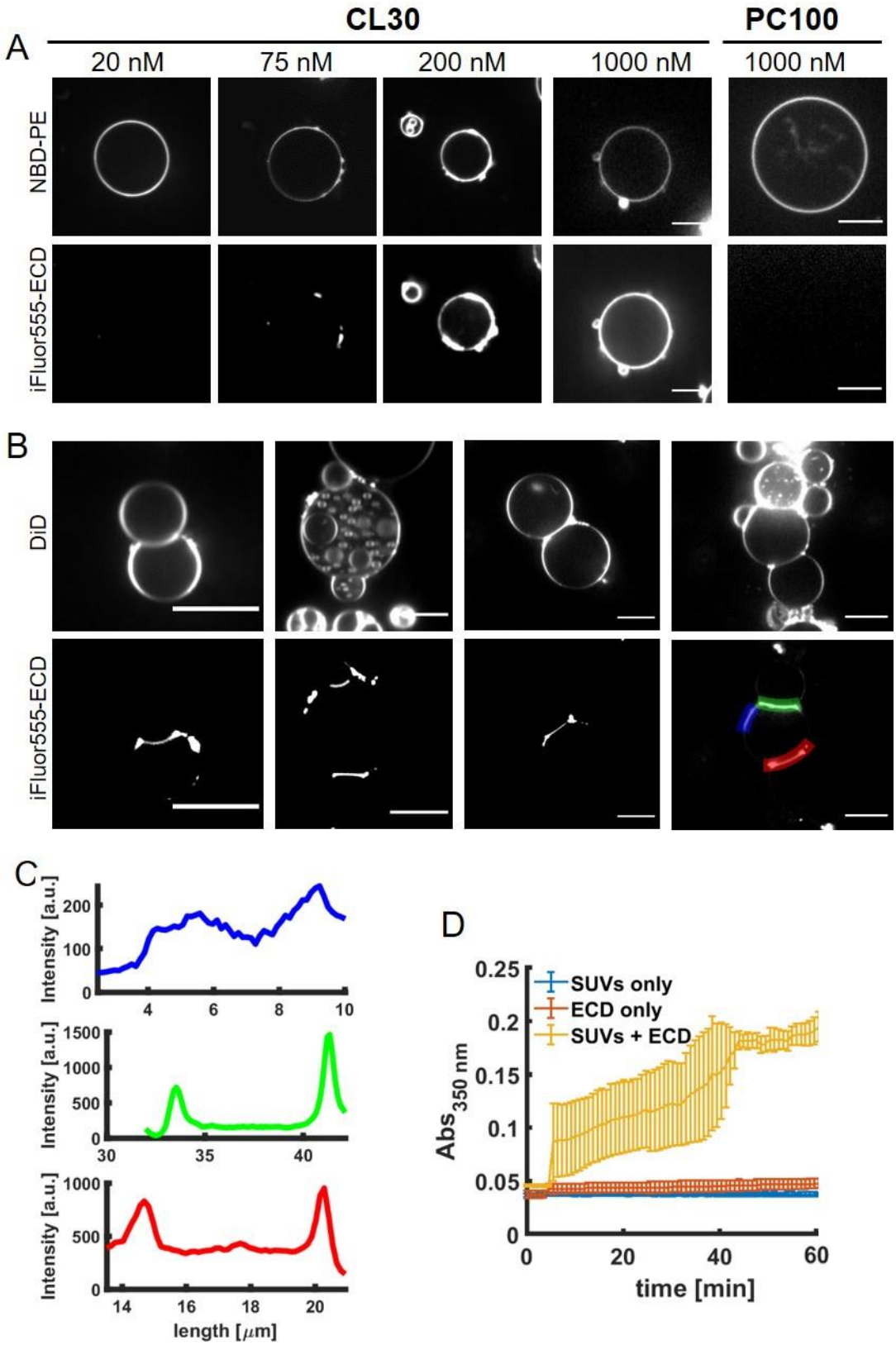

Figure 15. Interactions of FisB(ECD) with GUV membranes.

2.2.2 FisB(ECD) forms a stable, extended network on GUV membranes

To monitor interactions of iFluor555-FisB(ECD) with GUVs over time, I added 3 µl of a 25 µM iFluor555-FisB(ECD) solution to one corner of the open observation chamber shown in Figure 16C (volume = 300 µl) filled with GUVs (final concentration of iFluor555-FisB(ECD) was 250 nM). The composition of the GUVs was 50 mole % *E. coli* PG, 25 mole % *E. coli* PE, 19 mole % eggPC, 5 mole % *E. coli* CL and 1 mole % NBD-PE (BS mix). This composition was chosen to mimic the membranes of *B. subtilis* which usually contain a high amount of PG and PE [58].

At various times after iFLuor555-FisB(ECD) addition, I imaged iFLuor555 and NBD channels. Small, mobile spots appeared within 20 min after addition of iFluor555-FisB(ECD) to the GUV chamber (Figure 16A). As more and more protein binds over time, the GUV becomes more uniformly covered. After ~1 h of incubation, large deformations appeared in the GUV membranes. These deformations were stable for at least 1-2 h, i.e., the shape of a deformed GUV was fixed during this time. About 50% of the GUVs showed deformed membrane regions which were covered continuously and quite homogeneously with iFluor555-FisB(ECD). These results suggested that FisB(ECD) may form an extended network stabilizing the membrane shape.

To test how stable the FisB(ECD) network is, I added the detergent Triton X-100 (1.7 mM final concentration) to the GUVs after deformations had formed. 5 to 10 minutes after addition of detergent the lipid signal disappeared, suggesting that the membranes were dissolved. Remarkably, iFLuor555-FisB(ECD) signals were intact (Figure 16B), indicating that once formed, the three-dimensional FisB(ECD) network was stable even after the removal of the membrane.

Importantly, I only observed the deformations when GUVs and FisB(ECD) were incubated in the open imaging chamber and not when protein and GUVs were first incubated in a closed Eppendorf tube and only transferred into the imaging chamber for imaging. When experiments were carried out in the open imaging chamber, the initial osmolarity of the outside solution was only slightly hypertonic by ~20 mOsm/l. Over 3 hrs approximately 2/3 of the original buffer had evaporated, effectively increasing the osmolarity of the outside buffer 3-fold. This leads to deflation of the GUVs. Since deflated GUVs have a lower membrane tension, they are more easily tubulated by curvature sensing/inducing proteins. This has been described for the eukaryotic protein endophilin [118]. However, we only saw large scale deformations and no correlation of iFluor555-FisB(ECD) intensity with the positive or negative curvatures of theses GUVs was found (Figure 21B), indicating FisB might not behave as eukaryotic curvature sensing proteins. A more detailed discussion of this can be found in section 2.2.5.

Instead, we hypothesize, that FisB forms a stable extended network on GUV membranes. Over the course of the experiment the osmolarity difference between the inner and outer GUV solution increases. Due to this osmolarity difference between the inner and outer solutions, the volume of the inner GUV solution decreases over the course of the experiment. However, the FisB(ECD)-covered GUV membrane surface area remains the same. This results in large scale deformations to account for this imbalance, similar to a deflating volleyball.

Figure 16. FisB(ECD) forms a stable, extended network on GUV membranes. ***(A)*** GUVs composed of BS mix were free floating in the imaging chamber illustrated in *(C).* 3 µl of a 25 µM iFluor555-FisB(ECD) solution was added to one corner of the imaging chambers. Lipid and protein channel were monitored for 3h. Representative images of GUVs before (0h) and after (0.5h and 3h) protein addition are shown. iFluor555-FisB(ECD) first forms small mobile clusters on the GUV membrane. After about 1h some GUVs are fully and mostly uniformly covered and show large inward deformations. ***(B)*** After GUVs started to show deformations, Triton X-100 was added to a final concentration of 1.7 mM to dissolve the GUV membrane. 5 to 10 min after Triton X-100 addition no fluorescence in the lipid channel could be detected, indicating that the GUV membrane had been dissolved (top row). In contrast, the 3-dimensional structure formed by FisB(ECD) is still intact (middle and bottom row). ***(C)*** Schematic of the imaging chamber. 2 cover glasses are separated with a spacer leaving 2 sites open to the environment.

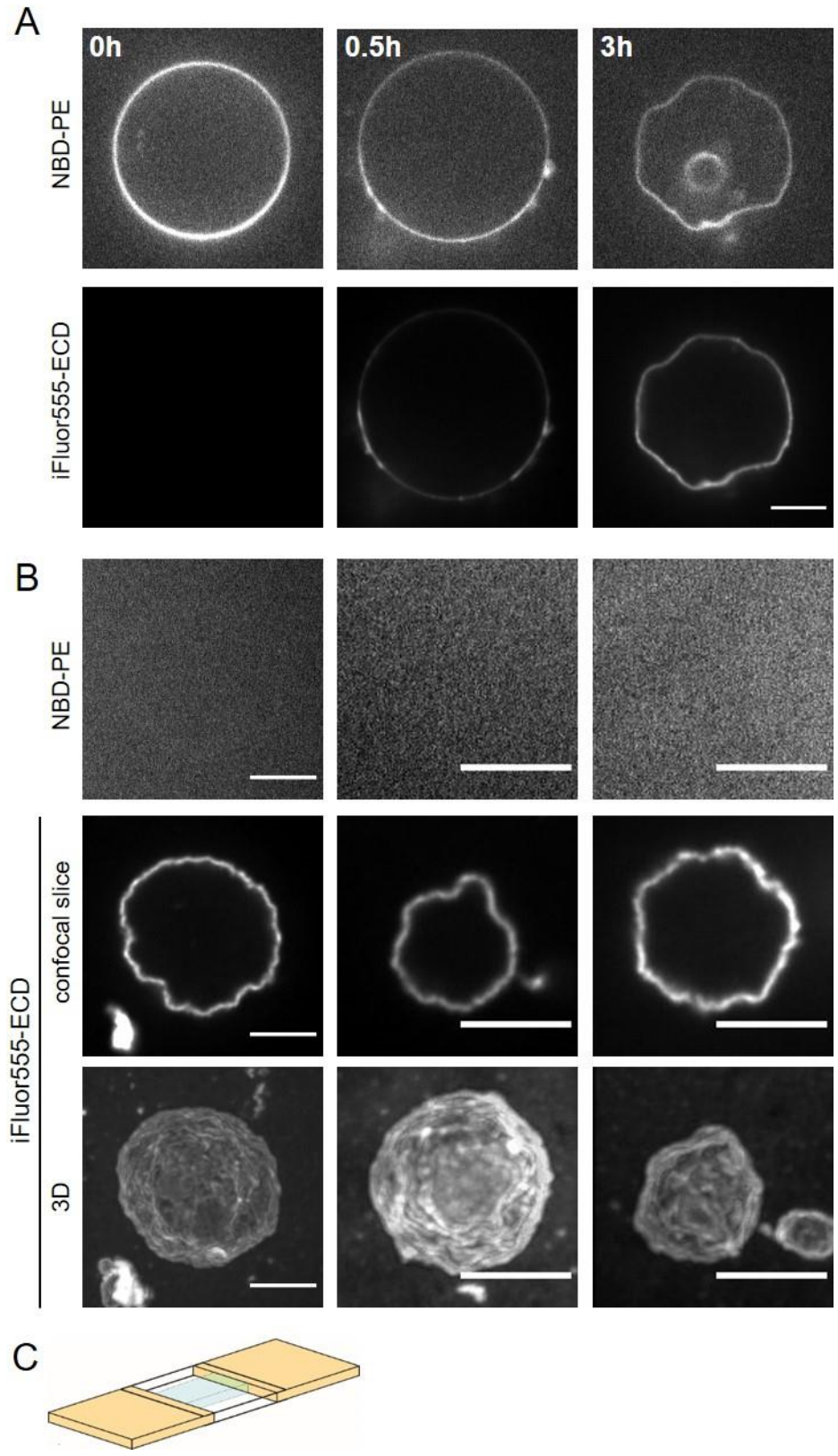

Figure 16. FisB(ECD) forms a stable, extended network on GUV membranes.

We reasoned that if FisB(ECD) does indeed form a stable extended network on GUV membranes, its mobility should be low in such regions. To test this hypothesis, I performed fluorescence recovery after photobleaching (FRAP) experiments (Figure 17). I incubated 1 μM iFLuor555-FisB(ECD) with BS mix GUVs for 2 h in our imaging chamber. After incubation, a wide range of iFLuor555-FisB(ECD) coverages on GUVs can be observed. While some GUVs were uniformly covered by iFLuor555-FisB(ECD), others were covered only partially by iFLuor555-FisB(ECD) patches (Figure 17A). I bleached the iFLuor555-FisB(ECD) fluorescence in a rectangular region of interest (ROI) and monitored the subsequent recovery on a given GUV as indicated with the blue and orange boxes in Figure 17A. Recovery was faster for GUVs that had partial, patchy iFLuor555-FisB(ECD) coverage, as new patches diffused into the bleached region. By contrast, there was virtually no recovery for GUVs that were uniformly covered by iFLuor555-FisB(ECD). To relate FisB(ECD) membrane coverage to mobility, we plotted the mean iFLuor555-FisB(ECD) signal along the contour of the GUV, F_{mean}^{ECD}, against the fractional fluorescence recovery 45 s after bleaching, $((F_{45} - F_o)/(1 - F_o)$, where F_{45} is the fluorescence value at 45 s and F_o is the intensity just after bleaching), as shown in (Figure 17). This analysis showed that increasing FisB(ECD) coverage led to decreased FisB(ECD) mobility, consistent with the idea that FisB(ECD) forms a denser, less dynamic network as coverage increases.

Together, these results show that FisB(ECD) forms an extended, stable network in which individual FisB molecules are immobile. The network is stable even if the membrane is completely removed.

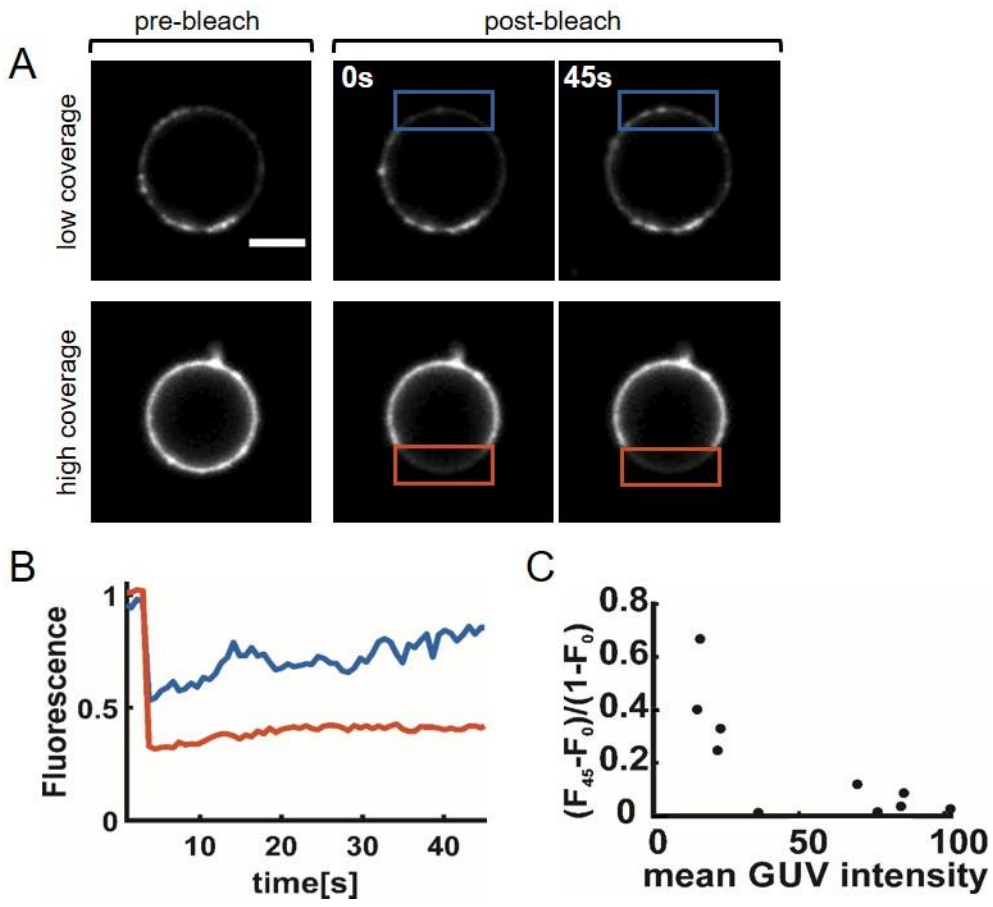

Figure 17. FisB(ECD) forms a stable network on GUV membranes. ***(A)*** Top row shows a GUV with low iFluor555-FisB(ECD) coverage before bleaching, 0 s and 45 s after bleaching. Bottom row shows a GUV fully covered with iFluor555-FisB(ECD) before bleaching, 0 s and 45 s after bleaching. Bleached regions are indicated with boxes. Scale bar is 5 μm. **(B)** Normalized fluorescence intensity over time of the boxes indicated in *(A).* ***(C)*** Relation of protein coverage (mean GUV intensity) to protein mobility. Plotted is the fractional fluorescence recovery at 45 s after bleaching ($(F_{45} - F_o)/(1 - F_o)$, where F_{45} is the fluorescence intensity at 45 s and F_o is the intensity just after bleaching) against the mean GUV intensity.

2.2.3 FisB does not permeabilize membranes

We observed many deflated GUVs in the presence of FisB(ECD) such as the one depicted in Figure 16A . Such GUVs were rare in the absence of FisB(ECD), which could be due to at least two possibilities that are not mutually exclusive: a) FisB(ECD) helps deflate GUVs, e.g. by making pores in them, b) FisB(ECD) stabilizes deflated GUVs against collapse caused by an osmotic imbalance between the inner and outer solution. Our observations that FisB(ECD) forms a stable, extended network on GUV membranes (Figure 16 and Figure 17) support the second possibility, but do not exclude the first one.

Therefore, we tested if deflated GUVs with FisB(ECD)-induced large-scale stable membrane deformations like the example in Figure 16A had lost their membrane integrity, i.e. whether FisB(ECD) permeabilizes membranes. To this end, we first encapsulated carboxyfluorescein (CF) in GUVs composed of the BS lipid composition (Figure 18A) and determined the ratio of fluorescence from a region of interest inside to outside the GUVs in the presence and absence of 1 μM FisB(ECD) at the time points indicated in Figure 18B. Since the dye is encapsulated inside the GUVs, initially this ratio should be >1. However, if a GUV had lost its encapsulated dye due to permeabilization, this ratio should be closer to 1.

These experiments were again carried out in the open imaging chamber, leading to increased osmolarity of the outer solution over the course of the experiment. In line with the fact that GUV membranes are permeable to small molecules [119], after 3h, protein-free GUVs lost their CF fluorescence to varying degrees, and the distribution of GUV lumenal CF fluorescence shifted to lower values and broadened (Figure 18B).

In the presence of FisB(ECD), the loss of CF fluorescence depended on whether a given GUV had deformations. The distribution of lumenal CF fluorescence from GUVs that

remained spherical was comparable to those in the absence of FisB(ECD) (Figure 18B). In contrast, deformed GUVs lost essentially all their content.

GUVs that have completely lost their internal fluorescence are very rare in the absence of any protein. This is consistent with the idea that in the absence of protein, GUVs might eventually collapse due to the osmotic imbalance between inner and outer solution. The presence of FisB(ECD) may prevent the GUVs from collapse even if internal solution is lost due to osmotic imbalance between inner and outer solution. This idea is supported by the experiments described in section 2.2.2, which showed that the extended network formed by FisB(ECD) on GUVs persists, even if the GUVs are permeabilized with detergent.

Finally, we also tested if FisB(ECD) permeabilizes membranes of large unilamellar vesicles. To this end, we first prepared 400 nm LUVs (using the BS lipid composition) filled with 50 mM sulforhodamine B (SRB). At this concentration, the fluorescence of SRB is self-quenched. If LUVs become leaky, dequenching of SRB would result into an increase in fluorescence. We measured the fluorescence of LUVs (~ 50 μM total lipid) for 5 min and then added a total of 4 or 8 μM FisB(ECD) and continued to measure fluorescence for another 2.5h (Figure 18C). To determine the maximum increase in SRB dequenching, we added Triton X-100 at a final concentration of 2 mM to release all SRB cargo. Consistent with the GUV experiments with encapsulated CF, no increase in fluorescence was observed when LUVs were incubated with FisB(ECD), indicating that LUVs were not permeabilized. The slight decrease of fluorescence as a function of time observed in Figure 18C is most likely the result of bleaching.

Altogether our results suggest that up to ~ 1 μM FisB(ECD) does not induce leakage of membranes. Thus, FisB does not behave like membrane-permeabilizing proteins such as Adenylate cyclase (ACT) [120].

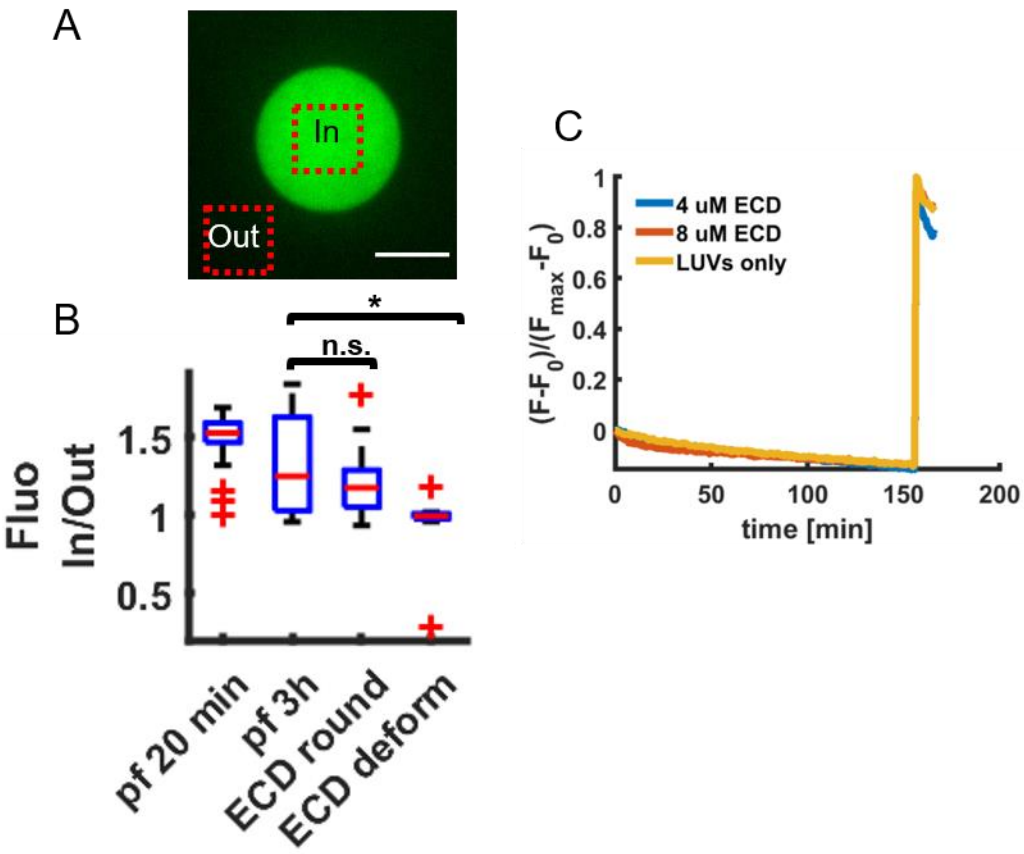

Figure 18. FisB does not permeabilize membranes at 1 µM. ***(A)*** Example of a GUV filled with 10 µM carboxyfluorescein. Boxes indicate the area used to determine the mean pixel intensity used for quantification of permeabilization. ***(B)*** Ratio of the mean pixel intensity inside to outside of the GUVs for protein free GUVs and in the absence and presence of 1 µM FisB(ECD) after 3h in the imaging chamber. ***(C)*** FisB(ECD) does not permeabilize membranes of LUVs. LUVs have 50 mM of SRB encapsulated. At this concentration SRB is self-quenched. Fluorescence of LUVs was measured for 5 min before addition of 4 or 8 µM FisB(ECD). No dequenching of SRB was observed, indicating that LUVs are not permeabilized.

2.2.4 At very high concentrations FisB(ECD) deforms and disrupts membranes

To observe acute effects of FisB(ECD) binding to GUVs at high concentration, we administered fluorescently labeled FisB(ECD) directly onto free floating GUVs using a micropipette and imaged the resulting events with high time resolution using SDC microscopy. We applied a 12 μM Cy5.5-FisB(ECD) solution through a micropipette directly onto free floating GUVs composed of 30 mol % CL and 70 mol % eggPC, or 100 mole % eggPC (Figure 19A,B).

Observed in brightfield, the flow generated by the pipette solution pushed away GUVs made of 100% eggPC (Figure 19A), consistent with our observation that FisB(ECD) does not bind neutral membranes. In sharp contrast, when 30 mol % CL was present, the GUVs rapidly aggregated, as seen both in brightfield and the Cy5.5 channel (Figure 19C). Cy5.5-FisB(ECD) signals initially appeared as small clusters (Figure 19C) which grew over time as more protein bound. Concomitantly, GUVs aggregated strongly. Some GUVs were observed to fuse, while others burst. Some of these GUV transformations were likely due to increased mechanical stress in the GUV aggregates. However, some deformations and membrane disruptions were unlikely to be due to increased stress in the GUV aggregate, because they were observed in GUV membranes that were not in contact with others and the deformations were inward, i.e. opposite of what would be expected from increased internal pressure due to compressive forces generated by aggregation (Figure 19D,E). In some cases, the inward deformations proceeded to implosion and collapse, as shown in Figure 19E.

Together, these experiments show that at ~ 10 μM, FisB(ECD) can strongly bridge negatively charged membranes and is able to deform them. It also suggests that

FisB(ECD) might disrupt the membranes.

These results seem to contrast with experiments in which we used up to ~1 uM FisB(ECD) (sections 2.2.1and 2.2.2). However, in addition to an increased protein concentration, in the experiments described here, FisB(ECD) covered GUV membranes rapidly, presumably without sufficient time to equilibrate. As shown in Figure 19C-D, the flow created by the micropipette results in inhomogeneous labeling along the GUV contour. Thus, the membrane disrupting-activity of FisB(ECD) we observed here may be at least partially caused by non-equilibrium effects.

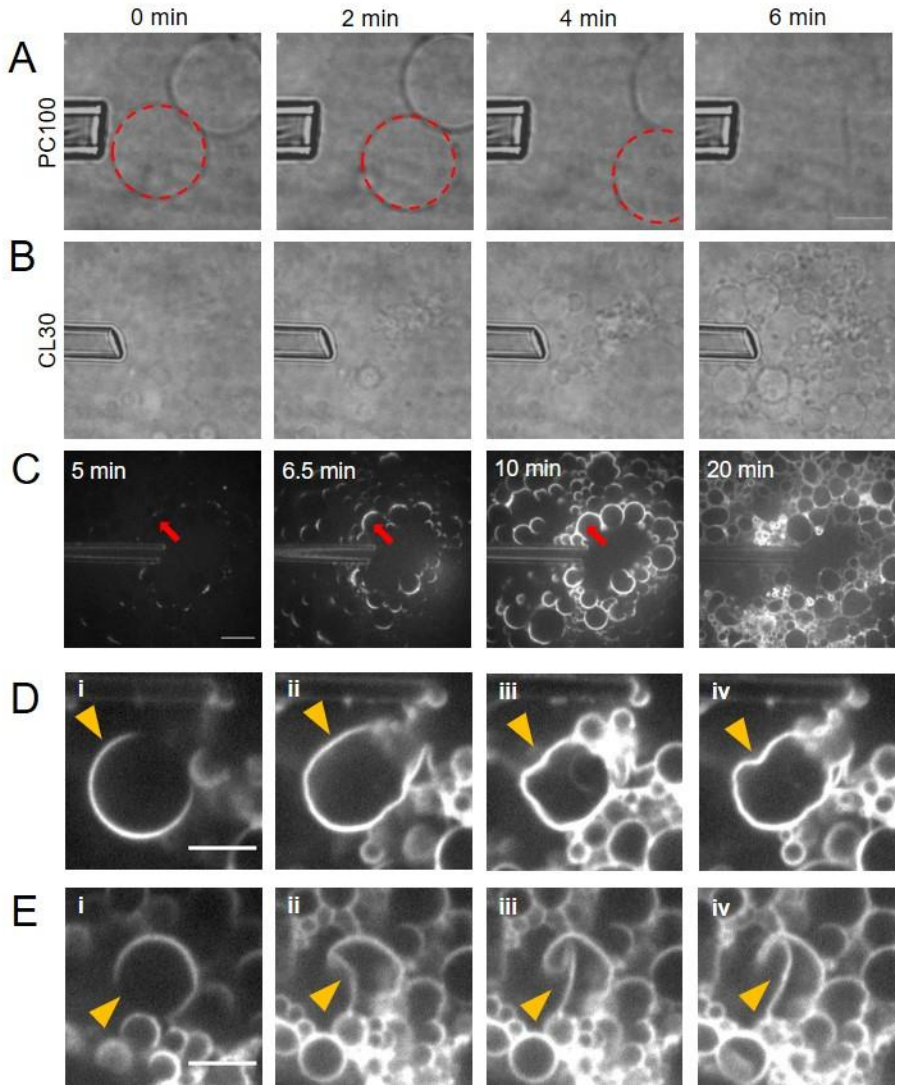

Figure 19. At high coverage, FisB(ECD) causes membrane invaginations and collapse.*(A,B)* A micropipette is puffing a 12 μM solution of Cy5.5-FisB(ECD) onto free floating GUVs consisting of 100 mole % eggPC *(A*) or 30 mole % CL and 70 mole % eggPC *(B).* In the absence of acidic lipids, the flow generated by the protein solution pushes the GUVs away. In contrast, massive aggregation of GUVs can be observed when CL is present in the GUVs. ***(C)*** Puffing a 12 μM solution of Cy5.5-FisB(ECD) onto free floating GUVs containing 30 mole % CL and 70 mole % eggPC. Initially small spots can be observed. These spots grow over time until GUVs become mostly uniformly labeled. ***(D)*** Example of a GUV that gets deformed upon binding of Cy5.5-FisB(ECD). ***(E)*** Example of a collapsing GUV upon binding of Cy5.5-FisB(ECD).

2.2.5 FisB does not sense or induce membrane curvature

At the end of engulfment, the membrane neck connecting the engulfment membrane to the rest of the mother cell membrane is the most highly curved membrane region in the cell (Figure 21A). The predicted crescent shape of FisB together with our findings that localization of FisB and membrane fission do not depend on lipid domains or interaction partners other than acidic lipids and FisB itself, suggest that FisB could be recruited to the fission site due an intrinsic affinity for highly curved membrane regions. That is, localization of FisB to the membrane fission site could involve an intrinsic membrane curvature sensing/inducing activity. I would like to clarify curvature "sensing" vs. "inducing" by proteins that interact with membranes. All proteins that have an intrinsic preference for binding curved membranes "sense" membrane curvature at low coverage (Figure 20). That is, the protein binds preferentially to regions of the membrane that have a curvature close to the protein's intrinsic curvature. As the area fraction of bound protein on the membrane (coverage) increases, the proteins on the membrane can induce membrane deformations due to cooperative effects. Membrane tension and bending rigidity oppose membrane deformation. Deflating GUVs (low membrane tension) and a lipid composition that leads to a low bending rigidity (e.g. with a high PE content) facilitate membrane deformations by proteins that have an intrinsic curvature preference. For example, the protein endophilin preferentially binds to membrane tubules with a diameter of < 100 nm at low coverage (bulk protein concentration < 1 μM) [8]. At this coverage, the protein is not able to induce any membrane curvature. However, at high bulk concentration (> 2.5 μM), it can tubulate SUVs/LUVs resulting into tubules with a radius of 20 - 100 nm [121].

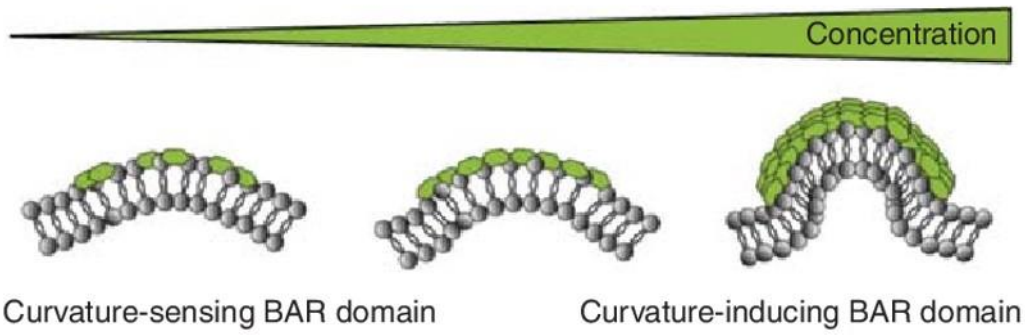

Figure 20. Curvature-sensing versus curvature-inducing. Borrowed from [122]. At low concentrations, curvature sensing dominates. The protein is enriched in membrane regions that match the intrinsic curvature of the protein. No mechanical effects on the membrane are observed. As the concentration increases cooperative effects induce membrane deformations.

However, several lines of evidence suggest that FisB does not sense or induce membrane curvature. First, if FisB had a preference for highly curved membrane regions, we would expect a higher density of FisB at regions of higher membrane curvature. To test this, I plotted the mean fluorescence intensity of iFluo555-FisB(ECD) against curvature of the GUV membrane in Figure 21B. The curvature of the GUV membrane was determined by manually fitting a circle into the curved regions as indicated in the inset. I was unable to find a correlation between membrane curvature and iFluor555-FisB(ECD) intensity.

Second, interactions of FisB(ECD) with GUV membranes suggest it can only generate or stabilize large, micrometer scale deformations at high membrane coverage on deflated GUVs (Figure 16). By contrast, eukaryotic curvature sensing proteins involved in endocytosis and membrane fission typically cause extensive membrane tubulation at low μM concentrations [118, 123]. For example, the N-BAR domain containing protein endophilin A1 has been shown to induce membrane curvature at high enough surface coverage [118, 124, 125]. I used Endophilin A1 as a positive control, by showing it can extensively tubulate GUVs under our experimental conditions. I incubated 2 μM endophilin A1 labeled with Atto395 (a present from Aurélien Roux's laboratory) with GUVs composed of 45% DOPS, 24.5% DOPC, 30% DOPE and 0.5% DiD for 1h in an Eppendorf tube, which resulted in extensive tubulation of GUV membranes (Figure 21F). By contrast, under similar conditions 2 uM FisB(ECD) was not able to generate membrane deformations despite high GUV coverage (Figure 21G).

Thus, under our experimental conditions, 2 μM Endophilin A1 can extensively tubulate GUV membranes containing 45 % DOPS, while FisB(ECD) at concentrations ranging from 0.1 – 12 μM cannot tubulate GUVs containing either 30 % CL and 70 % eggPC or GUVs composed of BS mix. This is not due a weaker affinity of FisB(ECD) for membranes ($K_d \approx$

$1\ \mu M$ for membranes with 45 mole % CL) compared to endophilin ($K_d = 1.15\ \mu M$ for membranes containing 45%DOPS, 30% DOPE, 24.5% DOPC, 0.5% TR-DHPE [126]).

Third, I tested if FisB's localization in *B. subtilis* cells depended on geometric cues of the cell membranes using curved filamentous cells. To avoid potentially confounding effects of other cues that may be present during sporulation, I expressed GFP-FisB from an inducible promoter during vegetative growth. Additionally, cell division was blocked by inducing expression of MciZ [127]. MciZ normally blocks binary cell division during sporulation, but when expressed during vegetative growth, cells grow into long flexible filaments that bent to varying degrees (Figure 21C). I imaged GFP-FisB spots along curved edges of these filaments and plotted the linear density of GFP-FisB spots (spots/μm) as a function of curvature (Figure 21E).

For the outer edge of a curved cell (blue) the curvature is $C_o = \frac{1}{R_o} + \frac{1}{r_t}$ and for the inner edge (red) the curvature is $C_i = \frac{-1}{R_i} + \frac{1}{r_t}$ where R_i and R_o are the inner or outer radii of the bent cell (Figure 21D blue or red dotted lines) and r_t is the radius of the tubular cell itself (Figure 21D black arrow). There was no clear correlation between GFP-FisB spot density and filament curvature. This might be because the actual range of curvatures tested with this assay is very small. The minimum curvature I was able to test was C_i = 0.5 μm^{-1} (for R_i = 0.65 μm) and the maximum curvature was 2.85 μm^{-1} (for R_o = 1.2 μm). Since r_t = 0.5 μm is fixed and smaller than R_i or R_o, the curvature tested with this assay will always be positive. Assuming the membrane tube connecting the forespore to the environment at the end of engulfment is a cylinder (Figure 21A), FisB at the fission site would only encounter highly negatively curved membranes (approximately -20 μm^{-1}). Therefore, this assay may not be ideal for testing the curvature preference of FisB. However, the same assay was successfully used to show that DivIVA has a preference for negatively curved

membranes [128]. Thus, if FisB has any curvature preference, it must be weaker than DivIVA's.

Fourth, I overexpressed FisB in eukaryotic HEK293 cells to see if it caused membrane tubulation and/or preferred highly curved regions. Overexpression of membrane curvature-inducing proteins such as phospholipase Cβ1 or amphiphysin1 N-BAR causes extensive tubulation of the plasma membrane [129, 130]. Full-length GFP-FisB was found mostly retained in the endoplasmic reticulum and was not informative. GFP-FisB(ECD) was expressed but was cytosolic and did not bind to the plasma membrane (PM). As an alternative, we used Lyn N-terminal sequence (Lyn11) to anchor mEGFP-sg-FisB^{ECD} to the plasma membrane [131]. The plasma membrane was stained with CellMask™ Deep Red. We did not observe any tubulation or invaginations in the presence of if Lyn11-mEGFP-sg-FisB^{ECD}) (Figure 21H). We tested if Lyn11-mEGFP-sg-FisB^{ECD} would accumulate at membrane regions with high negative curvature, similar to what FisB encounters during sporulation inside the membrane neck connecting the engulfment membrane to the rest of the mother cell membrane (Figure 21A). To create a high curvature region in the cell, we extruded a thin membrane tether from the cell surface using a small latex bead trapped with optical tweezers. To quantify enrichment or depletion of Lyn11-mEGFP-sg-FISB(ECD) in the tether, we calculated the sorting ratio [132], $S = (I_{FisB}^{tether}/I_{MB}^{tether})/(I_{FisB}^{cell}/I_{MB}^{cell})$, where I_{FisB}^{tether} is the fluorescence intensity of FisB in a region of interest in the tether, I_{MB}^{tether} is the same in the membrane channel, and I_{FisB}^{cell} and I_{MB}^{cell} are the corresponding intensities from a region in the cell membrane. A small (high) sorting ratio indicates depletion (enrichment) of the protein in the tether, whereas a value close to 1 indicates no preference. We found $S = 0.94 \pm 0.22$ for Lyn11-mEGFP-sg-FISB^{ECD} (3 tethers), indicating Lyn11-mEGFP-sg-FisB^{ECD} has little curvature preference. However, since GFP-FisB(ECD) alone did not bind to the PM, it is possible that the GFP-tag might

interfere with membrane binding and/or curvature sensing. Additionally, the TMD might be needed for curvature sensing. Therefore, these experiments should ideally be repeated with a construct that directly binds the plasma membrane. We will explore the use of different tags, such as a SNAP-tag [133] or FlAsH-tag [134] in the future.

Altogether, these results may suggest that FisB does not rely on curvature cues for its localization to the membrane fission site, at least within the range of curvatures we were able to generate. However, ideally, we would test FisB's curvature preference directly by pulling thin membrane tethers from GUVs with either encapsulated FisB(ECD) or reconstituted FisB full-length. Unfortunately attempts to do so were unsuccessful so for (see Appendix).

Figure 21. FisB does not sense or induce membrane curvature.*(A)* During sporulating FisB localizes to regions of negatively curved membranes in the engulfing membrane of the mother cell as well as the fission site. ***(B)*** iFluor555-FisB(ECD) is not enriched in large scale deformations of GUVs. Plotted is the mean pixel intensity along curved regions (as indicated in red for negative curvature and cyan for positive curvature) against the membrane curvature of this regions. The membrane curvature was determined by manually fitting a circle to the curved region. No correlation between iFluor555-FisB(ECD) intensity and membrane curvature was observed. ***(C)*** Cells of strain BMB014 are grown on an agar pad containing xylose and IPTG. Xylose induced the expression of MciZ which inhibits cell division leading to long filamentous curved cells. IPTG induces the expression of GFP-FisB. ***(D)*** Detection of foci along highly curved cells using the ImageJ plugin TrackMate [135] ***(E)*** GFP-FisB foci per micrometer plotted against the total membrane curvature. For the outer edge of a curved cell (cyan) the curvature is $C_o = \frac{1}{R_o} + \frac{1}{r_t}$ and for the inner edge (red) the curvature is $C_i = \frac{-1}{R_i} + \frac{1}{r_t}$. No correlation between curvature and foci density was observed. ***(F)*** GUV composed of 45% DOPS, 24.5% DOPC, 30% DOPE and 0.5% DiD were incubated with 2 µM Atto395 labeled Endophilin A1 for 1h at room temperature in an Eppendorf tube. Tubulation of GUVs is clearly visible in the protein and lipid channel. ***(G)*** GUV composed of BS mix were incubated with 2 µM iFluor555-FisB(ECD) for 1h at room temperature in an Eppendorf tube. In contrast to endophilin A1, no tubulation is visible. ***(H)*** Wild-type HEK cells and HEK cells expressing Lyn11-mEGFP-sg-FisB(ECD). No difference between the two cell types were observed. ***(I)*** Using optical tweezers, a latex bead is used to pull a thin membrane tether from cells expressing Lyn11-mEGFP-sg-FISB(ECD). No enrichment of FisB(ECD) in the tether is observed.

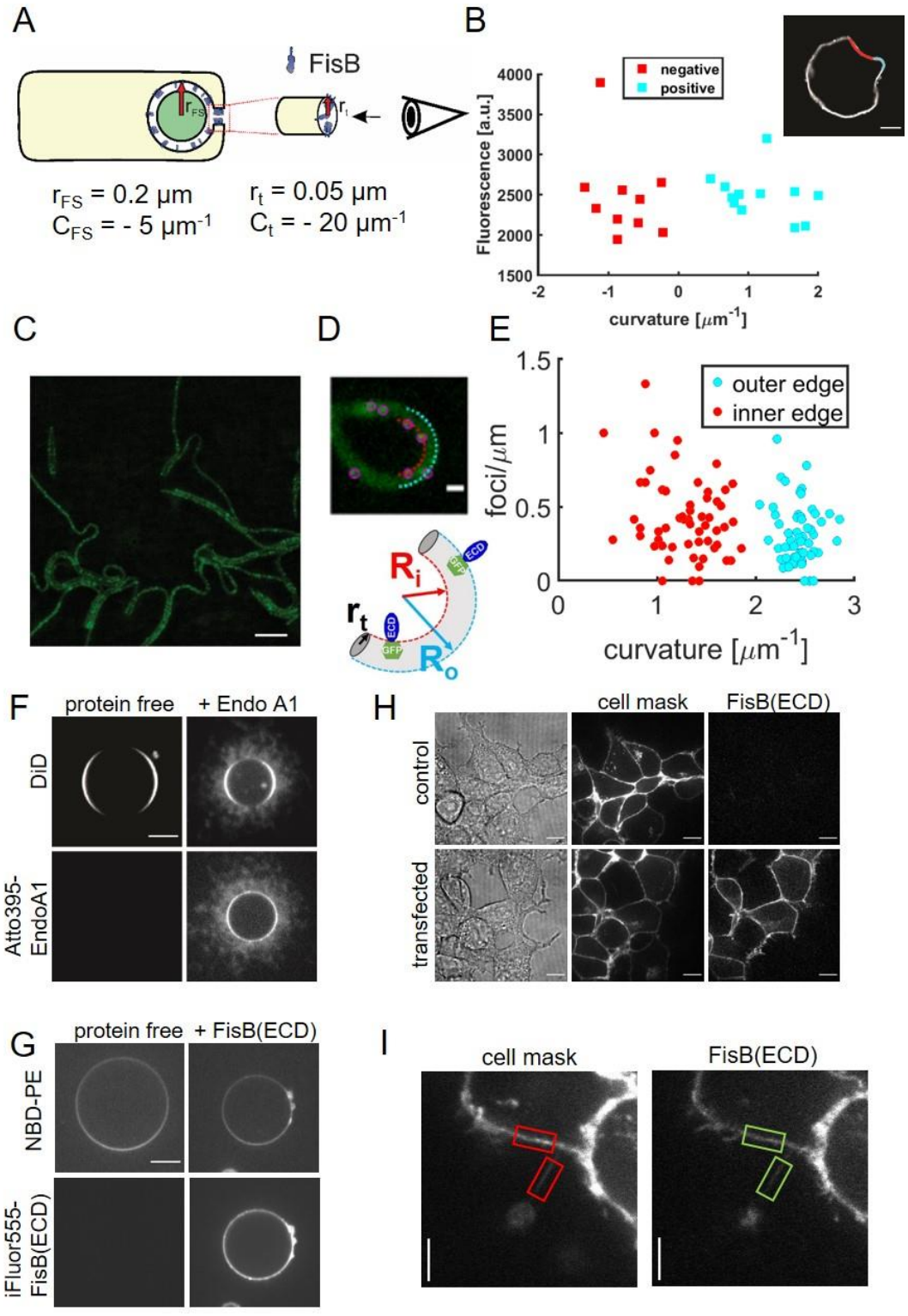

Figure 21. FisB does not sense or induce membrane curvature.

2.2.6 Interaction of FisB(ECD) mutants with artificial membranes

So far, we have shown that FisB self-oligomerization (GIII mutant) as well as lipid – binding (KK mutant) are important for localization of FisB to the fission site during sporulation. To gain insight into why these mutants fail to form a cluster at the membrane fission site, I tested the interactions of the mutant ECDs with GUV membranes. Similar to FisB(ECD) WT, the ECDs of the mutants were expressed and purified from *E. coli* and subsequently labeled with iFluor555 at position 123 (iFluor555-FisB^{GIII}(ECD) and iFluor555-FisB^{KK}(ECD)).

Based on our results in section 2.1.9, at low concentrations (<1 μM) we expected the GIII mutant to bind GUV membranes as well as WT but distribute more evenly since oligomerization is impaired. However, for the KK mutant we expected less binding, but clusters on GUVs as observed for WT. When I incubated 100 nM WT or mutant FisB(ECD) with GUVs composed of BS mix both mutants formed small mobile clusters at low concentration (Figure 22A), with potentially subtle differences that were not immediately obvious.

I plotted the iFluor555-FisB(ECD) fluorescence intensity along the contours of a few GUVs incubated with WT (left), GIII (middle) the KK(right) variants (Figure 22B, for more examples see Figure 31 in the Appendix). It appeared that the GIII mutant formed less and smaller clusters, while the overall fluorescence intensity was lower for the KK mutant, consistent with our expectations (section 2.1.10).

To better quantify clustering of FisB(ECD) variants on GUV membranes, I determined the mean fluorescence pixel intensity as well as the index of dispersion (ID) of iFluor555-FisB(ECD) fluorescence along the membrane contours for individual GUVs. The index of dispersion is a measure of fluctuations relative to the mean and is defined as the ratio of the variance to the mean:

$$ID = \frac{< (I - < I >)^2 >}{< I >}$$

where I is the fluorescence intensity and <> denote the averages over the contour length. A larger dispersion indicates larger fluctuations in fluorescence along the contour and hence more clustering of the protein. Only single free floating GUVs were analyzed, that is, GUVs which were attached to another GUV were excluded from this analysis.

I wrote a MATLAB script which first automatically detects GUV membranes (Figure 22C) using the lipid channel. The contour of a GUV membrane is binarized, then expanded to 10 pixels wide (Figure 22C,ii) This binary contour is used as a mask to compute the mean pixel intensity and the ID of protein fluorescence (Figure 22C, iii). I analyzed 46 GUVs incubated with WT FisB(ECD), 126 GUV incubated with the GIII mutant and 32 GUV incubated with the KK mutant. While the mean pixel fluorescence intensity was similar for WT ($1.26 \times 10^3 \pm 1.43 \times 10^3$, mean ± standard deviation) and KK ($1.91 \times 10^3 \pm 1.69 \times 10^3$), the intensity for the GIII ($0.48 \times 10^3 \pm 1.22 \times 10^3$) was lower (Figure 22D). Similar results emerged for the ID analysis. While no difference between WT ($5.80 \times 10^3 \pm 5.14 \times 10^3$) and KK ($4.51 \times 10^3 \pm 4.49 \times 10^3$) exists, the ID for the GIII mutant ($1.46 \times 10^3 \pm 1.58 \times 10^3$) is significantly lower (Figure 22E). Since the binding constants for WT and GIII for binding to negatively charged lipids are similar (chapter 2.1.9), we expected that the mean pixel intensity per GUV along the contour length should be similar, since the total amount of protein bound to the membrane should be the same. However, we observed that the mean pixel intensity per GUV is smaller for GIII than for WT. Usually where a protein cluster is found on the GUV, the fluorescence of the lipid channel is also enhanced. This could be due to FisB(ECD) mediating small local membrane deformations/folds or FisB(ECD)-mediated docking of smaller vesicles. If the GIII mutant has less ability to induce these kinds of deformations or aggregation, this would also result

into a reduced mean pixel intensity for the GIII mutant. Nevertheless, our expectation that the oligomerization-deficient GIII mutant display a lower ID was confirmed (Figure 22E).

The mean GUV intensity and ID for the KK mutant were similar to those for WT. While we expected to see a reduction in binding for the KK mutant, the similar mean GUV fluorescence intensity along the GUV contour as well as ID for KK and WT could be due to two reasons. First, every GUV analyzed, even from the same imaging chamber, showed a large range of protein coverages with some GUVs fully covered and others not covered at all. Therefore, no difference may have been observed simply because of the GUVs that were chosen to be analyzed. Secondly, another factor influencing the results is the labeling efficiency (see Materials and Methods). While the labeling efficiency was similar for WT and GIII (~75%) and therefore should not have an influence on the analyses, it was significantly higher for the KK mutants (~95 %). This higher labeling efficiency could be the reason why the mean GUV intensity is similar for WT and KK, even if the actual amount of protein bound to the GUV is lower for the KK mutants.

Our results so far suggest that the GIII mutant might be reduced in its ability to self-aggregate and or bridge membranes. Therefore, we I sought additional analyses and experimental approaches.

Figure 22. Interaction of FisB(ECD) WT and mutants with GUV membranes. ***(A)*** GUVs composed of BS where incubated with iFluor555-FisB(ECD) WT or mutants for 1h***. (B)*** Examples of GUVs incubated with 100 nM WT or mutant iFluor555-FisB(ECD) with their corresponding fluorescence intensity along the GUV membrane. ***(C)*** Schematic for determination of mean fluorescence intensity and ID for individual GUVS using MATLAB. The lipid channel (i) is used to create a mask (ii), which in turn is used to detect the protein fluorescence (iii) for a given GUV. ***(D)*** Cumulative distribution function of mean GUV intensity for WT and mutant iFluor555-FisB(ECD). ***(E)*** Cumulative distribution function of the index of dispersion (ID) for GUVs incubated with WT and mutant iFluor555-FisB(ECD).

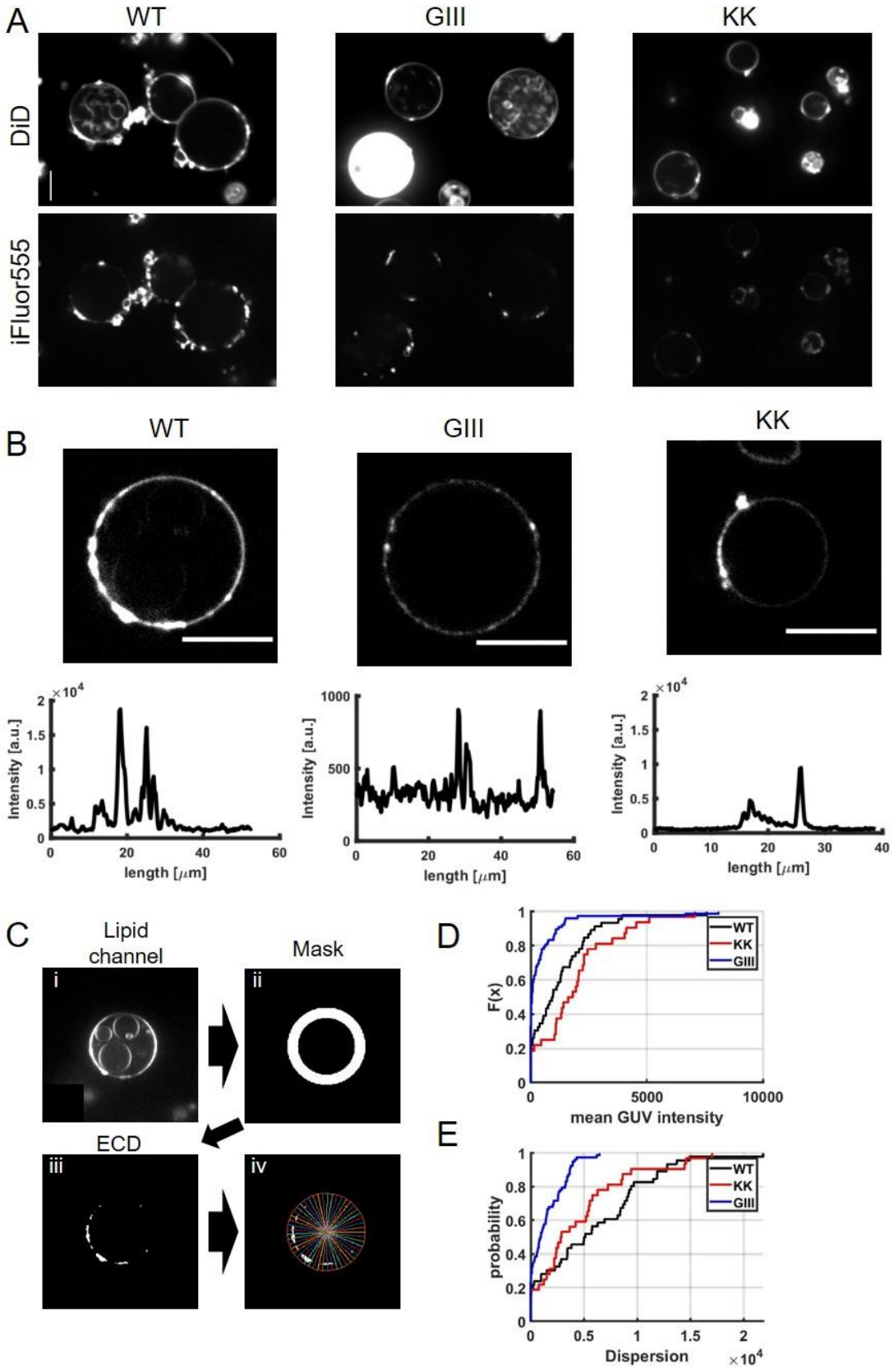

Figure 22. Interaction of FisB(ECD) WT and mutants with GUV membranes.

To further investigate if the mutants are reduced in their ability to bridge membranes, I used two different approaches. First, I determined the number of GUV doublets, triplets, etc. in each image for WT, GIII and KK as shown in Figure 23A, B and C. The presence of WT or mutant FisB(ECD) decreased the number of single free floating GUVs slightly while the number of GUVs attached to one or more GUVs increased. No clear difference between WT and mutants was observed. Using the Kolmogorov - Smirnov statistical test revealed that the distributions of WT and mutants are not significantly different.

It should be noted that all results and analyses shown in this section involving GUVs included data from only a single imaging chamber for each protein. To determine if there is an actual difference between WT and mutants in cluster formation and their ability to aggregate membranes, experiments and analyses would need to be repeated. Additionally, it would also be interesting to see if the mutants at high concentration would be able to aggregate GUVs as robustly as WT in the micropipette puffing experiments (chapter 2.2.4, Figure 19)

Second, I analyzed the ability of the mutants to aggregate SUVs as described in chapter 2.2.1. The absorbance of 50 μM (total lipid) SUVs composed of BS lipid mixture was measured for 5 min before WT or mutant FisB(ECD) was added to a total concentration of 1 μM (Figure 23D). Upon protein addition, SUVs start to aggregate, measured by an increase in absorbance at 350 nm. SUVs or proteins alone (Figure 23E) did not increase the absorbance significantly. The data for WT is copied from Figure 15D. While the increase in absorbance for WT and GIII mutant was similar, less aggregation was observed for the KK mutant. This is in line with our results that the binding affinity for acidic lipids of the KK mutant is about 10 – fold smaller compared to WT.

Similar aggregation for WT and GIII mutant could be due to the high protein concentration used. This might not be surprising if we assume that the ability of FisB(ECD)

to bridge membranes is linked to self-oligomerization. While self-oligomerization of GIII is reduced, it is not completely abolished as shown using SEC (chapter 2.1.9). 1 μM of GIII might therefore be enough to induce SUVs aggregation at similar levels compared to WT.

To determine if there is an actual difference in the ability of GIII, KK or WT protein to aggregate SUVs, this experiment would need to be carried out using a range of protein concentrations.

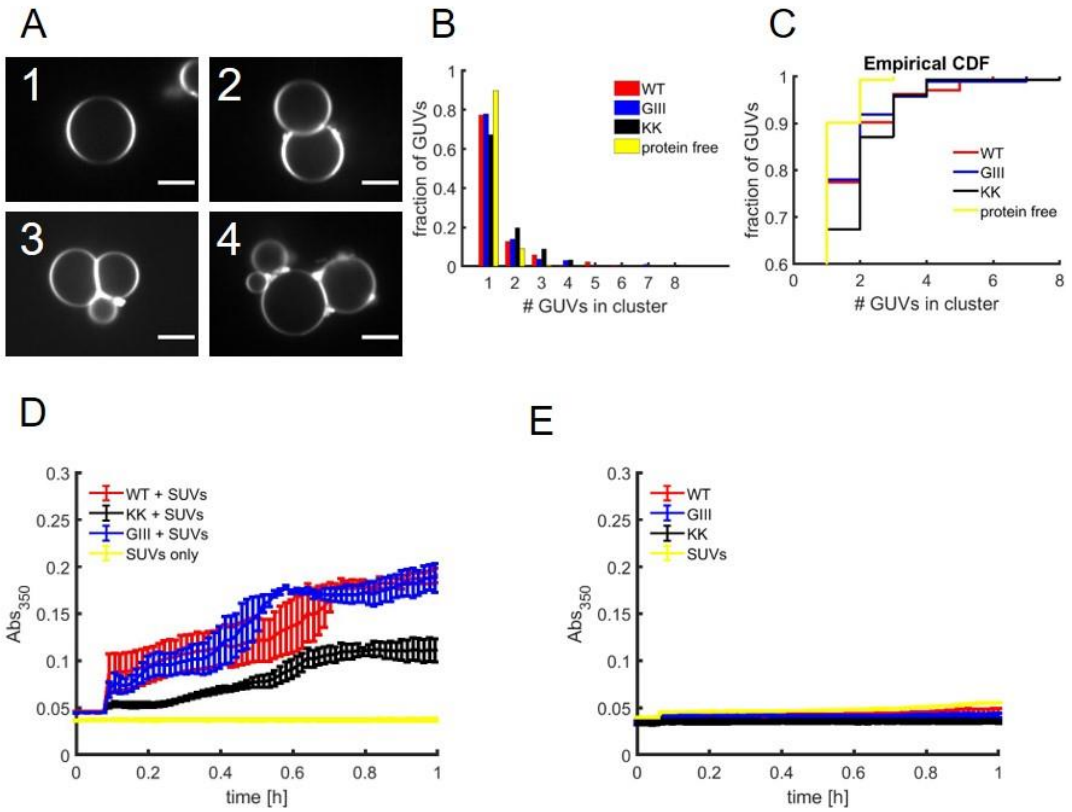

Figure 23. FisB(ECD) WT and mutants aggregate membranes of GUVs and SUVs. ***(A)*** Method for determining the number of GUVs in a cluster. A single free floating GUV is counted as 1, two GUVs attached to one another is 2, etc. ***(B)*** Fraction of GUVs that are single, double, etc..total number of GUVs counted: WT:133, GIII:186, KK:147, protein free: 141. ***(C)*** Empirical cumulative distribution function (CDF) of *(B).* (***D,E)*** SUVs aggregate upon addition of FisB(ECD) and WT. Absorbance (at 350 nm) of SUVs is measured. After 5 min, 1 μM of FisB(ECD) WT or mutants is added resulting in an increase in absorbance, indicating that SUVs are aggregating. No difference between WT and GIII mutant is observed. Reduced aggregation upon addition of the KK is consistent with the mutant being impaired in lipid binding. Proteins or vesicles alone do not aggregate. 3 independent experiments (mean ± SEM).

Finally, I tested if the GIII and KK mutants can form a stable network on GUV membranes similar to FisB(ECD) WT. When deflated GUVs composed of BS lipid mixture were incubated with 1 μM of mutant FisB(ECD), uniform labeling of GUVs was observed in all cases and the same large-scale deformations as with WT FisB(ECD) were formed (Figure 24A) . The percentage of GUVs showing these deformations was also comparable for WT and mutants (Figure 24B). Again, in order to observe a difference between WT and mutants, these experiments would need to be carried out using a range of protein concentrations.

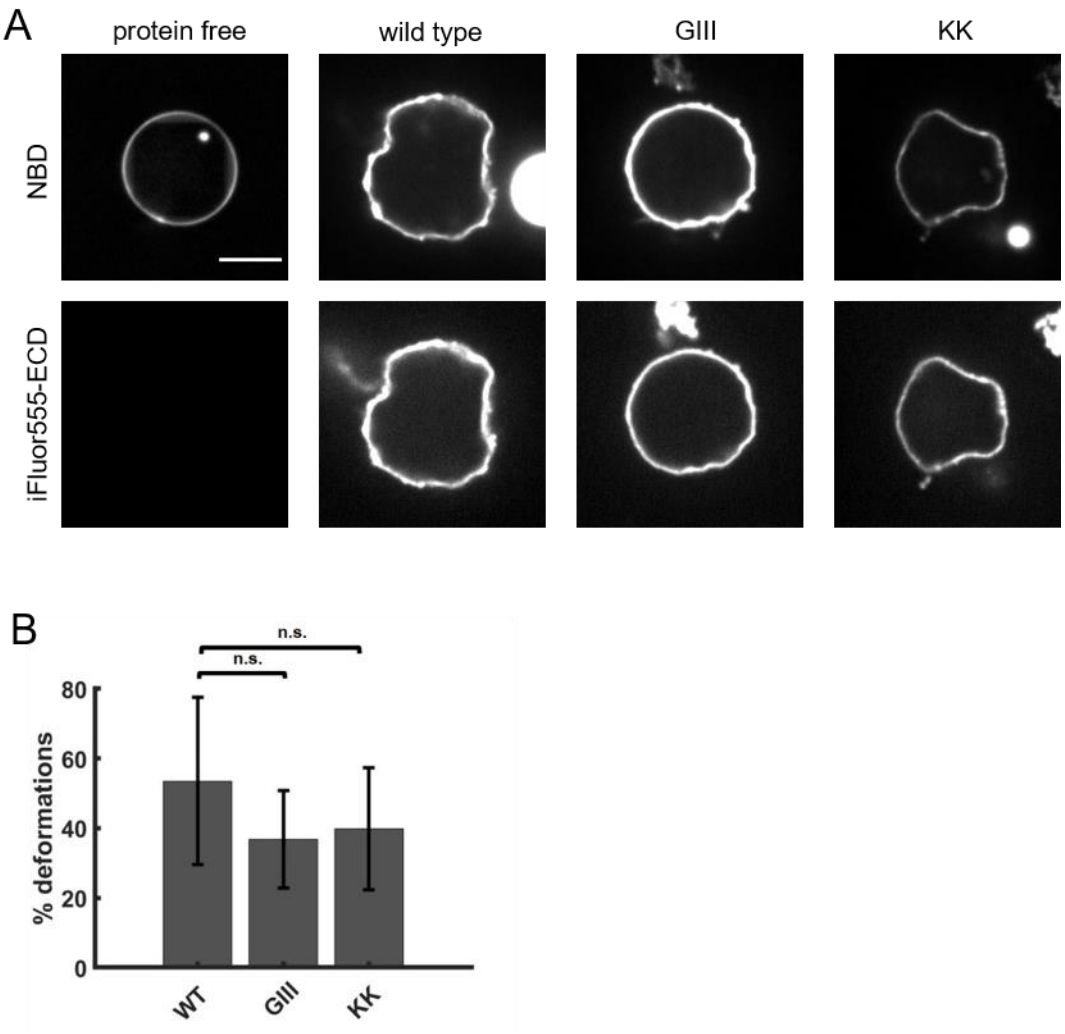

Figure 24. At 1 µM FisB(ECD) mutants also form a stable network on GUV membranes.*(A)* GUVs composed of BS were incubated with 1 µM of FisB(ECD) WT or mutants for 2h in the open imaging chamber. ***(B)*** Percentage of GUVs showing deformations after 2h. GUVs were incubated with either 1 µM of FisB(ECD) WT or mutants for 2h in the open imaging chamber.

2.2.7 Correlation between forespore size and membrane fission

Contribution statement: Images were acquired by Ane Landajuela. All analysis was carried out by me.

We showed that membrane fission during sporulation is always accompanied by a FisB cluster at the fission site (section 2.1.2). Formation of the FisB cluster at the fission site requires FisB self-oligomerization as well as lipid binding. However, we also noticed that forespores of post-fission cells are larger than forespores of pre-fission cells. To quantify the forespore surface area of pre- and post-fission cells, I first used the ImageJ plugin JFilament 2D to detect the outlines of forespores stained with TMA-DPH (Figure 25A, top). Using MATLAB, I then fitted an ellipse to the forespore outline (Figure 25B, dashed red line). Half of the forespore outline (solid red line) was finally rotated around the symmetry axis of the ellipse (blue line) to create a 3D surface (Figure 25C). In Figure 25D, I plotted the forespore area for pre- and post-fission cells 2.5h, 3h and 3.5h after sporulation was induced. We found that 3h after induction of sporulation the spore surface area of post – fission cells is on average 1.7 x larger than the spore surface area of pre – fission cells, suggesting a link between forespore size and membrane fission. To exclude any artifacts introduced through labeling with TMA-DPH, I also analyzed the forespore surface area by detecting the forespore outlines using a CFP forespore marker (Figure 25A, bottom) and obtained similar results. At T3 forespores of post-fission cells are about 1.4 x larger than forespores of pre-fission cells.

It was previously reported that forespores inflate during sporulation due to SpoIIIE-mediated DNA-translocation into the forespore thereby increasing the forespore turgor pressure. However, to the best of our knowledge, no link between forespore inflation and membrane fission has been reported. A model of how forespore inflation and FisB-mediated membrane fission could be linked will be described in the next section.

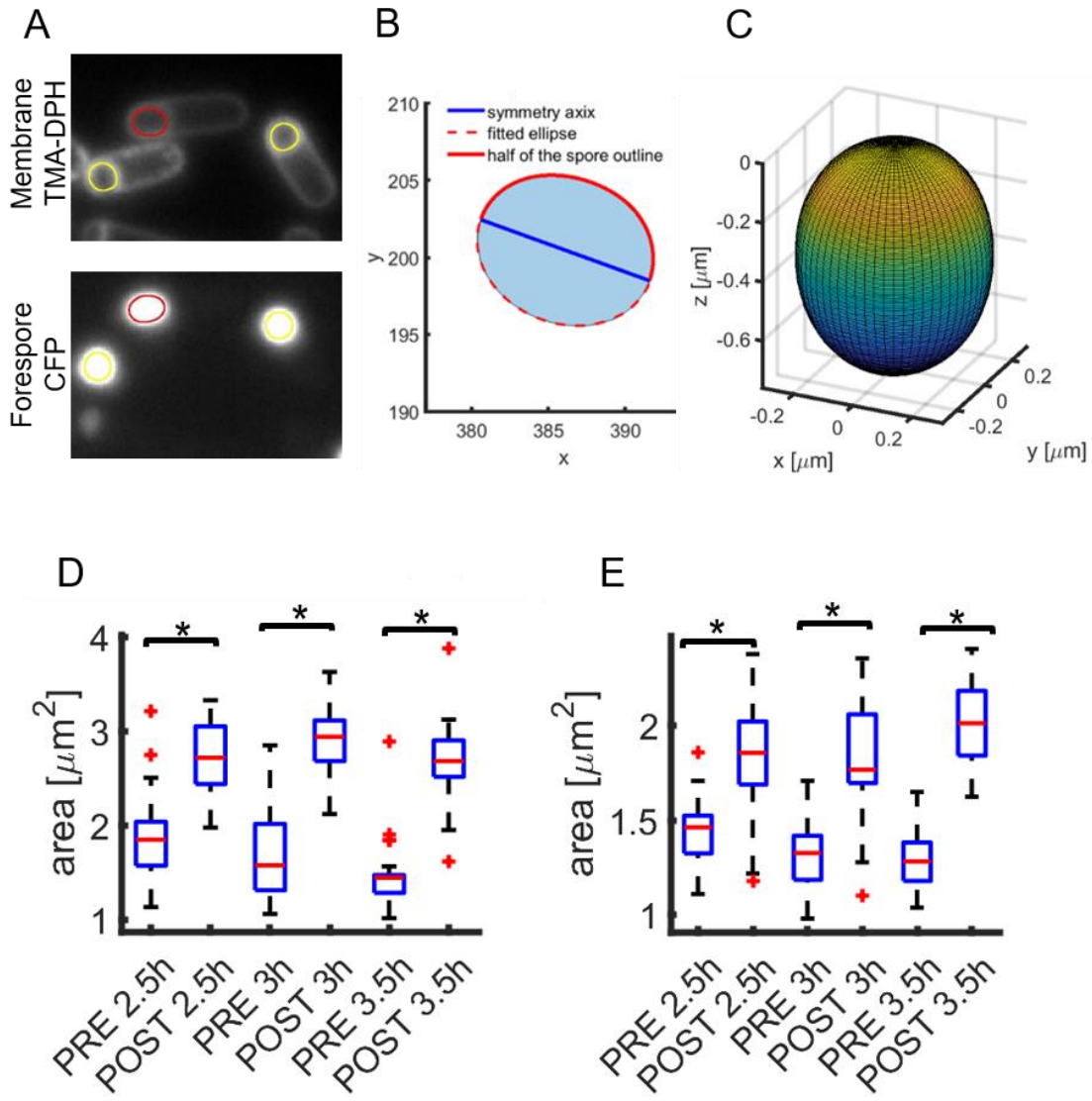

Figure 25. Determination of forespore surface area. ***(A)*** Top: Cells at T3 were stained with TMA-DPH to distinguish between pre- and post-fission cells. Bottom: The same cells also express CFP inside the forespores. Outlines of spores in both channels were detected by fitting snakes using the ImageJ plugin JFilament 2D [136]. Pre-fission cells are indicated in yellow, post-fission cells are indicated in red. ***(B)*** Outlines determined in *(A)* were further analyzes in MATLAB. First, an ellipse is fitted to the forespore outlines (red dashed line). ~ ½ of the forespore outline (solid red line) is then rotated around the symmetry axis of the ellipse (blue line) to create a 3D surface. x and y-axis are in pixel. ***(C)*** 3D surface of the spore shown in (B). ***(D)*** Spore surface area for pre- and post-fission cells at T2.5, T3 and T3.5 determined using the TMA-DPH channel. N=30 for each condition. ***(E)*** Spore surface area for pre- and post-fission cells at T2.5, T3 and T3.5 determined using the CFP channel in (A). Pre – and post fission cells were distinguish using the TMA-DPH stain. N=30 for each condition.

2.2.8 A possible mechanism for FisB mediated membrane fission

We found that forespores of post-fission cells are larger than forespores of pre-fission cells. During sporulation, SpoIIIE-mediated DNA-translocation into the forespore leads to forespore inflation. While the volume of the forespore increases, the volume of the mother cell decreases [42]. Therefore, lipids must flow from the peripheral mother cell membrane into the engulfing membrane through the membrane neck connecting the two regions (Figure 26 i). During engulfment, FisB forms small mobile clusters and we hypothesize that once a small FisB cluster reaches the membrane neck when engulfment is complete, it can interact with other FisB molecules and/or lipids in *trans* across the membrane neck (Figure 26 ii). These in *trans* interactions could trap a FisB cluster at the fission site. From our GUV experiments described in sections 2.2.1 and 2.2.1, we know that FisB can form a stable extended network on GUV membranes. We therefore propose that FisB forming a stable network at the membrane neck could resist membrane flow and FS inflation (Figure 26 ii). Increased resistance to lipid flow is likely to increase the probability of membrane fission by friction between the FisB molecules and the membrane (Figure 26 iii). Therefore, future work will test if forespore enlargement drives membrane fission by modulating forespore enlargement. This can be achieved by either inhibition of lipid synthesis by addition of the antibiotic cerulenin or by mutations in SpoIIIE that either abolish or slow down DNA transport into the forespore (see Outlook).

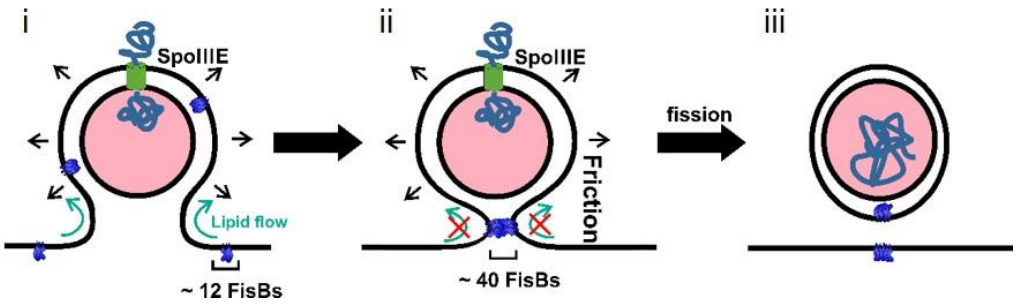

Figure 26. Possible mechanism for FisB mediated membrane fission. ***(i)*** During engulfment, FisB forms dim mobile clusters containing approximately 12 FisB molecules in the engulfment membrane as well as the peripheral mother cell membrane. Simultaneously, SpoIIIE transports DNA from the mother cell into the forespore which results into an increase in forespore size. This requires lipid flow from the mother cell into the forespore membrane through the membrane neck. ***(ii)*** When engulfment is complete, a large cluster of FisB (~ 40 molecules) can be found at the fission site. We propose that FisB gets trapped within the membrane neck by interacting with the membrane or other FisB molecules in *trans*. By forming a stable network in the membrane neck, FisB could resist membrane flow through the neck, which would result in friction, which if high enough, can lead to membrane fission ***(iii)***.

2.3 Discussion

Membrane fission is essential to all forms of life and it is still an active field of research. In recent years, an increasing number of membrane fission mechanisms has been described [1]. However, most of these studies were focused on eukaryotic proteins. While bacteria also rely on membrane fission for binary division and sporulation, studies of membrane fission mechanisms in bacteria are lacking. Our lab and collaborators previously showed that the protein FisB is required for membrane fission at the end of engulfment during sporulation in *B. subtilis* [38].

FisB localization to the fission site

When I started my thesis work, how FisB is recruited to the fission site and how fission is achieved was not known. We could not detect proteins interacting with FisB other than itself using an anti-GFP resin pulling on GFP-FisB [38]. Lipid microdomains (CL or PE), cell wall remodeling machinery, pH or voltage gradients across the membrane have all been described as factors guiding protein localization. However, our results suggest that none of these factors impact the localization of FisB and membrane fission. Surprisingly, we found that CL and PE, phospholipids that tend to form non bilayer structures and which have been implicated in membrane fission and fusion reactions, are not important for FisB localization and membrane fission. While these non-bilayer forming lipids might not be an absolute requirement for fission and fusion reactions, they usually affect the kinetics and/or the extent of fusion/fission. Still, the time course of membrane fission in cells lacking CL, PE or both were comparable to wild type *B. subtilis.*

In contrast, using mutagenesis, we found that FisB localization to the fission site requires FisB self-oligomerization as well as lipid-binding.

We found that the extracellular domain of FisB binds to acidic lipids non-specifically using electrostatic interactions involving residues within or close to the consensus domain. In addition to the bacterial lipids CL and PG, FisB(ECD) also binds to PS, a phospholipid usually not present in the membranes of *B. subtilis*. FisB(ECD) binds PG and CL with comparable affinity after adjusting for charge density and we therefore suspect that *in vivo* FisB is more likely to interact with PG as it is much more abundant (~50%) in the membrane than CL (~ 5%).

That lipid binding might be important for FisB's functions is supported by our result that the ECD of the FisB homolog of the thermophile *C. islandicus* also binds negatively charged lipids. While lipid binding might be a conserved property, we were unable to identify highly conserved positively charged residues between FisB homologs. Neutralizing or inverting only a single positively charged residue did not or only slightly affect lipid binding or sporulation efficiency. Only when multiple residues were mutated, we found that lipid binding was impaired *in vitro,* and that FisB failed to accumulate at the engulfment pole *in vivo*. We saw a 10-fold reduction in binding affinity and a reduction of membrane fission when positively charged residues within the consensus region where mutated (FisB(K168,170D) = $FisB^{KK}$). Importantly, $FisB^{KK}$(ECD) retained the ability to form oligomers. However, we did not look at these oligomeric structures using TEM. It would be interesting to see if these complexes resemble the wild type rod-like structures or if neutralizing the two lysines leads to structural changes which in turn could be responsible for reduced lipid binding and/or mislocalization of the protein.

We propose, that FisB binds membranes through a patch of positively charged residues (most likely within or close to the consensus sequence) on one site of the protein and that this interaction is important for FisB localization to the fission site. This hypothesis is further supported by our finding that a peptide corresponding to FisB(173-220) still binds CL containing liposomes via electrostatic interactions.

During sporulation, FisB forms small mobile clusters in the engulfing membrane. When engulfment is complete FisB forms a large immobile cluster at the fission site. Purified recombinant FisB(ECD) also forms soluble oligomers of various sizes. When we mutated highly conserved residues within the consensus domain, we were able to identify a mutant which is impaired in oligomerization *in vitro* ($FisB^{GIII}$(ECD)). *In vivo*, this mutant also fails to accumulate at the fission site suggesting that FisB self-oligomerization is important for localization of FisB to the site of membrane fission.

Together, the above results suggest FisB-FisB and FisB-lipid interactions are key drivers for FisB clustering and accumulation at the membrane fission site.

Many eukaryotic proteins involved in endocytosis and membrane fission sense and/or induce membrane curvature [1, 8, 137-139]. Examples include Bin/Amphiphysin/Rvs (BAR) domain proteins such as amphiphysin [130] or endophilin [140]. At low bulk concentration, these proteins preferentially localize to curved regions of membranes that match their intrinsic curvature. At high concentrations, binding of these proteins induces membranes to curve [141, 142]. However, our results indicate that FisB does not sense or induce membrane curvature. While endophilin induced tubulation of GUV membranes, addition of FisB(ECD) resulted in large scale deformations with no enrichment of FisB(ECD) within the curved regions. We did not see any enrichment of GFP-FisB to regions of higher membrane curvature in filamentous curved cells. Finally, we were unable to detect enrichment of Lyn11-mEGFP-sg-$FisB^{ECD}$ in membrane tethers pulled from HEK293 cells.

Using the curved filamentous *B. subtilis* cells, only a very small range of positive curvatures (0.5 – 3 μm^{-1}) can be tested. However, the curvature FisB encounters at the fission site is negative and approximately -20 μm^{-1}. While we were able to generate regions of much higher membrane curvature by pulling thin membrane tethers from

eukaryotic cells, the construct that we used (Lyn11-mEGFP-sg-FisB^{ECD}) may have been impaired in sensing membrane curvature. mGFP-FisB(ECD) alone was located in the cytosol and did not bind to plasma membrane of HEK cells, indicating that the GFP tag might hinder FisB(ECD) – membrane interactions. While these results imply that FisB does not sense or induce membrane curvature, more research is necessary to support this claim (see Outlook).

We propose that FisB's abilities to form a stable extended protein network and to bridge membranes, coupled with the unique geometry of the membrane neck at the end of engulfment may be sufficient for FisB accumulation at the fission site. *In vivo,* the only time FisB could interact with another FisB molecule or lipids in *trans* would be at the end of engulfment when a thin membrane tube is formed (Figure 27B). This idea is supported by our finding that no accumulation of FisB at the leading edge can be observed during engulfment until a thin neck has formed when engulfment is complete. Interaction of FisB with other FisB molecules and/or the lipids across the neck leads to formation of a stable FisB cluster. Once this stable interaction is formed, this cluster would be trapped and unable to leave the fission site. That FisB is able to form a large stable cluster is supported by our size exclusion chromatography results. When high molecular weight peaks collected from the initial chromatogram were re-injected into the column, no size redistribution was observed. Additionally, after a FisB(ECD) network on GUV membranes is formed, it is able to persist even when the membranes were dissolved with detergent. These results suggest that once formed, oligomeric structures of FisB are stable for an hour or longer.

Thus, FisB localizes to the site of membrane fission by utilizing the high membrane curvatures generated at the end of engulfment, without an intrinsic preference for curved membranes.

A model for FisB-mediated membrane fission

We found that membrane fission is always accompanied by a FisB cluster at the fission site. However, membrane fission in the ΔfisB strain is not completely abolished. At native expression, 3h after induction of sporulation about 80% of the cells have undergone membrane fission. At these expression levels about 40 FisB molecules have accumulated at the fission site. Lowering expression levels by ~8-fold also decreases the number of molecules accumulating at the fission site to about 6 copies [90]. In this case only 30% of cells have undergone membrane fission 3h after induction of sporulation. In the absence of FisB, ~5% of cells still undergo fission by T3, suggesting that FisB is not absolutely required for membrane fission and might help to catalyze the fission reaction, possibly by working together with another cellular process.

Since fission can be achieved with different numbers accumulated at the fission site together with our results that FisB forms clusters of various sizes *in vivo* indicates that FisB does not oligomerize into a defined quaternary structure with a definite stoichiometry. Our results are in line with observations that have been made for SNARE mediated membrane fusion [143-145] or dynamin mediated membrane fission [146].

During the time course of sporulation, the protein SpoIIIE translocates DNA into the forespore (Figure 26) [41] which is proposed to inflate the forespore [42]. Interestingly, our analysis shows that all cells that have undergone membrane fission have a 1.7 x larger forespore surface area then pre-fission cells suggesting a link between forespore size and membrane fission that has not been reported before. Previous research showed that the forespore volume increases at the expense of the mother cell and that lipid synthesis is required for this process [42]. In order to increase the size of the forespore, membrane would need to flow from the mother cell through the neck connecting the engulfment membrane to the rest of the mother cell membrane (Figure 26). Accumulation of FisB

inside the neck might form a barrier for lipid flow by forming a stable network. If the membrane cannot flow, stress might be created which ultimately could lead to membrane fission. This hypothesis is also supported by our finding that membrane fission can be achieved with various numbers of molecules at the fission site. At lower expression of FisB, less molecules accumulate at the fission site resulting in a delay in membrane fission. According to our model, membrane fission would be delayed, because in the presence of a lower number of FisB molecules at the fission site, more time is needed to create enough stress in the membrane neck for fission to occur.

We will test this hypothesis in the future by modulating forespore enlargement. To this end we will use SpoIIIE mutants and/or block lipid synthesis and correlate FisB cluster formation, forespore size and membrane fission (see Outlook).

In addition to DNA translocation of the chromosome into the forespore, SpoIIIE is also required to complete asymmetric division at the beginning of sporulation [147]. The Pogliano lab had previously suggested that SpoIIIE is also required for membrane fission that releases the forespore into the cytoplasm of the mother cell at the end of sporulation [43, 44]. They observed that cells lacking SpoIIIE are also defective in membrane fission. However, more recent studies showed that cells lacking SpoIIIE are impaired in engulfment, displaying bulged septal membranes or invaginations, which could prevent membrane fission [41, 148]. While SpoIIIE is a membrane protein, the bulk of the protein is located within the cytosol. During asymmetric division, SpoIIIE would facilitate membrane fission from the inside of the membrane neck. However, the membrane topology at the end of sporulation is reversed and SpoIIIE would have to facilitate membrane fission from the outside of the membrane neck. It is hard to imagine that any protein could mediate membrane fission from the inside as well as the outside of a membrane neck. Therefore, by linking SpoIIIE-mediated forespore inflation to FisB-

mediated membrane fission, we have explained the indirect role of SpoIIIE in membrane fission at the end of engulfment.

Finally, Ane Landajuela found that the FisB homologue of *Clostridium perfringens* can rescue sporulation in *B. subtilis* cells lacking FisB, despite only 23 % sequence identity [90] which ultimately supports the idea that FisB may act as an independent module which only relies only on self-oligomerization and lipid binding for localization to the fission site. Friction between the FisB cluster and the underlying membrane upon forespore inflation could, if high enough, lead to membrane fission.

Comparison with other membrane fission proteins

While FisB shares some characteristics with well-known eukaryotic membrane fission proteins such as the ESCRT machinery or the endocytic proteins dynamin and endophilin, it does not show any sequence homology and therefore might represent a new class of fission proteins. Similar to dynamin or proteins or the ESCRT machinery, FisB forms oligomers both *in vivo* and *in vitro* and we showed that this property is important for FisB localization to the fission site. While endophilin and dynamin assemble on the outside of a membrane neck (Figure 27D and F), proteins of the ESCRT machinery assemble on the inside of a membrane neck to mediated fission (Figure 27E). Since most of FisB faces the extracytoplasmic space, from a topological standpoint, FisB might work similar to the ESCRT proteins. However, it was shown that the ESCRT-III snf7 and its homologs assemble into spirals *in vitro* while FisB assembles into flexible rod-like structures, although those need more characterization.

Endocytic proteins, ESCRT proteins and FisB have in common that they all bind to acid lipids. The ESCRT machinery is involved in diverse cellular membrane fission reactions such as multivesicular body (MVB) genesis [149, 150], cytokinetic abscission [151], autophagy [152] and budding of some enveloped viruses from the host membrane [153].

Phosphoinositides were shown to direct the ESCRT machinery to different subcellular locations. For example, the ESCRT machinery is targeted to endosomes for MVB vesicle formation by interaction with the endosome-specific phospholipid PI(3)P [154, 155]. However, during HIV-1 budding, ESCRT proteins are directed the plasma membrane through interaction with $PI(4,5)P_2$ [156].

During clathrin-mediated endocytosis (CME), $PI(4,5)P_2$ and PS are enriched in the plasma membrane where endocytic sites form. While PS is involved in localizing endocytic proteins to the membrane and for initiation of endocytosis [157], $PI(4,5)P_2$ was shown to be required for endocytic membrane invagination but less important for initiation of endocytosis [157]. Additionally, the pleckstrin homology (PH) domain of dynamin also binds to $PI(4,5)P_2$ and PI(4)P [158]. This interaction is important for activation of dynamin's GTPase domain. In the absence of the PH domain the GTPase domain cannot be activated by $PI(4,5)P_2$ and membrane fission is inhibited [159]. The picture emerges that specific lipids seem to be required for targeting proteins of the ESCRT pathway and endocytic proteins to a certain subcellular localization and are required for the fission reaction. While we showed that lipid binding is required for targeting FisB to the fission site, a specific lipid was not required. Removing lipids previously implicated in membrane fission reactions (CL and PE) did not affect FisB localization and membrane fission. Additionally, membrane fission by dynamin or the ESCRT machinery requires a cellular energy source, whereas no ATP or GTP binding site was identified for FisB.

During clathrin-independent endocytosis (CIE), the N-BAR domain containing protein endophilin A2 was shown to mediate membrane fission through membrane friction [8, 160] (Figure 27F). Endophilin A2 can form a protein scaffold on a membrane tube, which generates a frictional barrier for diffusion of lipids. Upon elongation of this tube by molecular motors, friction between the protein scaffold and the underlying membrane leads to an increase in membrane tension and finally membrane fission. We hypothesize

that FisB mediates membrane fission in a similar way. An increase in forespore size upon SpoIIIE mediated chromosome transfer into the forespore causes the engulfment area to increase, which in turn drives lipid flow from the mother cell membrane into the engulfment membrane though the membrane neck (Figure 27C). FisB forming a stable network in the membrane neck might resist membrane flow, resulting in membrane friction and subsequently could lead to fission.

Finally, in contrast to the other proteins, FisB is the only protein with a transmembrane domain. While the role of the TMD is still unclear, it might simply be to attach the extracellular domain to the membrane to avoid its loss in the extracellular space.

Altogether, we have shown that FisB localization to the fission site requires FisB-FisB and FisB-lipid interactions. We hypothesize that FisB accumulates at the fission site by interacting with other FisB molecules and/or lipids across the membrane neck at the end of engulfment. Due to this in *trans* interaction, the FisB cluster gets trapped and would be unable to leave. Thus, FisB localizes to the fission site by exploiting the membrane geometry at the fission site without relying on an intrinsic membrane curvature preference. Finally, our results indicate that membrane fission and forespore inflation are linked. Since forespore inflation requires lipid flow from the mother cell into the forespore, we propose that by forming a stable network at the fissions site, FisB opposes lipid flow, leading to increased stress in the membrane neck and ultimately membrane fission.

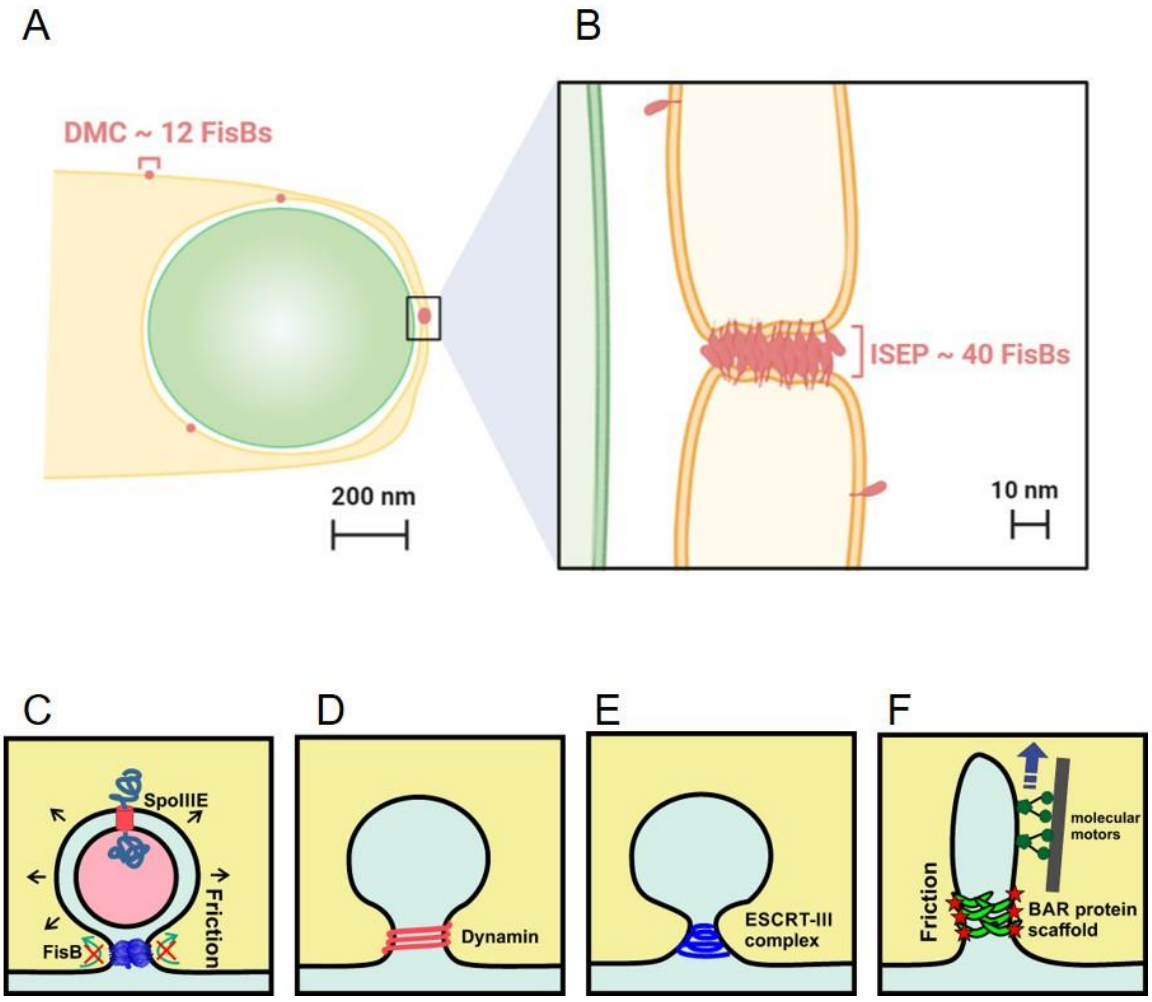

Figure 27. Comparison of FisB with eukaryotic fission proteins. **(*A)*** Schematic of completed engulfment, when a small fission pore connects the engulfment membrane to the rest of the mother cell membrane. ***(B)*** Schematic of FisB accumulation at the fission site. FisB freely moves around the engulfment membrane and other regions of the mother cell membrane in clusters of ~12 molecules. These motions are independent of lipid microdomains, flotillins, the cell-wall synthesis machinery, and voltage or pH gradients. About 40 copies of FisB accumulate at the fission site into an immobile cluster, possibly because leaving this region would require disruption of the cluster. We cannot exclude the presence of FisB monomers, which are below our detection limit (~3-4 mEGFP molecules). ***(C-F)*** **Comparison of fission proteins.** ***(C)*** FisB forms an immobile cluster at the fission site. DNA translocation into the forespore, increases the forespore size and requires lipid flow from the mother cell into the forespore. FisB restricts lipid flow and generates frictions which if high enough can lead to fission. ***(D)*** Dynamin polymerizes around the membrane neck from the outside. Upon GTP hydrolysis, a conformational change in dynamin mediates membrane fission. ***(E)*** Proteins of the ESCRT-III complex polymerize inside the membrane neck in form of an inward growing spiral to mediate membrane fission. ***(F)*** Pulling forces exerted by molecular motors induce friction between a BAR protein scaffold and the membrane neck which results in membrane fission.

2.4 Outlook

FisB curvature preference

We found that FisB self-oligomerization as well as lipid binding are required for FisB localization to fission site. While several of our results imply that curvature does not play a role in FisB localization, more research is necessary to rigorously support this claim. As mentioned above, the range of curvatures we were able to test using curved filamentous cells was very small (0.5 – 3 μm^{-1}) and different from the curvatures FisB encounters during sporulation (approximately -20 μm^{-1}). We were able to generate regions of much higher membrane curvature by pulling thin membrane tethers from eukaryotic cells but the construct that we used (Lyn11-mEGFP-sg-FisB^{ECD}) may have been impaired in sensing membrane curvature. mGFP-FisB(ECD) alone did not bind to the plasma membrane of HEK293 cells and was cytosolic, indicating that the GFP tag might hinder FisB(ECD) – membrane interactions. In the future we will try different C- or N-terminal tags, such as SNAP-tag [133] or FlAsH-tag [134] in combination with different linker lengths between the tag and FisB(ECD) to identify a construct that binds to the plasma membrane of eukaryotic cells own its own a repeat the tether pulling experiments.

If we are unable to identify a membrane binding construct, we will continue our efforts to investigate the curvature preference of FisB by pulling membrane tethers from giant *B. subtilis* protoplasts expressing FisB or GUVs with reconstituted FisB. To this end, I successfully established a protocol for generating giant *B. subtilis* protoplasts expressing FisB full-length, which can be aspirated by micropipettes (Figure 28C). As described in section 2.2.5, I created a strain (BMB014) in which we can express GFP-FisB from an inducible promoter during vegetative growth (Figure 28A, left). In the same strain, cell division can be blocked with addition of xylose which induces the expression of MciZ which in turn leads to long filamentous cells (Figure 28A, right). Finally, the cell wall can be

digested with lysozyme, resulting in giant *B. subtilis* protoplasts with a diameter of 5 – 10 µm which can be aspirated by micropipettes (Figure 28C). From these protoplasts we will try to pull a membrane tether using a latex bead held by optical tweezers and observe FisB localization. However, in contrast to what is shown in Figure 28D, the larger part of FisB would face outside into the extracellular space. Only if FisB would be depleted from the tether, it would indirectly show that FisB prefers less curved membranes or even negative membrane curvature. However, these experiments might still be informative even if FisB does not specifically localize to or is excluded from the tether (see below).

FisB uses membrane friction to mediate membrane fission

The force needed to pull a tether from a protoplast can be calculated by the displacement of the bead from the center of the optical trap. Breaking of a tether can be detected by a sudden drop in the force with which the tether pulls on the bead. Additionally, breaking of the tether can be determined by imaging.

If friction between a FisB scaffold and the membrane helps to achieve membrane fission, tethers should break easier in the presence of FisB. However, as mentioned above, the ECD faces outside the cell and FisB-FisB as well as FisB-lipid interactions across the thin membrane tube may be necessary for FisB localization to the tether and friction mediated membrane fission. Therefore, to mimic the membrane geometry FisB encounters during sporulation the ECD would have to face inside the cell (Figure 28D).
To achieve the correct topology, we tried using GUVs instead of giant *B. subtilis* protoplasts. However, encapsulation of FisB(ECD) inside GUVs by electroformation [161] or inverted emulsion [162] was unsuccessful (see Appendix). Encapsulating a maleimide dye using inverted emulsion was successful. However, when FisB(ECD) was used, no GUVs formed or no protein encapsulation was observed. However, I only tested GUVs containing 15 % CL and 85% eggPC and protein concentrations > 250 nM. It is possible that FisB(ECD) somehow prevents GUV formation by interacting with the lipids. Varying

the lipid composition as well as adjusting the protein concentrations could potentially help with encapsulating FisB(ECD).

We will also further test our hypothesis that FisB mediates membrane fission by friction *in vivo*. We hypothesized that an increase in forespore area upon DNA translocation into the forespores requires lipid flow from the mother cell into the engulfing membrane. FisB may form a stable network at the fission site and restrict membrane flow, which in turn would lead to friction between the FisB network and the membrane and thereby facilitating membrane fission. To further test this hypothesis, we will modulate the increase in forespore size by using mutants of SpoIIIE. A point mutation of SpoIIIE (SpoIIIE36) still binds DNA but is impaired in DNA translocation into the forespore [163] and therefore forespore inflation is impaired. In this mutant, FisB levels were not affected [38]. We found that membrane fission always occurs in the presence of a FisB cluster at the fission site. If however forespore inflation is required for membrane fission, we should be able to observe a FisB cluster at the fission site without membrane fission in a strain in which forespore inflation is inhibited. Additionally, we will also use SpoIIIE(D584A) in which DNA transport is significantly slower than in WT cells [41]. If our hypothesis is correct, slowing down DNA transport should also slow down membrane fission. Since forespore enlargement also requires lipid synthesis, another way to modulate the forespore size is by controlling lipid synthesis [164]. This could be achieved by the addition of the antibiotic cerulenin which inhibits fatty acid synthesis [165].

Figure 28. Method for generating giant *B. subtilis* protoplasts. ***(A)*** BMB014 cells expressing GFP-FisB during vegetative growth. Upon addition of 1% xylose to the media, cells express MciZ. MciZ blocks cell division, leading to long filamentous cells with multiple GFP-FisB foci. ***(B)*** Addition of 1 mg/ml lysozyme to the cells in (A) removes the cell wall and leads to the formation of round protoplasts with a diameter of ~ 5-10 µm. Cell membranes are stained with CellMask™ Deep Red. ***(C)*** Example of a protoplast from *(B)* aspirated into a micropipette. ***(D)*** Schematic representation of an *in vitro* assay to study membrane fission and curvature preference of FisB. FisB full-length is reconstituted into membranes of GUVs. Alternatively, the ECD could be encapsulated. A thin membrane tether is pulled from the GUV using a latex bead and optical tweezers (OT) and protein localization can be analyzed using fluorescence.

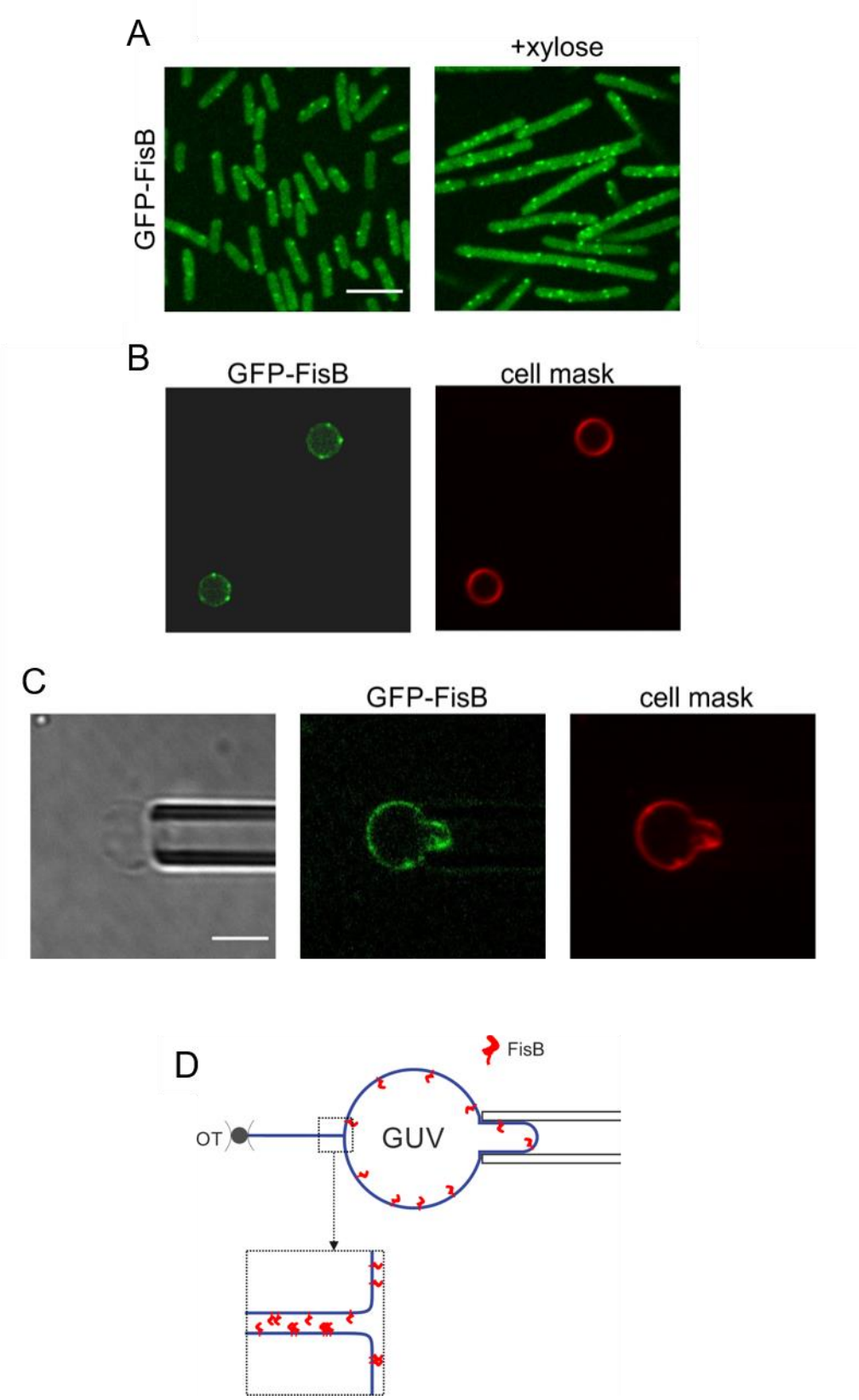

Figure 28. Method for generating giant *B. subtilis* protoplasts.

3 Materials and Methods

3.1 Materials

E. coli cardiolipin (CL), *E. coli* L-α-phosphatidylglycerol (PG), egg L-α-phosphatidylcholine (eggPC), *E. coli* L-α-phosphatidylethanolamine(PE), 1,2-dioleoyl-sn-glycero-3-phosphoethanolamine-N-(7-nitro-2-1,3-benzoxadiazol-4-yl) (NBD-PE), 1,2-dioleoyl-sn-glycero-3-phosphoethanolamine (DOPE), 1,2-dioleoyl-sn-glycero-3-phosphocholine (DOPC), 1,2-dioleoyl-sn-glycero-3-phospho-L-serine (DOPS) were purchased from Avanti Polar Lipids.

1-(4-Trimethylammoniumphenyl)-6-Phenyl-1,3,5-Hexatriene *p*-Toluenesulfonate (TMA-DPH) and *N*-(3-Triethylammoniumpropyl)-4-(6-(4-(Diethylamino) Phenyl) Hexatrienyl) Pyridinium Dibromide (FM™ 4-64 Dye) were from Thermofisher Scientific.

Molybdenum Blue spray reagent was from Sigma.

Carbonyl cyanide *m*-chlorophenyl hydrazone (CCCP), Valinomycin and zaragozic acid were purchased from Sigma. 4-acetamido-4′-maleimidylstilbene-2,2′-disulfonic acid (AMS) and zaragozic acid were from obtained from Cayman Chemical. Carbonyl cyanide m-chlorophenyl hydrazone (CCCP) and Valinomycin were purchased from Abcam and VWR. 3-(N-maleimidylpropionyl) biocytin) was from Invitrogen and the HRP-conjugated antibody from eBioscience.

3.2 Methods

3.2.1 Generation of *B. subtilis* Strains

B. subtilis strains were derived from the prototrophic strain PY79 [166]. Lipid synthesis mutants were obtained from the *Bacillus* knock-out (BKE) collection [167] and all were back-crossed twice into *B*. *subtilis* PY79 before assaying and prior to antibiotic cassette

removal. Antibiotic cassette removal was performed using the temperature-sensitive plasmid pDR244 that constitutively expresses Cre recombinase [167]. Cassette removal was further confirmed by PCR with primers flanking the deletion.

Other *B*. *subtilis* strains were constructed using plasmid or genomic DNA and a 1-step competence method. Briefly, a freshly streaked colony is used to inoculate 1 ml 1XMC (100 mM potassium phosphate pH, 7.03 mM sodium citrate, 2% glucose 22 mg/ml ferric ammonium citrate, 0.1% casein hydrolysate, 0.2 % potassium glutamate, 3 mM $MgSO_4$) and grown at 37°C for 4 h to create competent *B. subtilis* cells. 2 µl and 1:20 and 1:400 dilutions of either plasmid DNA (obtained from *E. coli* using QIAprep Spin Miniprep Kit (#27104)) or *B. subtilis* genomic DNA were added to 20 – 200 µl of competent cells and the transformation in grown for another 2h at 37°C. Finally, the entire transformation is plated on selective LB plates overnight at 37°C.

Site directed mutagenesis of plasmids was performed using Agilent's Quick-change Lightning kit (#210518) following manufacturer's instructions and mutations were confirmed by sequencing. The strains and plasmids used in this study are listed in Tables 1 and 2, respectively.

3.2.2 Overnight cultures of *B. subtilis*

Overnight cultures of *B. subtilis* strains were prepared by inoculating 5 ml of CH medium [168] with a freshly streaked colony. 1:5 and 1:25 dilutions were prepared, and all cultures were grown overnight at 22°C. The next morning the OD_{600} of all cultures is measured and only cultures that were in mid-log phase (OD_{600} = 0.4 - 1.0) were used in further experiments.

3.2.3 Sporulation by resuspension (synchronous sporulation)

Synchronous sporulation was induced by the method of Sterlini-Mandelstam [168]. An overnight culture was diluted in fresh CH medium to OD_{600} = 0.05 and grown at 37˚C until cultures reached mid-log phase (0.5-0.9). Cells were harvested by centrifugation for 5 min at 5 krpm in a room temperature centrifuge. To induce sporulation, the cell pellet was resuspended in an equal volume of Resuspension Medium [168] and transferred back to the original flasks. The cultures were returned to 37˚C. This is T_0 of sporulation. Accordingly, T1, T2 and T3 represent 1h, 2h and 3h after induction of sporulation.

3.2.4 Substituted Cysteine Accessibility Method (SCAM)

We used SCAM to determine the orientation of FisB within the membrane. Strains BMB034, BMB0035, BM0B36 were used to assess if residues C6, C137 and C245 were intra- or extracellular. SCAM relies on sulfhydryl-reactive membrane impermeable labeling reagents 3-(*N*-maleimidylpropionyl) biocytin (MPB, biotinylating reagent) and 4-acetamido-4′-maleimidylstilbene-2,2′-disulfonic acid (AMS, blocking reagent). For each strain, 500 ml of cells were harvested at T2.5 of sporulation and washed 2 x with protoplasting buffer (20 mM maleic acid, 20 mM MgCl2, 0.5 M sucrose). Protoplasts were created by addition of 0.5 mg/ml lysozyme and incubation at 37°C for 1h with gentle rocking. For each strain, cells were labeled under 3 different conditions:

1) To test if cysteines were accessible to biotinylation by MPB, protoplasts were lysed with a hypotonic shock using Buffer H (20 mM HEPES pH, 200 NaCl, 10 µg/ml DNase I and 20 µg/ml RNAse A) and subsequently incubated with 100 µM MPB for 1 h at room temperature with gentle rocking. The reaction was quenched with 50 mM DTT.

2) For labeling of extracellular cysteines only, protoplasts were made as described above but cells were not lysed. Cysteines in the extracellular space were labeled by adding

100 μM MPB during removal of the cell wall with lysozyme and for an additional 30 min. The reaction was quenched by addition of 50 mM DTT before cells were lysed with a hypotonic shock as described above.

3) For labeling intracellular cysteines, extracellular cysteines of protoplasts were blocked with 2 mM AMS for 30 min in the dark. AMS was removed by washing the protoplasts 3x with protoplasting buffer before cell lysis. 100 μM MPB is added to biotinylate any unblocked cytoplasmic cysteines. The reaction is quenched with 50 mM DTT.

For all conditions, membrane proteins were isolated from the cell lysates by ultracentrifugation at 100 000 x g for 1h at 4°C. The pellet was then solubilized in Buffer S (Buffer H + 20% glycerol, 100 μg/ml lysozyme, 0.5% digitonin, 2%LDAO) by vortexing the sample for 1h at room temperature. After solubilization, FisB was pulled down as described in [85]. Briefly, the samples were incubated with Anti-Myc antibody (mAb #2276) overnight at 4°C. Protein A/G-agarose affinity resin was added and incubated at 4°C for 1.5h. The resin was washed with 1 ml of IP1 (50 mM Tris–HCl, pH 8.1, 0.15 M NaCl, 1 mM EDTA, 2% LDAO, 0.4% SDS), vortexed for 1 min, washed with 1ml IP2 (50 mM Tris–HCl, pH 8.1, 1 M NaCl, 1 mM EDTA, 2% LDAO, 2%, 0.4% SDS), vortexed and finally washed with 10 mM Tris–HCl, pH 8.1. 50 ul of SDS sample buffer was added and the sample was vortexed for 15 min at room at room temperature, incubated 15 min at 37°C and again vortexed for 15 min. The resin was spun down and the supernatant, which contains FisB, is collected and analyzed by Western Blot.

3.2.5 Western Blot

To access if a cysteine was labeled with MPB, the samples were subjected to Western Blot analysis. Proteins were transferred onto a PVDF membrane using the

XCell II Blot Module (Thermo Fisher Scientific) for 1.5h, 30 V at room temperature. The membrane was blocked for 1h at room temperature with TBST (20 mM Tris pH 7.6, 150mM NaCl, 0.1 % (w/v) Tween® 20) containing 5% milk. The membrane was washed 3 x 5 min with TBST. Avidin-HRP was added at a final dilution of 1:5000 from 2 mg/ml stock in TBS containing 0.3% BSA and incubated for 1h at room temperature. The membrane was washed 6 x 5 min with TBST and developed with Pierce ECL Western Blotting Substrate and biotinylated proteins were detected using chemiluminescence. The membrane is then stripped, blocked, washed, and incubated overnight at 4°C with anti-FisB antibody [38] at a dilution of 1:5000. After washing, the blot was incubated with the secondary antibody (Thermo Fisher Scientific #31460) for 1h. After washing the blot was developed and FisB was visualized using chemiluminescence.

3.2.6 Inhibition of cell wall synthesis and analyses of FisB motions

Overnight cultures of BDR2061 or BMB014 were diluted in CH medium to OD600 = 0.05. Expression of GFP-FisB was induced with 1 mM IPTG for 2h at 37°C. Expression of GFP-Mbl was induced with 10 mM xylose for 30 min after BDR2061 reached OD600 = 0.5. For imaging untreated cells, 1 ml of cells was washed twice with 1 ml PBS and finally resuspended in 10 µl PBS. 2 µl of cell suspension was spread on a 2% PBS agar pad for imaging. To inhibit cell-wall synthesis 50 µg/ml fosfomycin was added to the cultures 45 min before imaging. 1 ml of cells was washed twice with PBS containing 50 µg/ml fosfomycin and mounted on a PBS agar pad also containing 50 µg/ml fosfomycin. Cells were imaged using a Olympus IX81 microscope with a home-built polarized TIRF setup [169]. Exposure times were 50 ms for BDR2061 and 100 ms for BMB014. Movies were acquired at 1 frame/s. Movies collected for BMB014 were corrected for bleaching using the Bleaching Correction function (exponential method) in ImageJ. Kymographs were

created with ImageJ along the indicated axes. GFP fusion proteins were tracked using the ImageJ plugin TrackMate [135]. A Laplacian of Gaussian (LoG) filter was used to detect particles with an estimated blob diameter 400 μm. Particles were tracked using the Simple LAP tracker with a 0.25 μm maximum linking distance and no frame gaps. MATLAB (Mathworks, Natick, MA) was used for further processing of the tracks. Mean squared displacement (MSD) was calculated using the MATLAB class @msdanalyzer [170].

The asymmetry of individual tracks was calculated as described in [103] using:

$$Asym = -log\left(1 - \frac{(R_1^2 - R_2^2)^2}{(R_1^2 + R_2^2)^2}\right)$$

where R_1 and R_2 are the principal components of the radius of gyration, equal to the square roots of the eigenvalues of the radius of gyration tensor R_g:

$$\boldsymbol{R_g(i,j) = \langle x_i x_j \rangle - \langle x_i \rangle \langle x_j \rangle.}$$

3.2.7 Dissipation of membrane potential

Cells were concentrated by centrifugation (3300xg for 30 s) and 100 μM CCCP or 30 μM valinomycin was added just prior to mounting cells onto a 2% PBS agar pad also containing 100 μM CCCP or 30 μM valinomycin.

3.2.8 Thin Layer Chromatography (TLC)

Lipids were extracted from *B. subtilis* cells at T3 of sporulation according to the method of Lacombe and Lubochinsky [171]. Lipid extracts were analyzed by TLC on silica gel plates in mixtures of chloroform:hexane:methanol: acetic acid (50:30:10:5). Phospholipids were detected with Molybdenum Blue Reagent (Sigma-Aldrich).

3.2.9 Determination of sporulation efficiency (Heat Kill assay)

A freshly streaked colony was used to inoculate 2 ml of $DSM_{complete}$(0.8 % (w/v) Difco Nutrient Broth, 1 mM $MgSO_4$, 13.2 mM KCl, 0.5 mM NaOH, 1mM $Ca(NO_3)_2$, 10 μM $MnCl_2$, 1 μM $FeSO_4$) in an 18 x 150 mm glass test tube and incubated for 24 – 36 hours at 37˚C. The culture was serially diluted 6 times (10^{-1} - 10^{-6} dilution) in Dilution Medium (150 mM $NH_4)_2SO_4$, 0.8 M K_2HPO_4, 0.44 M KH_2PO_4, 34 mM $Na_3C_6H_5O_7 \cdot 2H_2O$,1 mM $MgSO_4$). To kill non-sporulated cells, the serial dilutions were placed in an 80˚C water bath for 20 min. Heat resistant, colony forming units were determined by plating the dilutions on DSM agar plates. Agar plates were incubated at 37˚C overnight and colonies were counted the next day. Sporulation efficiency is determined as spores/WT spores.

3.2.10 Determination of membrane fission efficiency

To determine the percentage of cells that have undergone membrane fission, the membranes of sporulating cells were stained with 1-(4-trimethylammoniumphenyl)-6-phenyl-1,3,5-hexatriene p-toluenesulfonate (TMA-DPH; Molecular Probes) at a final concentration of 100 μM. TMA-DPH does not fluoresce in the aqueous solution and crosses membranes inefficiently. Prior to membrane fission, the dye has direct access to the engulfment, forespore and mother cell membranes and therefore shows intense labeling where these membranes are adjacent to one another (Figure 8D, top row). After fission, the dye only has direct access to the mother cell membrane and consequently weaker labeling around the forespore is observed (Figure 8D, bottom row).

3.2.11 Widefield live-cell fluorescence microscopy of *B. subtilis*

For imaging *B. subtilis*, 1 ml of cells was concentrated by centrifugation (3300 x g for 30 sec) and mounted on a 2% agarose pad. Fluorescence microscopy was performed using a Leica DMi8 wide-field inverted microscope equipped with an HC PL APO 100×DIC objective (NA=1.40) and an iXon Ultra 888 EMCCD Camera from Andor Technology. Membranes were stained with TMA-DPH at a final concentration of 100 µM. Excitation light intensity was set to 50% and exposure times were 300 ms for TMA-DPH (λ_{ex}=395/25 nm; λ_{em}=460/50 nm); 500 ms for m(E)GFP (λ_{ex}=470/40; λ_{em}=500-550) and 1 s for mYFP (λ_{ex}=510/25; λ_{em}>530) respectively. Images were acquired with Leica Application Suite X (LAS X) and analysis and processing were performed using the ImageJ software.

3.2.12 Expression and purification of recombinant FisB(ECD)

His_6-FisB(ECD) was purified as described in [38] but with slight modifications. Briefly, His_6-FisB(ECD) was expressed in *E. coli* BL21 (DE3) from New England Biolabs and purified using HisPur™ Ni-NTA Resin from Thermo Fisher Scientific. Protein expression was induced with 1 mM IPTG at OD_{600} = 0.6 overnight at 16°C. Cells were harvested by centrifugation and the pellet was resuspended in Lysis Buffer (20 mM HEPES, 500 mM NaCl, 0.5 mM TCEP, 20 mM Imidazole, 2% glycerol, 20 mM $MgCl_2$) and flash-frozen in liquid nitrogen. Pellets were thawed on ice and subsequently lysed by 5 passes through a high-pressure homogenizer (Avestin EmulsiFlex-C3). The lysate was spun down at 100,000 × g and the soluble fraction was incubated with HisPur™ Ni-NTA Resin for 2.5 h at 4°C while rotating. The bound protein was washed with Lysis Buffer, Lysis Buffer containing 50 mM and finally 100 mM Imidazole. The protein was eluted with Elution Buffer (20 mM HEPES, 500 mM NaCl, 0.5 mM TCEP, 200 mM Imidazole, 2% glycerol, 20 mM $MgCl_2$). The protein was concentrated using a Vivaspin (MilliporeSigma) centrifugal

concentrator with a 10 kDa molecular weight cutoff and the concentration determined by Bradford protein assay. The protein was stored at -80ºC.

In experiments with labeled FisB(ECD), we used a cysteine mutation, G123C (FisB(ECD) does not have any endogenous cysteines). After expression and purification as described above, iFluor555-maleimide (AAT Bioquest) or Cy5.5 (Lumiprobe) was reacted with purified $FisB^{G123C}$ (ECD) following the manufacturer's instructions. G123 is in a loop that if removed does not interfere with FisB's function (Figure 13B,C).

We determined the labeling efficiency as the ratio of the dye concentration to the protein concentration. Protein and dye concentration were determined using absorbance with a NanoVue spectrophotometer (GE Healthcare).

3.2.13 Liposome preparation

Small unilamellar vesicles (SUVs) were prepared by mixing 1 µmol of total lipids at desired ratios. A thin lipid film was created using a rotary evaporator (Buchi). Any remaining organic solvent was removed by placing the lipid film under high vacuum for 2h. The lipid film was hydrated with 1 ml of RB-EDTA buffer (also referred to as flotation buffer) (25 mM HEPES at pH 7.4, 140 mM KCl, 1 mM EDTA, 0.2 mM tris(2-carboxyethyl) phosphine) by shaking using an Eppendorf Thermomix for >30 min. The lipid suspension was then frozen and thawed 7 times using liquid nitrogen and a 37°C water bath and subsequently extruded 21 times through a 100 nm pore size polycarbonate filter using a mini-extruder (Avanti). All SUVs contained 1% NBD-PE to determine the final lipid concentration by fluorescence.

3.2.14 Liposome-protein co-floatation

For initial experiments, 40 nmol total lipid was incubated with 200 pmol FisB(ECD) for 1h at room temperature in a total volume of 100 µl. 200 µl of 60% Optiprep (iodixanol, Sigma-Aldrich) was added to the sample creating a 40% Optiprep solution. The sample was then layered at the bottom of a 5 mm x 41 mm Beckman ultracentrifuge tube (#344090) and overlaid with 200 µl of 20% Optiprep and finally 150 µl of buffer (Figure 9B). Liposome-bound proteins co-float to a light density, while unbound proteins pellet upon ultracentrifugation for 1.5 h at 48 krpm. Fractions were collected as shown in Figure 9B and the amount of recovered protein was determined by SDS-PAGE (Nu-PAPGE 12% Bis-tris gel, Thermo Fisher Scientific) stained with SYPRO™ Orange (Invitrogen).

3.2.15 Determination of binding constants

For determination of binding constants, the floatation protocol was slightly modified. Varying amounts of lipids were incubated with 100 nM iFluor555-FisB(ECD) for 1 h at room temperature in a total volume of 100 µl. Density gradients were created as before using Optiprep, however only 2 fractions were collected (Figure 12H). The protein concentration in fraction A was too small to be quantified by SDS-PAGE. Therefore, the sample was concentrated by trichloroacetic acid (TCA) precipitation. Briefly, 50 µl of TCA was added to fraction A and incubated for 30 min at 4°C. The sample was spun at 14 krpm in an Eppendorf microfuge for 5 min. The pellet was washed twice with ice-cold acetone and subsequently dried for 10 min in a 95°C heating block. 10 µl of 2X SDS sample buffer was added to the dried pellet and the sample was boiled for 10 min at 95°C and loaded on a 12% bis-tris gel. The amount of recovered protein was determined by fluorescence intensity of the labeled FisB(ECD) band on the gel using a Typhoon FLA 9500 (GE Healthcare). The dissociation constant K_d was determined following [114]. Titration curves

were fitted to:

$$f_b = \frac{K[L]}{1+K[L]}, \qquad (1)$$

where f_b is the fraction of bound protein and K the apparent association constant ($K = 1/K_d$). Eq. (1) assumes that the total lipid concentration $[L]$ is much larger than the concentration of bound protein, a condition satisfied in our experiments for $[L] > 10^{-7}$ M.

3.2.16 Analytical size-exclusion chromatography (SEC) and negative-stain electron microscopy (EM)

For SEC analysis His_6-FisB(ECD) was loaded onto a Superose 6 Increase 10/300 GL column (GE) previously equilibrated with 20 mM HEPES, pH 7.5, 500 mM NaCl, 0.5 mM TCEP, 2% glycerol, 20 mM $MgCl_2$, running at a flow rate of 0.5 ml/min at 4ºC. The column was calibrated with Bio-Rad's Gel Filtration Standards. For negative stain EM analysis, 4 µl of the indicated elution fractions were applied to 200-mesh copper grids coated with ~10 nm amorphous carbon film, negatively stained with 2% (w/v) uranyl acetate, and air-dried. Images were collected on a FEI Tecnai T12 microscope, with a LaB6 filament operating at 120 kV, and equipped with a Gatan CCD camera.

3.2.17 Image analysis

For the analysis shown in Figure 14E and F, we calculated the total intensity (sum ox pixel values) inside the cell contour (indicated in yellow in Figure 14E) using MicrobeJ [172]. Mean integrated auto-fluorescence (~1300 a.u) was calculated by analyzing in the same way an equivalent number of individual wild-type cells, imaged under identical conditions.

For the analyses shown in Figure 8J and Figure 14C, FisB foci were semi-automatically selected using SpeckleTrackerJ [109]. For each spot the sum of pixel values in a 6 × 6 pixel (0.5 µm × 0.5 µm) box around the center of the spot were calculated. For each

corresponding cell, the same operation was performed at a membrane area where no clusters were present and subtracted from the FisB cluster intensity.

3.2.18 Giant Unilamellar Vesicles (GUVs)

GUVs were formed by the method of electroformation [173]. Briefly, in chloroform dissolved lipids were mixed in a glass tube at desired ratios and spotted on two indium tin oxide (ITO) coated glass slides. Organic solvent was removed by placing the lipid films in a vacuum desiccator for at least 2 h. A short strip of copper conductive tape was attached to each ITO slide which were then separated by a PTFE spacer and held together with binder clips. The chamber was filled with 500 µl Swelling Buffer (SweBu, 1mM HEPES, 0.25M sucrose, 1mM DTT) and sealed with Critoseal (Leica Camera AG). GUVs were formed by applying a sinusoidal voltage of 10 Hz and an amplitude of 1.8 V for at least 2 h at room temperature.

For experiments involving FisB(ECD) the GUVs contained 25% *E. coli* PE, 5% *E. coli* CL, 50% *E. coli* PG, 19% eggPC and 1% DiD or 1% NBD-PE (BS mix) unless otherwise noted. For experiments in which EndoA1 was used, GUVs contain 45% DOPS, 24.5% DOPC, 30% DOPE and 0.5% DiD.

GUVs were imaged using a Nikon Eclipse TE2000-E microscope with a micropipette setup. Micropipettes were pulled from borosilicate glass capillaries (1 mm outer diameter, 0.58 mm inner diameter) using a P1-1000 micropipette puller from Sutter Instruments (Novato, USA). A MF-830 Microforge from Narishige (East Meadow, U.S.A.) was used to precisely break the pulled micropipette to produce an opening of a few micrometers.

3.2.19 Permeabilization of giant unilamellar vesicles

GUVs were prepared as described above, but using Swelling Buffer containing 10 µM carboxyfluorescein (CF). GUVs were diluted 1:50 in RB-EDTA and incubated with 1 µM unlabeled FisB(ECD) for up to 3 h. To determine if FisB(ECD) permeabilizes the membrane, the fluorescence intensity of a box of 20 x 20 pixel inside and outside of the GUV was determined and the ratio was calculated.

3.2.20 Permeabilization of large unilamellar vesicles (LUVs)

To prepare LUVs with encapsulated Sulforhodamine B (SRB) the same basic protocol as for preparation of SUVs was followed with slight modifications. Here, the lipid film was hydrated with RB-EDTA containing 50 mM SRB. At this concentration SRB is self-quenched. After hydration, the lipid suspension was frozen and thawed 7 times using a 37°C water bath and liquid nitrogen. LUVs were then created by passing the lipid suspension through a 400 nm pore size polycarbonate filter using a mini-extruder. Not incorporated SRB was removed with a PD-10 Desalting Colum (GE Healthcare).

The permeabilization experiment was carried out using Synergy™ H1 microplate reader (BioTek Instruments). LUVs were diluted to 50 µM total lipid and the fluorescence at 590 nm was recorded for 5 min. FisB(ECD) was added to 4 or 8 µM and the fluorescence was measured for another 1.5 h. Finally, 2 mM Triton™ X-100 (MilliporeSigma) was added to dissolve the LUVs to determine the maximum amount of dequenching possible (F_{max}). Fluorescence is plotted as the fraction of F_{max}.

3.2.21 Fluorescence recovery after photobleaching (FRAP)

FRAP measurements were conducted using a Leica SP8 inverted microscope and the same open imaging chamber. As described above GUVs were diluted in RB-EDTA and incubated with 1uM iFluor555-FisB(ECD) for 2 h. A rectangular area was chosen for bleaching as indicated in Figure 17. 5 images (laser power 0.7%) were recorded before bleaching, 10 during bleaching (laser power 100%) and 60 after bleaching (laser power 0.7%).

3.2.22 Determination of mean GUV intensity

For analyzing the FRAP experiments, the mean GUV intensity was determined using ImageJ. A segmented line with a width of 10 pixels was used to manually follow the GUV contour. The line was smoothed using ‘fit spine’ and ImageJ was used to calculate the mean pixel intensity. The background was determined as the mean pixel value of a 20 x 20 pixel box (close to but outside the GUVs) and subtracted from the mean pixel intensity for the GUVs.

3.2.23 Transfection of HEK293 cells

HEK293T cells (HEK 293T/17, ATCC, CRL-11268) were maintained in 5% CO_2 at 37°C in Dulbecco's Modified Eagle's Medium (DMEM, Sigma-Aldrich), supplemented with non-essential amino acids (Sigma, Madrid, Spain) and 10% FBS (Lonza, Madrid, Spain). Cell were transiently transfected with Lipofectamine 2000 (Invitrogen, Carlsbad, CA) following manufacturer´s intructions.

3.2.24 Determination of spore surface area

Sporulating cells were stained with TMA-DPH as described in chapter 3.2.10. The outlines of spores were detected using the ImageJ plugin JFilament 2D. Snakes were fitted using contours with a point spacing of 0.1 and 100 deform iterations. Snakes were saved and further analyzed using MATLAB.

Using MATLAB an ellipse was fitted to each snake to determine the symmetry axis of the forespore. Half of the snake was then rotated around this symmetry axis and the surface of revolution was determined.

3.2.25 *Bacillus subtilis* giant protoplasts

Giant protoplasts were prepared from Strain BMB014. An overnight culture of BMB014 is diluted in CH medium to OD_{600} = 0.05. Cells were grown at 37°C for 30 min. GFP-FisB expression was then induced with 1 mM IPTG and MciZ expression was induced with 20 mM xylose. After 4 h filamentous cells were spun down (3300 x g for 30 s) and resuspended in protoplasting buffer. Cells were washed 2 x with protoplasting buffer and finally resuspended in $1/10^{th}$ volume protoplasting buffer. Lysozyme was added to 1 mg/ml and cells were incubated at 37°C. Protoplasting was complete after 30 min.

3.2.26 Micropipette aspiration

GUVs or protoplasts were aspirated using a hydrostatic system. The pressure difference between the two reservoirs was continuously read using a pressure sensor (Validyne DP-15) and transducer (Model CD223, Validyne Engineering, Northridge, CA). Gentle suction was applied with the micropipette (mounted on a Narishige MHW-3 3-axis manipulator) to pick up and lift the GUV/protoplast above the coverslip.

Table 1. *Bacillus subtilis* strains used in this study.

Strain	Genotype	% spo[a]	Source
PY79	*Prototrophic wild-type strain*	100±8.36	[166]
BDR1083	Δ*fisB::tet*	13.17 ± 1.97	[174]
BKM15	*amyE::PspoIIQ-cfp (spec)*	n.d	[38]
BAM003	Δ*fisB::tet ycgO::PfisB-mGFP -fisB (cat)*	90.17±12.65	[38]
BAL001	Δ*fisB::tet ycgO::PfisB-mEGFP -fisB (cat)*	n.d	This work
BAL002	Δ*fisB::tet, ycgO::PspoIID-RBSfisB(5n)-mYFP A206K-fisB (erm)*	83.54 ± 4.93	This work
BAL003	Δ*fisB::tet, ycgO::PspoIID-RBSfisB(5n)-mGFP A206K-fisB (erm)*	n.d	This work
BAL004	Δ*fisB::tet, ycgO::PspoIID-RBSfisB(5n)-mEGFP A206K-fisB (erm)*	n.d	This work
BAL005	Δ*fisB::tet ycgO::PfisB-mEGFP-fisB Clostridum perfringens sp. (cat)*	85 ± 5	This work
BAL006	Δ*fisB::tet, ycgO::PspoIID-RBSfisB(5n)-mYFP A206K-fisB* K168D K170D *(erm)*	16.91±7.03	This work
BAL007	Δ*fisB::tet, ycgO::PspoIID-RBSfisB(5n)-mYFP A206K-fisB* G175A I176S I194T I195S *(erm)*	3.03±2.51	This work
BAL008	Δ*fisB::tet, ycgO::PspoIID-RBSfisB(5n)-mYFP A206K-fisB Δ80-96 (erm)*	13.04±2.71	This work

BAL009	Δ*fisB::tet, ycgO::PspoIID-RBSfisB(5n)-mYFP A206K-fisB Δ122-132 (erm)*	99.42±15.03	This work
BAL010	Δ*fisB::tet, ycgO::PspoIID-RBSfisB(5n)-mYFP A206K-fisB Δ137-154 (erm)*	14.09±6.33	This work
BAL011	Δ*fisB::tet, ycgO::PspoIID-RBSfisB(5n)-mYFP A206K-fisB Δ167-182 (erm)*	16.70±6.99	This work
BAL012	Δ*fisB::tet, ycgO::PspoIID-RBSfisB(5n)-mYFP A206K-fisB Δ210-220 (erm)*	15.30±3.32	This work
BAL013	Δ*fisB::tet, ycgO::PspoIID-RBSfisB(5n)-mYFP A206K-fisB* Δ132-222*(erm)*	14.78±3.40	This work
BAL014	Δ*fisB::tet, ycgO::PspoIID-RBSfisB(5n)-mYFP A206K-fisB* L90T (erm)	104.31±0.00	This work
BAL015	Δ*fisB::tet, ycgO::PspoIID-RBSfisB(5n)-mYFP A206K-fisB L137S G138A (erm)*	16.74±2.39	This work
BAL016	Δ*fisB::tet, ycgO::PspoIID-RBSfisB(5n)-mYFP A206K-fisB L145TL146S (erm)*	16.52±2.60	This work
BAL017	Δ*fisB::tet, ycgO::PspoIID-RBSfisB(5n)-mYFP A206K-fisB G150A (erm)*	23.91±3.04	This work
BAL018	Δ*fisB::tet, ycgO::PspoIID-RBSfisB(5n)-mYFP A206K-fisB* V215S G217A *(erm)*	10.43±1.73	This work
BAL019	Δ*fisB::tet, ycgO::PspoIID-RBSfisB(5n)-mYFP A206K-fisB* V219T *(erm)*	23.48±0.00	This work
BAL020	Δ*fisB::tet, ycgO::PspoIID-RBSfisB(5n)-mYFP A206K-fisB* G175A I176S *(erm)*	9.91±5.14	This work

BAL021	Δ*fisB::tet, ycgO::PspoIID-RBSfisB(5n)-mYFP A206K-fisB* I194T I195S (erm)	45.65±12.97	This work
BAL022	Δ*fisB::tet, ycgO::PspoIID-RBSfisB(5n)-mYFP A206K-fisB* R56E *(erm)*	55.00±15.00	This work
BAL023	Δ*fisB::tet, ycgO::PspoIID-RBSfisB(5n)-mYFP A206K-fisB* E67R D68K *(erm)*	37.30±12.70	This work
BAL024	Δ*fisB::tet, ycgO::PspoIID-RBSfisB(5n)-mYFP A206K-fisB* K106D K109D *(erm)*	22.50±7.50	This work
BAL025	Δ*fisB::tet, ycgO::PspoIID-RBSfisB(5n)-mYFP A206K-fisB* K116D *(erm)*	65.70±14.30	This work
BAL026	Δ*fisB::tet, ycgO::PspoIID-RBSfisB(5n)-mYFP A206K-fisB* E119R *(erm)*	55.00±15.00	This work
BAL027	Δ*fisB::tet, ycgO::PspoIID-RBSfisB(5n)-mYFP A206K-fisB* R156E *(erm)*	65.50±22.50	This work
BAL028	Δ*fisB::tet, ycgO::PspoIID-RBSfisB(5n)-mYFP A206K-fisB K170D K172DE* (erm)	16.40±1.45	This work
BAL029	Δ*fisB::tet, ycgO::PspoIID-RBSfisB(5n)-mYFP A206K-fisB* K192D *(erm)*	55.16±14.80	This work
BAM234	Δ*ywnE::cat* Δ*ywjE::kan* Δ*ywiE::erm*	25.88 ± 8.53	[38]
BAM236	Δ*fisB::tet* Δ*ywnE::cat* Δ*ywjE::kan* Δ*ywiE::erm*	1.07 ± 0.52	[38]
BAL030	Δ*ywnE* Δ*ywjE* Δ*ywiE::kan* Δ*pssA::erm*	25.64 ± 2.56	This work
BAL031	Δ*pssA::erm*	85.10 ± 12.16	This work

BAL035	Δ*floA::erm*	35.9 ±12.18	This work
BAL036	Δ*floT::erm*	103.8±11.54	This work
BAL037	Δ*fisB::tet* Δ*ywnE* Δ*ywjE ywiE::kan ycgO::PspoIID-RBSfisB(5n)-mYFP -fisB (erm)*	n.d	This work
BDR2061	*amyE::PxylA-gfp-mbl (spec), mblΩpMUTIN4 (erm) trpC2*	n.d	[102]
BMB014	*amyE::PxylA-mciZ(cat), ycgO::Pspank-gfp-fisB (spec)*	n.d	This work
BMB031	*ycgO::PfisB-RBSfisB-Myc-fisB(erm)*	101 ± 7	This work
BMB032	*ycgO::PfisB-RBSfisB-Myc-fisB(G6C) (erm)*	68 ± 19	This work
BMB033	*ycgO::PfisB-RBSfisB-Myc-fisB(L137C) (erm)*	53 ± 3	This work
BMB034	*ycgO::PfisB-RBSfisB-Myc-fisB(A245C) (erm)*	83 ± 8	This work
BS168	*Wild-type strain trpC2*	n.d	BGSC[b]

a: Sporulation efficiency (% of WT spores at 24h after the onset of sporulation) for each indicated strain. Results are shown as means ± SD for four replicates per condition.
b: Bacillus Genetic Stock Center (www.bgsc.org)

Table 2. Plasmids used in this study.

Plasmid	Genotype	*E. coli*	Source
pAM002	ΔfisB::tet ycgO::PfisB-mGFP -fisB (cat)	amp	[38]
pVS001	ΔfisB::tet ycgO::PfisB-mYFP A206K -fisB (cat)	amp	This work
pAL001	ycgO::PfisB-mEGFP-fisB B.subtilis.(cat)	amp	This work
pAL002	ycgO::PspoIID-RBSfisB(5n)-mEGFP-fisB (erm)	amp	This work
pAL003	ycgO::PfisB-mEGFP-fisB Clostridium Perfringens sp.(cat)	amp	This work
pAL004	ycgO::PspoIID-RBSfisB(5n)-mYFP A206K-fisB (erm)	amp	This work
pAL005	ycgO::PspoIID-RBSfisB(5n)-mYFP A206K-fisB K168DK170D (erm)	amp	This work
pAL006	ycgO::PspoIID-RBSfisB(5n)-mYFP A206K-fisB G175A I176S I194TI195S (erm)	amp	This work
pKM110	his6-fisBECD WT	amp	[38]
pAL007	his6-fisBECD WT G123C	amp	This work
pDT390	his6-fisBECD G175A I176S I194T I195S	amp	[38]
pAL008	his6-fisBECD G175A I176S I194T I195S G13C	amp	This work
pAL009	his6-fisBECD K168D K170D	amp	This work

pAL010	his6-fisBECD K168D K170D G123C	amp	This work
pAL011	ycgO::PspoIID-RBSfisB(5n)-mYFP A206K-fisB ∆80-96 (erm)	amp	This work
pAL012	ycgO::PspoIID-RBSfisB(5n)-mYFP A206K-fisB ∆122-132 (erm)	amp	This work
pAL013	ycgO::PspoIID-RBSfisB(5n)-mYFP A206K-fisB ∆137-154 (erm)	amp	This work
pAL014	ycgO::PspoIID-RBSfisB(5n)-mYFP A206K-fisB ∆167-182 (erm)	amp	This work
pAL015	ycgO::PspoIID-RBSfisB(5n)-mYFP A206K-fisB ∆210-220 (erm)	amp	This work
pAL016	ycgO::PspoIID-RBSfisB(5n)-mYFP A206K-fisB ∆132-222 (erm)	amp	This work
pAL017	ycgO::PspoIID-RBSfisB(5n)-mYFP A206K-fisB L90T (erm)	amp	This work
pAL018	ycgO::PspoIID-RBSfisB(5n)-mYFP A206K-fisB L137SG138A (erm)	amp	This work
pAL019	ycgO::PspoIID-RBSfisB(5n)-mYFP A206K-fisB L145TL146S (erm)	amp	This work
pAL020	ycgO::PspoIID-RBSfisB(5n)-mYFP A206K-fisB G150A (erm)	amp	This work
pAL021	ycgO::PspoIID-RBSfisB(5n)-mYFP A206K-fisB V215SG217A (erm)	amp	This work

pAL022	ycgO::PspoIID-RBSfisB(5n)-mYFP A206K-fisB V219T (erm)	amp	This work
pAL023	ycgO::PspoIID-RBSfisB(5n)-mYFP A206K-fisB G175AI176S (erm)	amp	This work
pAL024	ycgO::PspoIID-RBSfisB(5n)-mYFP A206K-fisB I194TI195S (erm)	amp	This work
pAL025	ycgO::PspoIID-RBSfisB(5n)-mYFP A206K-fisB R56E (erm)	amp	This work
pAL026	ycgO::PspoIID-RBSfisB(5n)-mYFP A206K-fisB E67RD68K (erm)	amp	This work
pAL027	ycgO::PspoIID-RBSfisB(5n)-mYFP A206K-fisB K106D K109D (erm)	amp	This work
pAL028	ycgO::PspoIID-RBSfisB(5n)-mYFP A206K-fisB K116D (erm)	amp	This work
pAL029	ycgO::PspoIID-RBSfisB(5n)-mYFP A206K-fisB E119R (erm)	amp	This work
pAL030	ycgO::PspoIID-RBSfisB(5n)-mYFP A206K-fisB R156E (erm)	amp	This work
pAL031	ycgO::PspoIID-RBSfisB(5n)-mYFP A206K-fisB K170D K172DE (erm)	amp	This work
pDR244	PPA-cre-ori(ts) spec	amp	BGSC
pMB062	ycgO::PfisB-RBSfisB-Myc-fisB(erm)	amp	This work
pMB064	ycgO::PfisB-RBSfisB-Myc-fisB(G6C) (erm)	amp	This work

pMB065	ycgO::PfisB-RBSfisB-Myc-fisB(L137C) (erm)	amp	This work
pMB066	ycgO::PfisB-RBSfisB-Myc-fisB(A245C) (erm)	amp	This work

4 Leukocyte Cytoskeleton Polarization Is Initiated by Plasma Membrane Curvature from Cell Attachment

As a side project, I worked together with Chunguang Ren, a postdoc in Dianqing (Dan) Wu laboratory (Pharmacology), to investigate the membrane curvature preference of SLIT-ROBO Rho GTPase-activating protein 2 (SRGAP2), a eukaryotic BAR-domain containing protein which was previously shown to induce filopodia-like membrane protrusions to regulate neuronal migration and morphogenesis [175]. These results are published [176].

4.1 Introduction

Cell migration is a fundamental process required for processes such as embryonic development, wound healing, and tumor metastasis. Leukocytes require cell migration for infiltration, recruitment, trafficking, and homing [177].

The first step of cell migration is cell polarization which leads to the reorganization of signaling and structural molecules within the cell. This includes the formation of a polarized cytoskeleton where F-actin localizes to the leading edge of the cell and actomyosin accumulates at the back of the cell [178]. Usually, cells polarize upon chemoattractant stimulation. These chemoattractants are recognized by G-coupled receptors which for example can stimulate myosin light chain phosphorylation (pMLC) at the back of the cell [179].

However, in the absence of any chemoattractants, neutrophils can polarize upon integrin signaling [180]. Integrins are located at the cell surface and interact with the extracellular matrix. Circulating neutrophils can be captured by integrin-mediated adhesion during *in vivo* infiltration of inflamed tissues.

Previous research on cell polarization was mainly conducted using cells which had already attached to a surface and stochastic polarity was believed to be present in these cells [181]. However, the laboratory of Dianqing Wu found that free floating mouse neutrophils do not polarize upon chemoattracted stimulation, instead F-actin and pMLC were mainly colocalized. This finding suggested for the first time that cell attachment is a prerequisite for neutrophile polarization upon stimulation.

When the cell attaches to a surface the curvature of the plasma membrane (PM) increases locally. Bin-Amphiphysin-Rvs (BAR)-domain-containing proteins can sense and induce membrane curvature [130, 182]. Using a siRNA screen of BAR-domain containing proteins, the gene coding for SRGAP2 was identified to be required for polarized localization of pMLC. SRGAP2 has an inverse F-BAR domain, which prefers to bind to negatively curved membranes, where it can polymerize and thereby helps to stabilize the curved membrane [183]. Upon cell attachment, the highest membrane curvature can be found at the cusps of cell attachment (Figure 29A). SRGAP2 localizes to these cusps via its F-BAR domain and induces the sequential polarization of PtdIns4P (also referred to as PI4P), PIP5K1C90 (a lipid kinase involved in PtdIns4,5P_2 synthesis), and pMLC.

Together with Chunguang Ren, I investigated the membrane curvature preference of SRGAP2's Bar domain (FBAR-GFP) and PM PtdIns4P using micropipette aspiration and found that a local increase in PM curvature recruits FBAR-GFP and PtdIns4P independent of chemoattractants or integrins. Altogether our results show that chemical stimulation alone cannot be responsible for cell polarization in neutrophils. Instead, surface attachment of a cell leads to a local increase in plasma membrane curvature which in turn breaks the cellular symmetry by recruitment of the F-BAR domain containing protein SRGAP2 and subsequently PM PtdIns4P which are required for polarization of other proteins such as RPH3A, PIP5K1C90, RAB21 or pMLC.

4.2 Increasing membrane curvature drives SRGAP2 and PI4P polarization

Together with Chunguang Ren, I investigated if membrane curvature is the driving factor for FBAR-GFP recruitment to the cusps of cell attachment. To this end, we used mouse neutrophils expressing FBAR-GFP as well as a TdTomato labeled membrane-associated protein (memRed), which is not expected to have an intrinsic preference for curved membrane and therefore served as a control. To generate regions of defined membrane curvature, we aspirated free floating neutrophils using micropipettes of various diameters. Once a cell is aspirated into the micropipette, FBAR-GFP localized to regions of high membrane curvature within the micropipette (Figure 29C). We generated ratio images of FBAR-GFP to memRed to quantify FBAR-GFP enrichment to highly curved membranes as shown in Figure 29B. The aspirated part of the cell was divided into two regions, the tip and the tube, and the curvatures and fluorescence intensity for both regions were determined as shown in Figure 29B.

When plotting fluorescence intensity against curvature, a positive correlation between membrane curvature and FBAR-localization was observed Figure 29E, suggesting that membrane curvature is correlated with FBAR-GFP recruitment. With increasing membrane curvature more and more FBAR-GFP is recruited.

Similar to SRGAP2, the Wu laboratory observed polarized localization of PI4P upon cell attachment but no polarization in free floating neutrophils. Therefore, we also determined if PI4P polarized in a membrane curvature-dependent manner and independent of chemoattractant or integrin stimulation. PI4P localization was detected with the fluorescent PI4P probe GFP-P4M. P4M is a domain of the *L. pneumophila* protein SidM which has a high affinity and specificity for PI4P [184]. We aspirated neutrophils expressing GFP-P4M and memRed (Figure 29D) and similarly to FBAR-GFP, we found a

significant positive correlation between membrane curvature and localization of GFP-P4M (Figure 29F).

Altogether our results show that an increase in local membrane curvature because of cell surface attachment is the main mechanism for polarized localization of F-BAR and therefore most likely SRGAP2 in neutrophils, T cells, and probably other leukocytes. Additionally, we demonstrated that PM PI4P also polarizes upon cell attachment via local increase in membrane curvature and that this process in independent of chemoattractant or integrin signaling.

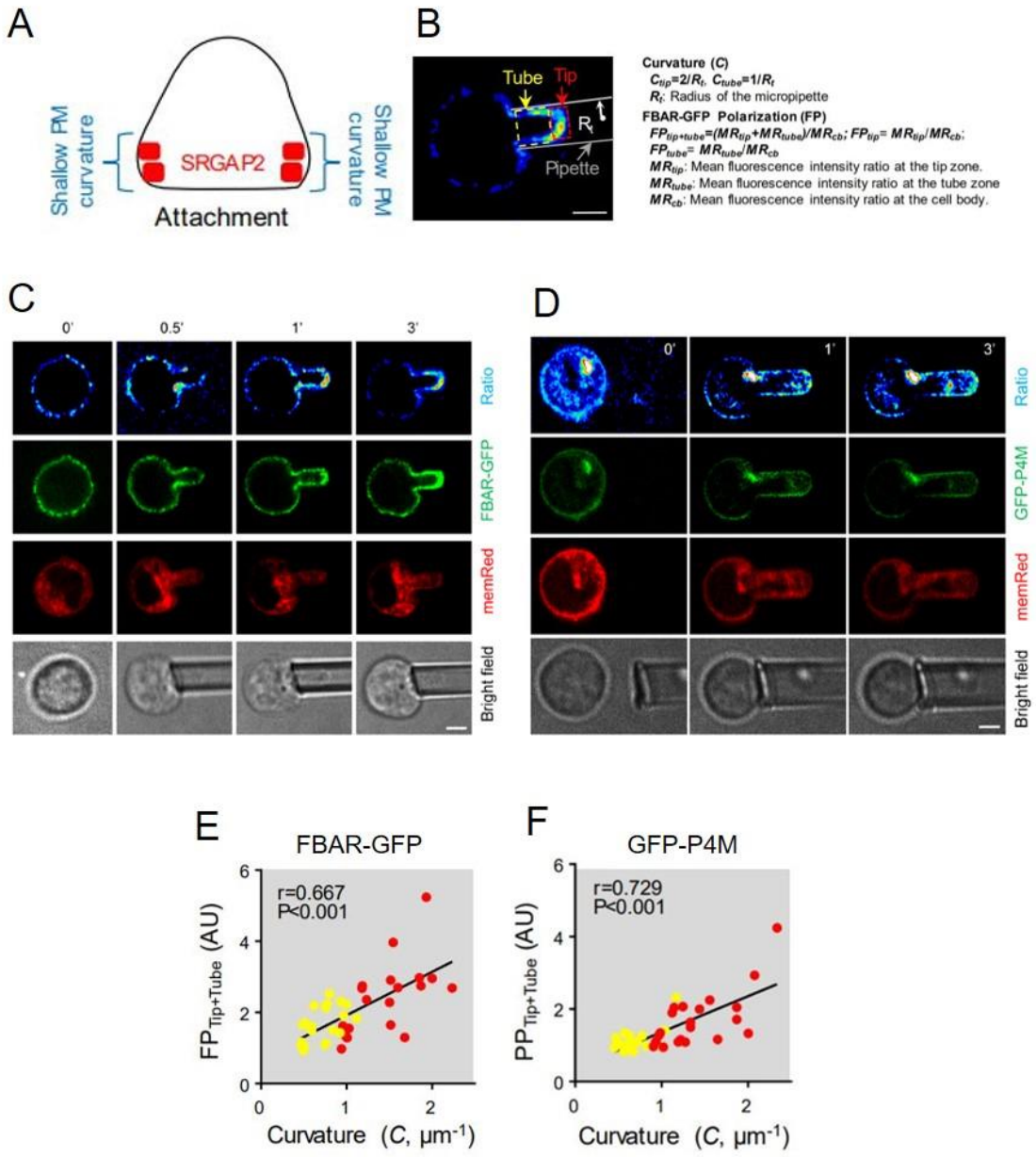

Figure 29. Curvature dependent localization of FBAR-GFP and GFP-P4M. ***(A)*** Schematic representation of SRGAP2 localization upon cell attachment. ***(B)*** Schematic representation for quantification of PM curvature and FBAR-GFP polarization. Ratio images of FBAR-GFP (or GFP-P4M) with memRed were generated. The aspirated tongue is divided into a tube and tip region for quantification. ***(C)*** Micropipette aspiration leads to polarization of SRGAP2 F-BAR-domain to regions of high concave curvature (relative to the cytosol), namely along the pipette walls and the semi-spherical tip of the aspirated tongue. Membrane-associated TdTomato (memRed) expressing neutrophils from mT/mG mice were transfected with FBAR-GFP. Images of a representative cell are shown. The experiments were repeated ten times. ***(D)*** Higher membrane curvature generated by micropipette aspiration leads to polarization of GFP-P4M. MemRed expressing neutrophils from mT/mG mouse were transfected with GFP-P4M. The bright spots are likely Golgi. Images of a representative cell are shown. The experiments were repeated ten times. ***(E,F)*** Correlation of PM curvature within the pipette with FBAR-GFP or GFP-P4M polarization. Yellow dots represent the curvature in the tube and red dots represent the curvature at the tip as shown in (B).

4.3 Discussion

It was previously believed that breaking of cellular symmetry in neutrophils was entirely dependent on extracellular stimulations such as chemoattractants or integrins. Here, we showed for the first time that chemical stimulation alone is not sufficient for cell polarization. We found that cell surface attachment is necessary for polarization of lamellar F-actin and pMLC, two cytoskeleton markers for cell polarization. Upon cell attachment, a local increase in membrane curvature recruits the FBAR-domain containing protein SRGAP2, which stimulates the activity of the lipid kinase PI4KA which converts PtdIns to PtdIns4P. The F-BAR domain of SRGAP2 can bind to PtdIns4P and is required for this process. Since SRGAP2 can bind to PtdIns4P, this interaction might serve as positive feedforward amplification mechanism. Interaction of SRGAP2 with PtdIns4P may help to stabilize PtdIns4P polarization, which in turn could recruit additional SRGAP2 molecules, leading to even more increased production of PtdIns4P which is ultimately required for polarization of pMLC.

The Wu laboratory also found that $CD8^+$ T cells also require PM curvature change for their cytoskeleton polarization. Hence, our results indicate that cell attachment as a prerequisite for cell polarization is likely also important for other circulating leukocytes [176].

Finally, our results suggest that earlier findings need to be interpreted with caution. Previously, it was believed that cells spontaneously polarize. However, these studies were conducted with cells attached to a surface. Our results reveal that this polarization is not spontaneous and in fact a result of polarized localization of SRGAP2 due to increased PM curvature.

4.4 Material and Methods

4.4.1 Neutrophil Preparation and Transfection

Murine neutrophils were purified from bone marrows as previously described ([185]). Briefly, bone marrow cells collected from mice were treated with the ACK buffer (155 mM NH4Cl, 10 mM KHCO3 and 127 mM EDTA) for red blood cell lysis, followed by a discontinuous Percoll density gradient centrifugation. Neutrophils were collected from the band located between 81% and 62% of Percoll. Transient transfection of neutrophils were done as previously described [185-187].

In brief, three million neutrophils were electroporated with 1.6 mg endotoxin-free plasmids or 300 nM of siRNA using the human monocyte nucleofection kit (Lonza, Switzerland) with an Amaxa electroporation system. The cells were then cultured for overnight in the medium supplied with the kit containing 10% FBS and 25 ng/ml recombinant GM-CSF (PeproTech, Rocky Hill, NJ). Cell sorting was done by a FACS Aria sorter (BD, San Jose, CA).

4.4.2 Micropipette Aspiration Assay

The micropipette pulling experiment was performed as previously reported [188]. Micropipettes were fabricated as described in chapter 3.2.18 and cells were imaged in our imaging chamber (Figure 16C). The chamber consisted of a pair of glass coverslips (#1.5, Waldemar Knittel Glasbearbeitungs-GmbH, Braunschweig, Germany) separated by 3 mm, attached to a metal block using vacuum grease. The coverslips were pretreated twice with 30% KOH in Ethanol with sonication for 5’ each, followed by twice washing in sterile-filtered H2O with sonication for 5’. The chamber and pipettes were filled with 0.5% BSA in HBSS with calcium, magnesium (14025092, Thermo Fisher). Neutrophils or CD8+ cells were suspended in the same solution, and introduced into a corner of the observation

chamber. Aspiration pressure was controlled as described in chapter 3.2.26.. Time lapse images were recorded every 6 seconds with an Ultraview spinning disk confocal microscope (Perkin-Elmer Life Sciences) equipped with a Hamamatsu C9100 EM-CCD camera and Nikon TE2000-E inverted microscope, and controlled by Volocity (Improvision) software. Images were further processed using ImageJ. (v1.48K).

Appendix: *In vitro* reconstitution of FisB into GUVs

We aimed to characterize the curvature preference of FisB in more detail and wanted to reconstitute the fission reaction *in vitro*. To this end we wanted to either encapsulate FisB(ECD) inside GUVs or reconstitute the full-length protein into GUV membranes and pull a thin membrane tether using optical tweezers to mimic the membrane geometries occurring during sporulation (Figure 28D).

Encapsulation of FisB(ECD) into GUVs

I tried to encapsulate FisB(ECD) using the method of inverted emulsion shown in Figure 30A [162]. In this assay, the lipids are first dissolved in diethyl ether. Then a 300 mM sucrose solution is added. This solution will be the inner GUV solution and can also contain any small molecules or proteins that need to be encapsulated. After vigorously mixing and centrifugation, a 300 mM glucose solution is added and after gently mixing and another slow a centrifugation step, the GUVs can be harvested. To test if I can successfully incorporate molecules into GUVs, I first encapsulated Cy5.5 dye only into GUVs composed of 84% eggPC, 15% *E. coli* CL and 1% DiI (Figure 30B).

Next, I tried encapsulating FisB(ECD) inside the GUVs, by adding 250 nM Cy5.5-FisB(ECD) to the inner sucrose solution. While weak fluorescence was visible in some of the GUVs, most GUVs appeared to be empty (Figure 30C). No binding of FisB(ECD) to the membrane was observed. This could be due to the fact, that 15% CL might not be enough to efficiently recruit FisB(ECD) to the membrane. Additionally, binding in the presence of 300 mM sucrose might be inhibited. One advantage of this assay is that different concentrations of sucrose/glucose should work and that in addition to sucrose, other more physiological relevant buffers could be used. Therefore, trying different inside and outside solutions that are more physiological relevant as well as a higher amount of

negatively charged lipids, might help to encapsulate FisB(ECD) inside the GUV as well as membrane binding in the future.

Reconstitution of FisB full-length into GUVs

Inverted emulsion: In principle the inverted emulsion method described above should also work for transmembrane proteins. I first introduced an N-terminal cysteine into FisB full-length (wild type FisB does not contain any cysteines) purified the protein from *E. coli* using a hexa-histidine tag as described by Doan et al. [38] and labeled the protein with Cy3 as described in section 3.2.12.

I tried adding either 200 nM (Lipid to protein ratio (L/P) = 3500) or 10 nM (L/P=50 000) FisB full-length to the inner sucrose solution. In the presence of 200 nM FisB no GUVs were formed. In the presence of 10 nM FisB, GUVs formed but no protein fluorescence inside the GUV membranes was observed. To prevent proteins containing transmembrane domains from aggregation in the absence of a membrane, detergent is added during the purification process. For purification of FisB, I used Fos-Choline-12 (Fos12) which has a critical micellar concentration (cmc) of 0.047%. When I added 200 nM, the total concentration of Fos12 was 0.02% and therefore should not have inhibited GUV formation. However, in the presence of 10 nM, the concentration of Fos12 was 0.001%. While for protein incorporation the concentration of detergent should be below the cmc, 0.001 % may have been too low to stabilize FisB and it is possible that FisB precipitated. In the future, we could try to optimize FisB reconstitution by varying the protein to lipid ratio, membrane composition, as well as the amount of detergent present to facilitate reconstitution of FisB.

A big advantage of the inverted emulsion method over electroformation is that is does not require drying the protein-containing lipid film under high vacuum, which may inhibit protein function. However, we still tried to use electroformation for reconstitution of FisB full-length.

Electroformation: Transmembrane domain proteins can also be reconstituted into GUVs by electroformation. During this process, FisB is first reconstituted into SUVs. These SUVs are subsequently dried on ITO coverslips and GUVs were formed as described in section 3.2.18. I have tried using SUVs composed of either 100% eggPC or 85% eggPC and 15% CL. Additionally, instead of using a 300 mM sucrose containing inner solution, I have tried forming GUVs in buffer containing 10 mM Tris, 2 mM EDTA, 100 mM NaCl. I also tried a lipid to protein ratio of 1:5000 and 1:10000. However, no GUVs were formed under the conditions, I tested. Instead, only protein-lipid aggregates were found after electroformation (Figure 30E). This may be due to FisB somehow preventing the formation of GUVs, possibly due to its interaction with the lipids present. While varying lipid to protein ratios as well as buffer and GUV composition may facilitate electroformation of GUVs containing FisB, overall, the inverted emulsion method to encapsulate FisB(ECD) seems to be the most promising method.

Figure 30. Reconstitution of FisB into GUVs. ***(A)*** Method for preparation of GUVs by inverted emulsion. Borrowed from [162]. ***(B)*** Using the protocol shown in (A), the dye Cy5.5 was successfully encapsulated in GUVs. ***(C)*** When 250 nM FisB(ECD) was added to the inner solution, most GUVs appeared to be either empty or showed a very faint protein fluorescence. However, no membrane binding was observed. ***(D)*** Reconstitution of FisB full-length into GUVs by inverted emulsion. No GUVs were formed in the presence of 200 nM FisB. GUVs were formed in the presence of 10 nM FisB, however no protein fluorescence within the membrane was observed. ***(E)*** Reconstitution of FisB full-length into GUVs by electroformation. No GUVs were formed and protein lipid aggregates were found in all conditions tested. ***(F)*** SDS gel showing that FisB is not degraded during the process of electroformation. Red arrow indicated the band corresponding to full-length FisB.

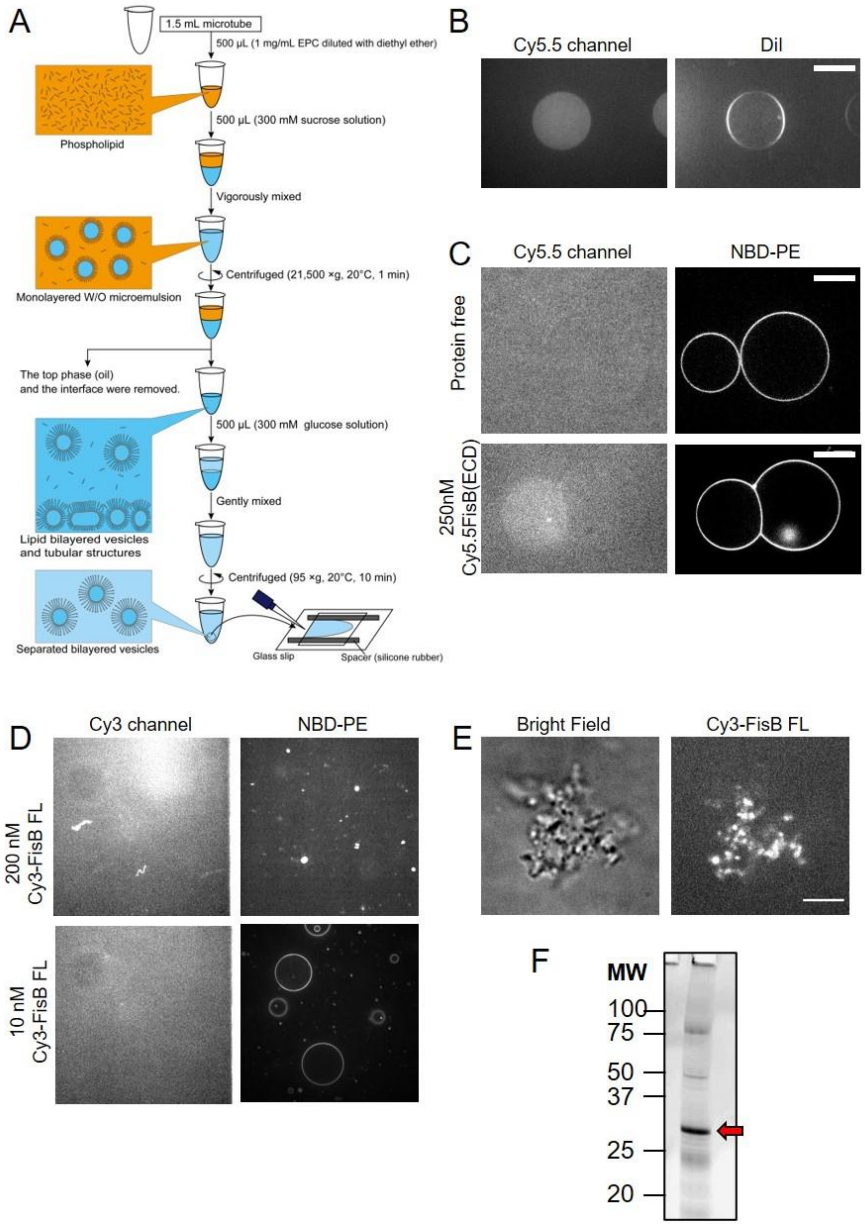

Figure 30. Reconstitution of FisB into GUVs.

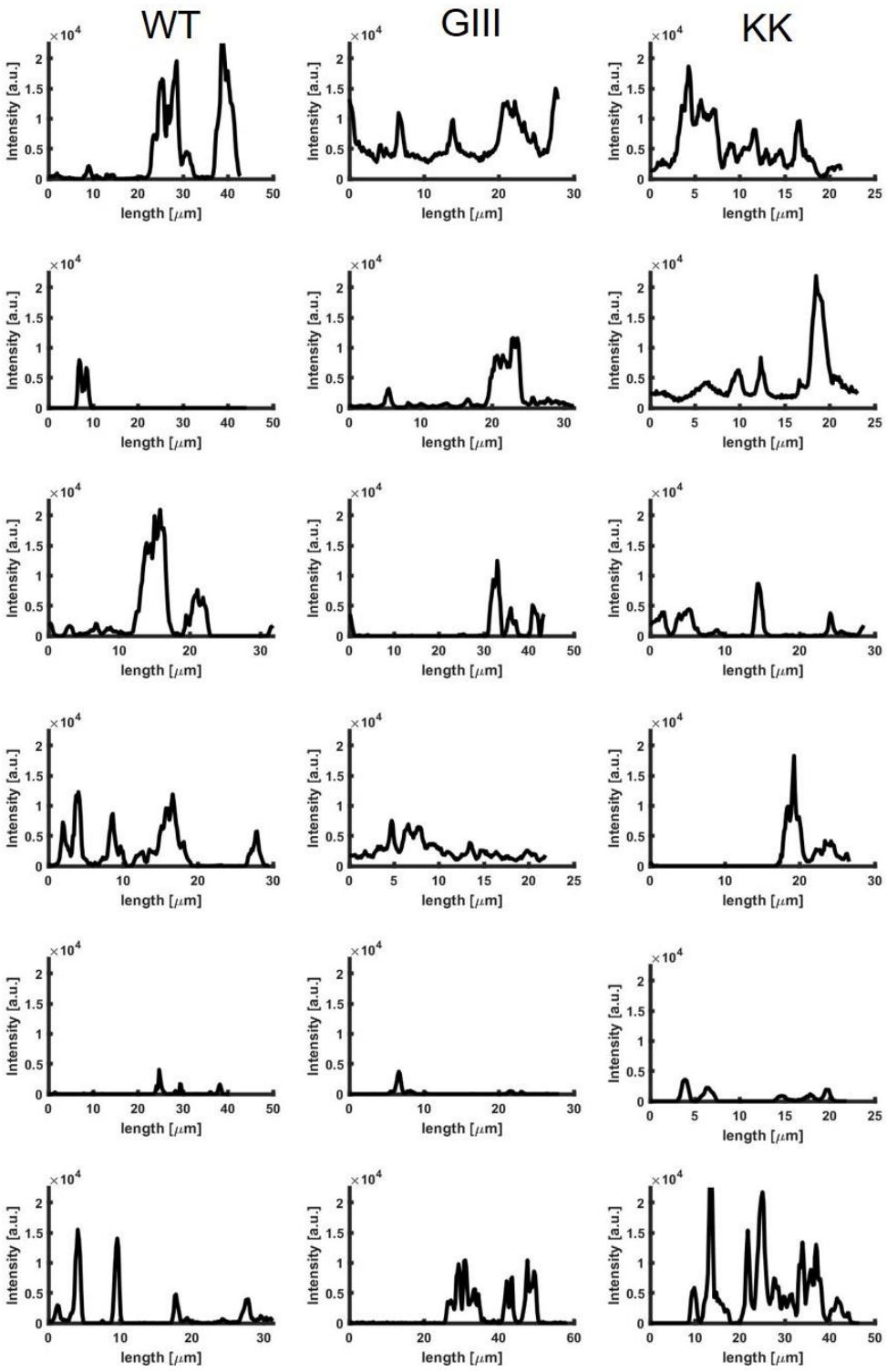

Figure 31. Fluorescence intensity profiles along GUV contours. GUVs composed of BS mix were incubated with 100 nM iFluor-FisB(ECD) wild-type (left column), GIII mutant (middle column) or KK mutant (right column). Plotted is the protein fluorescence along the GUV contour.

References

1. Renard, H.F., L. Johannes, and P. Morsomme, *Increasing Diversity of Biological Membrane Fission Mechanisms.* Trends Cell Biol, 2018. **28**(4): p. 274-286.
2. Gray, M. and R.J. Botelho, *Phagocytosis: Hungry, Hungry Cells.* Methods Mol Biol, 2017. **1519**: p. 1-16.
3. Khanna, K., J. Lopez-Garrido, and K. Pogliano, *Shaping an Endospore: Architectural Transformations During Bacillus subtilis Sporulation.* Annu Rev Microbiol, 2020.
4. Daumke, O. and G.J.K. Praefcke, *Mechanisms of GTP hydrolysis and conformational transitions in the dynamin superfamily.* Biopolymers, 2018. **109**(2).
5. McCullough, J., A. Frost, and W.I. Sundquist, *Structures, Functions, and Dynamics of ESCRT-III/Vps4 Membrane Remodeling and Fission Complexes.* Annu Rev Cell Dev Biol, 2018. **34**: p. 85-109.
6. Zhukovsky, M.A., et al., *Protein Amphipathic Helix Insertion: A Mechanism to Induce Membrane Fission.* Frontiers in Cell and Developmental Biology, 2019. **7**.
7. Snead, W.T., et al., *Membrane fission by protein crowding.* Proc Natl Acad Sci U S A, 2017. **114**(16): p. E3258-E3267.
8. Simunovic, M., et al., *Friction Mediates Scission of Tubular Membranes Scaffolded by BAR Proteins.* Cell, 2017. **170**(1).
9. Helm, C.A. and J.N. Israelachvili, *Forces between Phospholipid-Bilayers and Relationship to Membrane-Fusion.* Methods in Enzymology, 1993. **220**: p. 130-143.
10. Burger, K.N., *Greasing membrane fusion and fission machineries.* Traffic, 2000. **1**(8): p. 605-13.
11. Rand, R.P. and V.A. Parsegian, *Mimicry and mechanism in phospholipid models of membrane fusion.* Annu Rev Physiol, 1986. **48**: p. 201-12.
12. Wong, J.Y., et al., *Polymer-cushioned bilayers. II. An investigation of interaction forces and fusion using the surface forces apparatus.* Biophys J, 1999. **77**(3): p. 1458-68.
13. Kozlovsky, Y. and M.M. Kozlov, *Membrane fission: model for intermediate structures.* Biophys J, 2003. **85**(1): p. 85-96.

14. Bashkirov, P.V., et al., *GTPase cycle of dynamin is coupled to membrane squeeze and release, leading to spontaneous fission.* Cell, 2008. **135**(7): p. 1276-86.

15. Kozlov, M.M., H.T. McMahon, and L.V. Chernomordik, *Protein-driven membrane stresses in fusion and fission.* Trends Biochem Sci, 2010. **35**(12): p. 699-706.

16. Meinecke, M., et al., *Cooperative recruitment of dynamin and BIN/amphiphysin/Rvs (BAR) domain-containing proteins leads to GTP-dependent membrane scission.* J Biol Chem, 2013. **288**(9): p. 6651-61.

17. Kaksonen, M. and A. Roux, *Mechanisms of clathrin-mediated endocytosis.* Nat Rev Mol Cell Biol, 2018. **19**(5): p. 313-326.

18. Roux, A., et al., *GTP-dependent twisting of dynamin implicates constriction and tension in membrane fission.* Nature, 2006. **441**(7092): p. 528-531.

19. Jost, M., et al., *Phosphatidylinositol-4,5-bisphosphate is required for endocytic coated vesicle formation.* Current Biology, 1998. **8**(25): p. 1399-1402.

20. Ramachandran, R. and S.L. Schmid, *Real-time detection reveals that effectors couple dynamin's GTP-dependent conformational changes to the membrane.* Embo Journal, 2008. **27**(1): p. 27-37.

21. Lata, S., et al., *Helical structures of ESCRT-III are disassembled by VPS4.* Science, 2008. **321**(5894): p. 1354-7.

22. Lenz, M., S. Morlot, and A. Roux, *Mechanical requirements for membrane fission: common facts from various examples.* FEBS Lett, 2009. **583**(23): p. 3839-46.

23. Boucrot, E., et al., *Membrane Fission Is Promoted by Insertion of Amphipathic Helices and Is Restricted by Crescent BAR Domains.* Cell, 2012. **149**(1): p. 124-136.

24. Brown, W.J., K. Chambers, and A. Doody, *Phospholipase A2 (PLA2) enzymes in membrane trafficking: mediators of membrane shape and function.* Traffic, 2003. **4**(4): p. 214-21.

25. Lai, C.L., et al., *Membrane binding and self-association of the epsin N-terminal homology domain.* J Mol Biol, 2012. **423**(5): p. 800-17.

26. Zhang, C., et al., *The TIP30 protein complex, arachidonic acid and coenzyme A are required for vesicle membrane fusion.* PLoS One, 2011. **6**(6): p. e21233.

27. Martyna, A., et al., *Membrane remodeling by the M2 amphipathic helix drives influenza virus membrane scission.* Sci Rep, 2017. **7**: p. 44695.

28. Ryan, T., et al., *Cardiolipin exposure on the outer mitochondrial membrane modulates alpha-synuclein.* Nat Commun, 2018. **9**(1): p. 817.

29. Danne, L., et al., *Membrane Remodeling by a Bacterial Phospholipid-Methylating Enzyme.* mBio, 2017. **8**(1).

30. Bacia, K., P. Schwille, and T. Kurzchalia, *Sterol structure determines the separation of phases and the curvature of the liquid-ordered phase in model membranes.* Proc Natl Acad Sci U S A, 2005. **102**(9): p. 3272-7.

31. Baumgart, T., S.T. Hess, and W.W. Webb, *Imaging coexisting fluid domains in biomembrane models coupling curvature and line tension.* Nature, 2003. **425**(6960): p. 821-4.

32. Frolov, V.A., et al., *Geometry of membrane fission.* Chem Phys Lipids, 2015. **185**: p. 129-40.

33. Bisson-Filho, A.W., et al., *Treadmilling by FtsZ filaments drives peptidoglycan synthesis and bacterial cell division.* Science, 2017. **355**(6326): p. 739-743.

34. Mahone, C.R. and E.D. Goley, *Bacterial cell division at a glance.* J Cell Sci, 2020. **133**(7).

35. Tarrason Risa, G., et al., *The proteasome controls ESCRT-III-mediated cell division in an archaeon.* Science, 2020. **369**(6504).

36. Samson, R.Y., et al., *Molecular and structural basis of ESCRT-III recruitment to membranes during archaeal cell division.* Mol Cell, 2011. **41**(2): p. 186-96.

37. Low, H.H. and J. Lowe, *A bacterial dynamin-like protein.* Nature, 2006. **444**(7120): p. 766-9.

38. Doan, T., et al., *FisB mediates membrane fission during sporulation in Bacillus subtilis.* Genes Dev, 2013. **27**(3): p. 322-34.

39. Higgins, D. and J. Dworkin, *Recent progress in Bacillus subtilis sporulation.* FEMS Microbiol Rev, 2012. **36**(1): p. 131-48.

40. Barak, I. and K. Muchova, *The positioning of the asymmetric septum during sporulation in Bacillus subtilis.* PLoS One, 2018. **13**(8): p. e0201979.

41. Burton, B.M., et al., *The ATPase SpoIIIE transports DNA across fused septal membranes during sporulation in Bacillus subtilis.* Cell, 2007. **131**(7): p. 1301-12.

42. Lopez-Garrido, J., et al., *Chromosome Translocation Inflates Bacillus Forespores and Impacts Cellular Morphology.* Cell, 2018. **172**(4): p. 758-770 e14.

43. Sharp, M.D. and K. Pogliano, *The membrane domain of SpoIIIE is required for membrane fusion during Bacillus subtilis sporulation.* J Bacteriol, 2003. **185**(6): p. 2005-8.

44. Sharp, M.D. and K. Pogliano, *An in vivo membrane fusion assay implicates SpoIIIE in the final stages of engulfment during Bacillus subtilis sporulation.* Proc Natl Acad Sci U S A, 1999. **96**(25): p. 14553-8.

45. Ramamurthi, K.S. and R. Losick, *Negative membrane curvature as a cue for subcellular localization of a bacterial protein.* Proceedings of the National Academy of Sciences of the United States of America, 2009. **106**(32): p. 13541-13545.

46. Ramamurthi, K.S., et al., *Geometric cue for protein localization in a bacterium.* Science, 2009. **323**(5919): p. 1354-7.

47. Van Baarle, S., et al., *Protein-Protein Interaction Domains of Bacillus subtilis DivIVA.* Journal of Bacteriology, 2013. **195**(5): p. 1012-1021.

48. Lenarcic, R., et al., *Localisation of DivIVA by targeting to negatively curved membranes.* Embo Journal, 2009. **28**(15): p. 2272-2282.

49. Gill, R.L., Jr., et al., *Structural basis for the geometry-driven localization of a small protein.* Proc Natl Acad Sci U S A, 2015. **112**(15): p. E1908-15.

50. Lopez, D. and G. Koch, *Exploring functional membrane microdomains in bacteria: an overview.* Curr Opin Microbiol, 2017. **36**: p. 76-84.

51. Lopez, D. and R. Kolter, *Functional microdomains in bacterial membranes.* Genes Dev, 2010. **24**(17): p. 1893-902.

52. Good, M.C., J.G. Zalatan, and W.A. Lim, *Scaffold proteins: hubs for controlling the flow of cellular information.* Science, 2011. **332**(6030): p. 680-6.

53. Langhorst, M.F., A. Reuter, and C.A. Stuermer, *Scaffolding microdomains and beyond: the function of reggie/flotillin proteins.* Cell Mol Life Sci, 2005. **62**(19-20): p. 2228-40.

54. Donovan, C. and M. Bramkamp, *Characterization and subcellular localization of a bacterial flotillin homologue.* Microbiology (Reading), 2009. **155**(Pt 6): p. 1786-1799.

55. Planas-Iglesias, J., et al., *Cardiolipin Interactions with Proteins.* Biophys J, 2015. **109**(6): p. 1282-94.

56. Claypool, S.M. and C.M. Koehler, *The complexity of cardiolipin in health and disease.* Trends Biochem Sci, 2012. **37**(1): p. 32-41.

57. Renner, L.D. and D.B. Weibel, *Cardiolipin microdomains localize to negatively curved regions of Escherichia coli membranes.* Proc Natl Acad Sci U S A, 2011. **108**(15): p. 6264-9.

58. Kawai, F., et al., *Cardiolipin domains in Bacillus subtilis marburg membranes.* J Bacteriol, 2004. **186**(5): p. 1475-83.

59. Huang, K.C., R. Mukhopadhyay, and N.S. Wingreen, *A curvature-mediated mechanism for localization of lipids to bacterial poles.* PLoS Comput Biol, 2006. **2**(11): p. e151.

60. Romantsov, T., et al., *Cardiolipin promotes polar localization of osmosensory transporter ProP in Escherichia coli.* Mol Microbiol, 2007. **64**(6): p. 1455-65.

61. Romantsov, T., et al., *Cardiolipin controls the osmotic stress response and the subcellular location of transporter ProP in Escherichia coli.* J Biol Chem, 2008. **283**(18): p. 12314-23.

62. Claypool, S.M., et al., *Cardiolipin defines the interactome of the major ADP/ATP carrier protein of the mitochondrial inner membrane.* J Cell Biol, 2008. **182**(5): p. 937-50.

63. Acehan, D., et al., *Cardiolipin affects the supramolecular organization of ATP synthase in mitochondria.* Biophys J, 2011. **100**(9): p. 2184-92.

64. Schumacher, M.A., *Bacterial Nucleoid Occlusion: Multiple Mechanisms for Preventing Chromosome Bisection During Cell Division.* Subcell Biochem, 2017. **84**: p. 267-298.

65. Laloux, G. and C. Jacobs-Wagner, *How do bacteria localize proteins to the cell pole?* Journal of Cell Science, 2014. **127**(1): p. 11-19.

66. Ebersbach, G., et al., *A self-associating protein critical for chromosome attachment, division, and polar organization in caulobacter.* Cell, 2008. **134**(6): p. 956-68.

67. Laloux, G. and C. Jacobs-Wagner, *Spatiotemporal control of PopZ localization through cell cycle-coupled multimerization.* J Cell Biol, 2013. **201**(6): p. 827-41.

68. Mitchell, P., *Coupling of phosphorylation to electron and hydrogen transfer by a chemi-osmotic type of mechanism.* Nature, 1961. **191**: p. 144-8.

69. Strahl, H. and L.W. Hamoen, *Membrane potential is important for bacterial cell division.* Proc Natl Acad Sci U S A, 2010. **107**(27): p. 12281-6.

70. Seddon, J.M., *Structure of the inverted hexagonal (HII) phase, and non-lamellar phase transitions of lipids.* Biochim Biophys Acta, 1990. **1031**(1): p. 1-69.

71. Ban, T., et al., *OPA1 disease alleles causing dominant optic atrophy have defects in cardiolipin-stimulated GTP hydrolysis and membrane tubulation.* Human Molecular Genetics, 2010. **19**(11): p. 2113-2122.

72. Stepanyants, N., et al., *Cardiolipin's propensity for phase transition and its reorganization by dynamin-related protein 1 form a basis for mitochondrial membrane fission.* Mol Biol Cell, 2015. **26**(17): p. 3104-16.

73. Heymann, J.A.W. and J.E. Hinshaw, *Dynamins at a glance.* Journal of Cell Science, 2009. **122**(19): p. 3427-3431.

74. Vance, J.E. and G. Tasseva, *Formation and function of phosphatidylserine and phosphatidylethanolamine in mammalian cells.* Biochim Biophys Acta, 2013. **1831**(3): p. 543-54.

75. van Meer, G., D.R. Voelker, and G.W. Feigenson, *Membrane lipids: where they are and how they behave.* Nature Reviews Molecular Cell Biology, 2008. **9**(2): p. 112-124.

76. Patel, D. and S.N. Witt, *Ethanolamine and Phosphatidylethanolamine: Partners in Health and Disease.* Oxidative Medicine and Cellular Longevity, 2017. **2017**: p. 1-18.

77. Bogdanov, M., M. Umeda, and W. Dowhan, *Phospholipid-assisted refolding of an integral membrane protein. Minimum structural features for phosphatidylethanolamine to act as a molecular chaperone.* J Biol Chem, 1999. **274**(18): p. 12339-45.

78. Mileykovskaya, E., et al., *Localization and function of early cell division proteins in filamentous Escherichia coli cells lacking phosphatidylethanolamine.* J Bacteriol, 1998. **180**(16): p. 4252-7.

79. Matsumoto, K., et al., *Cloning, sequencing, and disruption of the Bacillus subtilis psd gene coding for phosphatidylserine decarboxylase.* J Bacteriol, 1998. **180**(1): p. 100-6.

80. Kikuchi, S., I. Shibuya, and K. Matsumoto, *Viability of an Escherichia coli pgsA null mutant lacking detectable phosphatidylglycerol and cardiolipin.* J Bacteriol, 2000. **182**(2): p. 371-6.

81. Dowhan, W., *Molecular basis for membrane phospholipid diversity: why are there so many lipids?* Annu Rev Biochem, 1997. **66**: p. 199-232.

82. Kawai, F., et al., *Cardiolipin enrichment in spore membranes and its involvement in germination of Bacillus subtilis Marburg.* Genes Genet Syst, 2006. **81**(2): p. 69-76.

83. Griffiths, K.K. and P. Setlow, *Effects of modification of membrane lipid composition on Bacillus subtilis sporulation and spore properties.* J Appl Microbiol, 2009. **106**(6): p. 2064-78.

84. El-Gebali, S., et al., *The Pfam protein families database in 2019.* Nucleic Acids Research, 2018. **47**(D1): p. D427-D432.

85. Bogdanov, M., et al., *Transmembrane protein topology mapping by the substituted cysteine accessibility method (SCAM(TM)): application to lipid-specific membrane protein topogenesis.* Methods, 2005. **36**(2): p. 148-71.

86. Bogdanov, M., P.N. Heacock, and W. Dowhan, *Study of polytopic membrane protein topological organization as a function of membrane lipid composition.* Methods Mol Biol, 2010. **619**: p. 79-101.

87. Schaeffer, P., J. Millet, and J.P. Aubert, *Catabolic repression of bacterial sporulation.* Proc Natl Acad Sci U S A, 1965. **54**(3): p. 704-11.

88. Ovchinnikov, S., et al., *Protein structure determination using metagenome sequence data.* Science, 2017. **355**(6322): p. 294-298.

89. Dobson, L., I. Remenyi, and G.E. Tusnady, *CCTOP: a Consensus Constrained TOPology prediction web server.* Nucleic Acids Res, 2015. **43**(W1): p. W408-12.

90. Landajuela, A., et al., *The bacterial membrane fission protein FisB requires homo-oligomerization and lipid-binding to catalyze membrane scission.* bioRxiv, 2020.

91. Ojkic, N., et al., *Cell-wall remodeling drives engulfment during Bacillus subtilis sporulation.* Elife, 2016. **5**.

92. Carballido-Lopez, R., et al., *Actin homolog MreBH governs cell morphogenesis by localization of the cell wall hydrolase LytE.* Dev Cell, 2006. **11**(3): p. 399-409.

93. Carballido-Lopez, R. and A. Formstone, *Shape determination in Bacillus subtilis.* Curr Opin Microbiol, 2007. **10**(6): p. 611-6.

94. Errington, J. and L.J. Wu, *Cell Cycle Machinery in Bacillus subtilis.* Subcell Biochem, 2017. **84**: p. 67-101.

95. Ojkic, N., et al., *Cell-wall remodeling drives engulfment during Bacillus subtilis sporulation.* Elife, 2016. **5**.

96. Meyer, P., et al., *Cell wall synthesis is necessary for membrane dynamics during sporulation of Bacillus subtilis.* Mol Microbiol, 2010. **76**(4): p. 956-70.

97. Jones, L.J., R. Carballido-Lopez, and J. Errington, *Control of cell shape in bacteria: helical, actin-like filaments in Bacillus subtilis.* Cell, 2001. **104**(6): p. 913-22.

98. Garner, E.C., et al., *Coupled, circumferential motions of the cell wall synthesis machinery and MreB filaments in B. subtilis.* Science, 2011. **333**(6039): p. 222-5.

99. Silver, L.L., *Fosfomycin: Mechanism and Resistance.* Cold Spring Harb Perspect Med, 2017. **7**(2).

100. Schirner, K., et al., *Lipid-linked cell wall precursors regulate membrane association of bacterial actin MreB.* Nat Chem Biol, 2015. **11**(1): p. 38-45.

101. Axelrod, D., *Total internal reflection fluorescence microscopy in cell biology.* Traffic, 2001. **2**(11): p. 764-74.

102. Carballido-Lopez, R. and J. Errington, *The bacterial cytoskeleton: in vivo dynamics of the actin-like protein Mbl of Bacillus subtilis.* Dev Cell, 2003. **4**(1): p. 19-28.

103. Huet, S., et al., *Analysis of transient behavior in complex trajectories: application to secretory vesicle dynamics.* Biophys J, 2006. **91**(9): p. 3542-59.

104. Koppelman, C.M., et al., *Escherichia coli minicell membranes are enriched in cardiolipin.* J Bacteriol, 2001. **183**(20): p. 6144-7.

105. Kunst, F., et al., *The complete genome sequence of the gram-positive bacterium Bacillus subtilis.* Nature, 1997. **390**(6657): p. 249-56.

106. Chernomordik, L.V. and M.M. Kozlov, *Mechanics of membrane fusion.* Nat Struct Mol Biol, 2008. **15**(7): p. 675-83.

107. Schmid, S.L. and V.A. Frolov, *Dynamin: functional design of a membrane fission catalyst.* Annu Rev Cell Dev Biol, 2011. **27**: p. 79-105.

108. Nishibori, A., et al., *Phosphatidylethanolamine Domains and Localization of Phospholipid Synthases in Bacillus subtilis Membranes.* Journal of Bacteriology, 2005. **187**(6): p. 2163-2174.

109. Smith, M.B., et al., *Interactive, computer-assisted tracking of speckle trajectories in fluorescence microscopy: application to actin polymerization and membrane fusion.* Biophys J, 2011. **101**(7): p. 1794-804.

110. Sohlenkamp, C. and O. Geiger, *Bacterial membrane lipids: diversity in structures and pathways.* FEMS Microbiology Reviews, 2015. **40**(1): p. 133-159.

111. Oliver, P.M., et al., *Localization of anionic phospholipids in Escherichia coli cells.* J Bacteriol, 2014. **196**(19): p. 3386-98.

112. Kobayashi, K., et al., *Essential Bacillus subtilis genes.* Proc Natl Acad Sci U S A, 2003. **100**(8): p. 4678-83.

113. den Kamp, J.A., I. Redai, and L.L. van Deenen, *Phospholipid composition of Bacillus subtilis.* J Bacteriol, 1969. **99**(1): p. 298-303.

114. Buser, C.A., et al., *Membrane binding of myristylated peptides corresponding to the NH2 terminus of Src.* Biochemistry, 1994. **33**(44): p. 13093-101.

115. Lopez, C.S., et al., *Role of anionic phospholipids in the adaptation of Bacillus subtilis to high salinity.* Microbiology (Reading), 2006. **152**(Pt 3): p. 605-16.

116. Bolanos-Garcia, V.M. and O.R. Davies, *Structural analysis and classification of native proteins from E. coli commonly co-purified by immobilised metal affinity chromatography.* Biochim Biophys Acta, 2006. **1760**(9): p. 1304-13.

117. Connell, E., P. Scott, and B. Davletov, *Real-time assay for monitoring membrane association of lipid-binding domains.* Anal Biochem, 2008. **377**(1): p. 83-8.

118. Shi, Z. and T. Baumgart, *Membrane tension and peripheral protein density mediate membrane shape transitions.* Nat Commun, 2015. **6**: p. 5974.

119. Nishimura, K., et al., *Identification of giant unilamellar vesicles with permeability to small charged molecules.* RSC Advances, 2014. **4**(66): p. 35224-35232.

120. Gonzalez-Bullon, D., et al., *Membrane Permeabilization by Bordetella Adenylate Cyclase Toxin Involves Pores of Tunable Size.* Biomolecules, 2019. **9**(5).

121. Farsad, K., et al., *Generation of high curvature membranes mediated by direct endophilin bilayer interactions.* J Cell Biol, 2001. **155**(2): p. 193-200.

122. Johannes, L., C. Wunder, and P. Bassereau, *Bending "on the rocks"--a cocktail of biophysical modules to build endocytic pathways.* Cold Spring Harb Perspect Biol, 2014. **6**(1).

123. Chen, Z., et al., *The N-Terminal Amphipathic Helix of Endophilin Does Not Contribute to Its Molecular Curvature Generation Capacity.* J Am Chem Soc, 2016. **138**(44): p. 14616-14622.

124. Ambroso, M.R., B.G. Hegde, and R. Langen, *Endophilin A1 induces different membrane shapes using a conformational switch that is regulated by phosphorylation.* Proc Natl Acad Sci U S A, 2014. **111**(19): p. 6982-7.

125. Masuda, M., et al., *Endophilin BAR domain drives membrane curvature by two newly identified structure-based mechanisms.* EMBO J, 2006. **25**(12): p. 2889-97.

126. Chen, Z.M., E. Atefi, and T. Baumgart, *Membrane Shape Instability Induced by Protein Crowding.* Biophysical Journal, 2016. **111**(9): p. 1823-1826.

127. Handler, A.A., J.E. Lim, and R. Losick, *Peptide inhibitor of cytokinesis during sporulation in Bacillus subtilis.* Mol Microbiol, 2008. **68**(3): p. 588-99.

128. Renner, L.D., et al., *Studying biomolecule localization by engineering bacterial cell wall curvature.* PLoS One, 2013. **8**(12): p. e84143.

129. Inaba, T., et al., *Phospholipase Cbeta1 induces membrane tubulation and is involved in caveolae formation.* Proc Natl Acad Sci U S A, 2016. **113**(28): p. 7834-9.

130. Peter, B.J., et al., *BAR domains as sensors of membrane curvature: the amphiphysin BAR structure.* Science, 2004. **303**(5657): p. 495-9.

131. Idevall-Hagren, O., et al., *Optogenetic control of phosphoinositide metabolism.* Proc Natl Acad Sci U S A, 2012. **109**(35): p. E2316-23.

132. Tsai, F.C., et al., *Ezrin enrichment on curved membranes requires a specific conformation or interaction with a curvature-sensitive partner.* Elife, 2018. **7**.

133. Cole, N.B., *Site-specific protein labeling with SNAP-tags.* Curr Protoc Protein Sci, 2013. **73**: p. 30 1 1-30 1 16.

134. Griffin, B.A., S.R. Adams, and R.Y. Tsien, *Specific covalent labeling of recombinant protein molecules inside live cells.* Science, 1998. **281**(5374): p. 269-72.

135. Tinevez, J.Y., et al., *TrackMate: An open and extensible platform for single-particle tracking.* Methods, 2017. **115**: p. 80-90.

136. Smith, M.B., et al., *Segmentation and tracking of cytoskeletal filaments using open active contours.* Cytoskeleton (Hoboken), 2010. **67**(11): p. 693-705.

137. Roux, A., et al., *Membrane curvature controls dynamin polymerization.* Proc Natl Acad Sci U S A, 2010. **107**(9): p. 4141-6.

138. Lee, I.H., et al., *Negative membrane curvature catalyzes nucleation of endosomal sorting complex required for transport (ESCRT)-III assembly.* Proc Natl Acad Sci U S A, 2015. **112**(52): p. 15892-7.

139. Blood, P.D. and G.A. Voth, *Direct observation of Bin/amphiphysin/Rvs (BAR) domain-induced membrane curvature by means of molecular dynamics simulations.* Proc Natl Acad Sci U S A, 2006. **103**(41): p. 15068-72.

140. Gallop, J.L., et al., *Mechanism of endophilin N-BAR domain-mediated membrane curvature.* EMBO J, 2006. **25**(12): p. 2898-910.

141. Makowski, S.L., R.S. Kuna, and S.J. Field, *Induction of membrane curvature by proteins involved in Golgi trafficking.* Adv Biol Regul, 2020. **75**: p. 100661.

142. McMahon, H.T. and E. Boucrot, *Membrane curvature at a glance.* Journal of Cell Science, 2015. **128**(6): p. 1065-1070.

143. Hernandez, J.M., et al., *Variable cooperativity in SNARE-mediated membrane fusion.* Proc Natl Acad Sci U S A, 2014. **111**(33): p. 12037-42.

144. Mostafavi, H., et al., *Entropic forces drive self-organization and membrane fusion by SNARE proteins.* Proc Natl Acad Sci U S A, 2017. **114**(21): p. 5455-5460.

145. Wu, Z., et al., *Dilation of fusion pores by crowding of SNARE proteins.* Elife, 2017. **6**.

146. Antonny, B., et al., *Membrane fission by dynamin: what we know and what we need to know.* EMBO J, 2016. **35**(21): p. 2270-2284.

147. Fleming, T.C., et al., *Dynamic SpoIIIE assembly mediates septal membrane fission during Bacillus subtilis sporulation.* Genes Dev, 2010. **24**(11): p. 1160-72.

148. Sullivan, N.L., K.A. Marquis, and D.Z. Rudner, *Recruitment of SMC by ParB-parS organizes the origin region and promotes efficient chromosome segregation.* Cell, 2009. **137**(4): p. 697-707.

149. Hanson, P.I., S. Shim, and S.A. Merrill, *Cell biology of the ESCRT machinery.* Curr Opin Cell Biol, 2009. **21**(4): p. 568-74.

150. Slagsvold, T., et al., *Endosomal and non-endosomal functions of ESCRT proteins.* Trends Cell Biol, 2006. **16**(6): p. 317-26.

151. Elia, N., et al., *Dynamics of endosomal sorting complex required for transport (ESCRT) machinery during cytokinesis and its role in abscission.* Proc Natl Acad Sci U S A, 2011. **108**(12): p. 4846-51.

152. Rusten, T.E. and H. Stenmark, *How do ESCRT proteins control autophagy?* Journal of Cell Science, 2009. **122**(13): p. 2179-2183.

153. Hurley, J.H. and P.I. Hanson, *Membrane budding and scission by the ESCRT machinery: it's all in the neck.* Nat Rev Mol Cell Biol, 2010. **11**(8): p. 556-66.

154. Misra, S. and J.H. Hurley, *Crystal structure of a phosphatidylinositol 3-phosphate-specific membrane-targeting motif, the FYVE domain of Vps27p.* Cell, 1999. **97**(5): p. 657-66.

155. Slagsvold, T., et al., *Eap45 in mammalian ESCRT-II binds ubiquitin via a phosphoinositide-interacting GLUE domain.* J Biol Chem, 2005. **280**(20): p. 19600-6.

156. Sundquist, W.I. and H.G. Krausslich, *HIV-1 assembly, budding, and maturation.* Cold Spring Harb Perspect Med, 2012. **2**(7): p. a006924.

157. Sun, Y. and D.G. Drubin, *The functions of anionic phospholipids during clathrin-mediated endocytosis site initiation and vesicle formation.* J Cell Sci, 2012. **125**(Pt 24): p. 6157-65.

158. Vallis, Y., et al., *Importance of the pleckstrin homology domain of dynamin in clathrin-mediated endocytosis.* Curr Biol, 1999. **9**(5): p. 257-60.

159. Salim, K., et al., *Distinct specificity in the recognition of phosphoinositides by the pleckstrin homology domains of dynamin and Bruton's tyrosine kinase.* EMBO J, 1996. **15**(22): p. 6241-50.

160. Renard, H.F., et al., *Endophilin-A2 functions in membrane scission in clathrin-independent endocytosis.* Nature, 2015. **517**(7535): p. 493-6.

161. Prevost, C., et al., *IRSp53 senses negative membrane curvature and phase separates along membrane tubules.* Nat Commun, 2015. **6**: p. 8529.

162. Tsumoto, K., et al., *A reverse-phase method revisited: Rapid high-yield preparation of giant unilamellar vesicles (GUVs) using emulsification followed by centrifugation.* Colloids and Surfaces a-Physicochemical and Engineering Aspects, 2018. **546**: p. 74-82.

163. Wu, L.J., et al., *A conjugation-like mechanism for prespore chromosome partitioning during sporulation in Bacillus subtilis.* Genes Dev, 1995. **9**(11): p. 1316-26.

164. Schujman, G.E., et al., *Response of Bacillus subtilis to cerulenin and acquisition of resistance.* J Bacteriol, 2001. **183**(10): p. 3032-40.

165. Schujman, G.E., et al., *De novo fatty acid synthesis is required for establishment of cell type-specific gene transcription during sporulation in Bacillus subtilis.* Mol Microbiol, 1998. **29**(5): p. 1215-24.

166. Youngman, P.J., J.B. Perkins, and R. Losick, *Genetic transposition and insertional mutagenesis in Bacillus subtilis with Streptococcus faecalis transposon Tn917.* Proc Natl Acad Sci U S A, 1983. **80**(8): p. 2305-9.

167. Koo, B.M., et al., *Construction and Analysis of Two Genome-Scale Deletion Libraries for Bacillus subtilis.* Cell Syst, 2017. **4**(3): p. 291-305.e7.

168. Sterlini, J.M. and J. Mandelstam, *Commitment to sporulation in Bacillus subtilis and its relationship to development of actinomycin resistance.* Biochem J, 1969. **113**(1): p. 29-37.

169. Nikolaus, J. and E. Karatekin, *SNARE-mediated Fusion of Single Proteoliposomes with Tethered Supported Bilayers in a Microfluidic Flow Cell Monitored by Polarized TIRF Microscopy.* J Vis Exp, 2016(114).

170. Tarantino, N., et al., *TNF and IL-1 exhibit distinct ubiquitin requirements for inducing NEMO-IKK supramolecular structures.* J Cell Biol, 2014. **204**(2): p. 231-45.

171. Lacombe, C. and B. Lubochinsky, *Specific extraction of bacterial cardiolipin from sporulating Bacillus subtilis.* Biochim Biophys Acta, 1988. **961**(2): p. 183-7.

172. Ducret, A., E.M. Quardokus, and Y.V. Brun, *MicrobeJ, a tool for high throughput bacterial cell detection and quantitative analysis.* Nat Microbiol, 2016. **1**(7): p. 16077.

173. Stockl, M., J. Nikolaus, and A. Herrmann, *Visualization of lipid domain-specific protein sorting in giant unilamellar vesicles.* Methods Mol Biol, 2010. **606**: p. 115-26.

174. Eichenberger, P., et al., *The sigmaE regulon and the identification of additional sporulation genes in Bacillus subtilis.* J Mol Biol, 2003. **327**(5): p. 945-72.

175. Guerrier, S., et al., *The F-BAR domain of srGAP2 induces membrane protrusions required for neuronal migration and morphogenesis.* Cell, 2009. **138**(5): p. 990-1004.

176. Ren, C., et al., *Leukocyte Cytoskeleton Polarization Is Initiated by Plasma Membrane Curvature from Cell Attachment.* Dev Cell, 2019. **49**(2): p. 206-219 e7.

177. de Oliveira, S., E.E. Rosowski, and A. Huttenlocher, *Neutrophil migration in infection and wound repair: going forward in reverse.* Nat Rev Immunol, 2016. **16**(6): p. 378-91.

178. Raman, R., C.S. Pinto, and M. Sonawane, *Polarized Organization of the Cytoskeleton: Regulation by Cell Polarity Proteins.* J Mol Biol, 2018. **430**(19): p. 3565-3584.

179. Hind, L.E., W.J. Vincent, and A. Huttenlocher, *Leading from the Back: The Role of the Uropod in Neutrophil Polarization and Migration.* Dev Cell, 2016. **38**(2): p. 161-9.

180. Xu, W., et al., *Integrin-induced PIP5K1C kinase polarization regulates neutrophil polarization, directionality, and in vivo infiltration.* Immunity, 2010. **33**(3): p. 340-50.

181. Woodham, E.F. and L.M. Machesky, *Polarised cell migration: intrinsic and extrinsic drivers.* Curr Opin Cell Biol, 2014. **30**: p. 25-32.

182. Salzer, U., J. Kostan, and K. Djinovic-Carugo, *Deciphering the BAR code of membrane modulators.* Cell Mol Life Sci, 2017. **74**(13): p. 2413-2438.

183. Sporny, M., et al., *Structural History of Human SRGAP2 Proteins.* Mol Biol Evol, 2017. **34**(6): p. 1463-1478.

184. Schoebel, S., et al., *High-affinity binding of phosphatidylinositol 4-phosphate by Legionella pneumophila DrrA.* EMBO Rep, 2010. **11**(8): p. 598-604.

185. Zhang, Y., et al., *Different roles of G protein subunits beta1 and beta2 in neutrophil function revealed by gene expression silencing in primary mouse neutrophils.* J Biol Chem, 2010. **285**(32): p. 24805-14.

186. Yuan, Q., et al., *PKN1 Directs Polarized RAB21 Vesicle Trafficking via RPH3A and Is Important for Neutrophil Adhesion and Ischemia-Reperfusion Injury.* Cell Rep, 2017. **19**(12): p. 2586-2597.

187. Basit, A., W. Tang, and D. Wu, *shRNA-Induced Gene Knockdown In Vivo to Investigate Neutrophil Function.* Methods Mol Biol, 2016. **1407**: p. 169-77.

188. Stachowiak, M.R., et al., *Mechanism of cytokinetic contractile ring constriction in fission yeast.* Dev Cell, 2014. **29**(5): p. 547-561.